NOTICE

The quality of this microform is heavily dependent upon the quality of the original thesis submitted for microfilming. Every effort has been made to ensure the highest quality of reproduction possible.

If pages are missing, contact the university which granted the degree.

Some pages may have indistinct print especially if the original pages were typed with a poor typewriter ribbon or if the university sent us an inferior photocopy.

Reproduction in full or in part of this microform is governed by the Canadian Copyright Act, R.S.C. 1970, c. C-30, and subsequent amendments.

AVIS

La qualité de cette microforme dépend grandement de la qualité de la thèse soumise au microfilmage. Nous avons tout fait pour assurer une qualité supérieure de reproduction.

S'il manque des pages, veuillez communiquer avec l'université qui a conféré le grade

La qualité d'impression de certaines pages peut laisser à désirer, surtout si les pages originales ont été dactylographiées à l'aide d'un ruban usé ou si l'université nous a fait parvenir une photocopie de qualité inférieure

La reproduction, même partielle, de cette microforme est soumise à la Loi canadienne sur le droit d'auteur, SRC 1970, c. C-30, et ses amendements subséquents

EXPERIMENTAL PERFORMANCE EVALUATION

OF

MULTI-ROW, PLATE FINNED-TUBE, DIRECT EXPANSION

AIR COOLING AND DEHUMIDIFYING COILS

Mal Turaga

A Thesis

in

Centre for Building Studies
The Faculty of Engineering

Presented in Partial Fulfillment of the Requirements
for the degree of Doctor of philosophy at
Concordia University
Montreal, Quebec, Canada

March 1989

ISBN 0-315-51339-X

ABSTRACT

Experimental studies are conducted on Plate finned-tube, Direct-Expansion (DX), air cooling and dehumidifying heat exchangers to determine the effects of significant coil geometric parameters and the fluid flow parameters on the coil performance. Tests are conducted on ten (10) coils with varied fin densities (3.1 to 5.5 fins/cm) and tube rows (3 to 8) under both dry and wet surface conditions for the air-side. Such studies, on the performance of DX-coils for comfort air conditioning applications, are very limited in the open literature.

Correlations for the average heat transfer and pressure drop factors for the working fluids (air and refrigerant) are developed from the experimental data; such correlations for refrigerant in DX-coils are very limited in the present literature. Regression analysis is used to determine the influential coil geometric parameters on the heat exchanger performance.

In the range of the air flow Reynolds number considered ($300 < Re_d < 1500$), the air-side average heat transfer and pressure drop factors (for both dry and wet surface conditions) are found to be independent of the number of tube rows and decrease when the fin density increases (for a given Reynolds number).

The refrigerant-side average Nusselt number (Nu_r) is found to be an increasing linear function of the two-phase heat transfer parameter ($Re^2_{r,l} K_f$) and the corresponding pressure drop factor (f_r) is found to be a decreasing linear function of the two-phase pressure drop parameter ($Re_{r,l}/K_f$). The presence of oil (about 2% by weight), is found to increase both the average Nusselt number (by 30 to 40%) and the average pressure drop factor (by 25%), compared to the corresponding oil free flow.

A method for selection of DX-coils is developed from the correlations for prediction of the average heat transfer and pressure drop factors. This selection method may be used for estimation of the part-load performance of DX-coils.

ACKNOWLEDGEMENTS

The author wishes to express his gratitude to the thesis Supervisors, Dr. S. Lin and Dr. P.P. Fazio, for their help and guidance.

Special thanks to Ting Hong Ngan and Hai Luong Pham for providing programming assistance, and to my colleagues in the Centre for Building Studies, for their support and help.

Financial assistance for the test facility was provided by a negotiated development grant, and the experimental study was made possible by grant # 4770, (P.P. Fazio) from the National Research Council (now National Science and Engineering Research Council of Canada).

Finally, my thanks to my wife Viviane and my family for their understanding and support.

TABLE OF CONTENTS

	PAGE
ABSTRACT	i
ACKNOWLEDGEMENTS	iii
TABLE OF CONTENTS	iv
NOMENCLATURE	viii
LIST OF FIGURES	xiii
LIST OF TABLES	xvii
CHAPTER 1: Introduction	1
CHAPTER 2: Literature Survey	7
1. Construction of DX-coils	8
2. Operation of DX-coils	12
3. Energy requirements due to DX-coils	13
4. Heat transfer and pressure drop processes in DX-coils	17
4.1 Review of the existing air-side studies	18
4.2 Discussion of the recent studies on the air-side performance	27
4.3 Summary of the existing literature on the air-side performance	43
4.4 Review of the existing methods for prediction of the heat transfer and pressure drop factors for boiling refrigerants	45
4.5 Effects of oil-refrigerant mixture on the heat transfer and pressure drop factors	49

PAGE

4.6 Discussion of the experimental studies on the boiling refrigerants 54

4.7 Summary of the existing studies on the refrigerant-side heat transfer and pressure drop factor predicition 63

CHAPTER 3: Description of the test facility and the measurement system 64

1. Operation of the test apparatus 65

2. Component description 73

3. Air-side measurements 77

4. Refrigerant-side measurements 85

5. Tube surface temperature measurement 89

6. Condenser water temperature measurement 89

7. Data acquisition system 91

CHAPTER 4: Description of the test procedure and the experimental data reduction method 92

1. Description of the test coils 93

2. General test conditions 95

3. Test procedure 95

3.1 Air-side wet surface tests 96

3.2 Air-side dry surface tests 96

4. Test data reduction method 97

CHAPTER 5: Analysis of the test results 112

1. Air-side dry surface average heat transfer factor 113

PAGE

2. Air-side dry surface average pressure drop factor 118

3. Air-side wet surface average heat transfer factor 122

4. Air-side wet surface average pressure drop factor 126

5. Refrigerant-side test results 129

6. Comparison of the air-side dry and wet surface test results 139

CHAPTER 6: Correlations for the heat transfer and pressure drop factors for DX-coils 144

1. Correlations for the heat transfer and pressure drop factors 145

2. Discussion of the correlations developed 151

CHAPTER 7: DX-coil selection method 166

1. General description of the selection method 167

2. Assumptions used in the selection method 172

3. Row-by-row heat balance calculations 176

4. Computer assisted selection method 186

CHAPTER 8: Conclusions and recommendations 190

1. Conclusion 190

2. Recommendations 192

LIST OF REFERENCES 193

BIBLIOGRAPHY 196

PAGE

APPENDICIES 201

1. Coil geometric data 201

2. Major equipment specifications 203

3. Test data summary 204

4. Sample test data 214

5. Sample calculations 217

6. Applications of the coil selection method 225

7. Uncertainty analysis 231

NOMENCLATURE

Symbol	Description	SI Units
A_o	Total surface area	m^2
A_F	Face area	m^2
A_I	Internal surface area	m^2
$A_{m,f}$	Minimum flow area	m^2
A_p	Primary surface area	m^2
A_s	Secondary surface area	m^2
b	Ratio of total surface area to tube internal surface area (A_o/A_I)	-
C_p	Specific heat	kJ/kg°K
C_H	Coil height	m
C_w	Coil width	m
D_h	Hydraulic diameter	m
D_I	Tube inside diameter	m
D_o	Tube outside diameter	m
F_s	Ratio of fin spacing to distance between fins	-
G	Mass flux	kg/m^2s
g_c	Gravitational Correction factor	kg m/N-s^2
H	Enthalpy	kJ/kg

Symbol	Description	SI Units
h	Heat transfer coefficient	$W/m^2\ °C$
h_d	Mass transfer coefficient	kg/sm^2
h_m	Flow coefficient ($= h_d/\rho$)	m/s
H_{fg}	Latent Heat	kJ/kg
J	Joules constant	-
k	Thermal conductivity	W/m°C
L_c	Length of fin collar	m
L_d	Depth of Plate fin	m
L_e	Equivalent length	m
$L_{e,RB}$	Equivalent length of return-bend	m
L_F	Height of plate fin	m
L_T	Length of tube	m
m	Mass flow rate	kg/s
N_f	Number of fins	-
N_R	Number of rows	-
N_T	Total number of tubes	-
N_{TR}	Number of tubes per row	-
p	Pressure	Pa
P_s	Number of fins per unit length	-
$\dot{Q}$	Heat transfer rate	W

Symbol	Description	SI Units
q	heat flux density	W/m^2
r	Tube radius ($= D_o/2$)	m
r'	Modified hydraulic radius	m
R	Thermal resistance	$m^2\,°C/W$
S_f	Fin spacing	m
S_L	Tube logitudinal spacing	m
S_T	Tube transverse spacing	m
t	Temperature	°C
t_t	Tube thickness	m
V	Velocity	m/s
v	Specific volume	m^3/kg
w	Humidity ratio	-
x	Vapour fraction	-
Y_f	Fin thickness	m
μ	Dynamic viscosity	$N.s/m^2$
ρ	Density	kg/m^3
σ	Ratio of coil face area to minimum flow area ($A_F/A_{n,f}$)	-

Symbol	Description

NON-DIMENSIONAL NUMBERS

J	Heat transfer factor ($S_t \ P_r^{2/3}$)
f	Friction factor (fanning factor)
K_f	Boiling number $[J(\Delta x)H_{fg}/L_e]$
Pr	Prandlt number ($\mu \ C_p/K$)
Re	Reynolds number (GD/μ)
Nu	Nusselt number ($h \ D/K$)
Sc	Schmidts number (momentum transfer coefficient / diffusivity coefficient)
St	Stanton number ($h/G \ C_p$)

Symbol	Description
	Subscripts
a	Air-side
AV	Average value
D	Dry surface condition
Exp	Experimental value
f	Fin related
l	Liquid phase
m	Metal, associated with R, and mean value, when associated witn 'X' and 'V'
m,f	Minimum flow
O	Overall
r	Refrigerant-side
s	Surface temp. associated witn 't', standard conditions associated with 'V'
sat	Saturated condition
T	Total, tube when associated with 'L'
W	Wet surface condition
1	Entering condition
2	Leaving condition

LIST OF FIGURES

FIGURE NO.		PAGE NO.
2.1	Pictorial view of a 4-row DX-coil	9
2.2	Geometric parameters for DX-coils	11
2.3	Schematic plan view of a typical DX-coil	15
2.4	Typical fluid and surface temperature variations along tube	15
2.5	Typical psychrometric representation of a cooling and dehumidifying process	16
2.6	Pressure-enthalpy variations in a typical vapour compression refrigeration system	16
2.7	Fin effects on heat transfer and pressure drop factors - Rich	26
2.8	Row effects on heat transfer factor - Rich	26
2.9	Correlation for the air-side dry surface heat transfer factors - Elmahdy	31
2.10	Correlation for the air-side wet surface heat transfer factor - Elmahdy	32
2.11	Comparison of the air-side dry and wet surface heat transfer factor correlations - Elmahdy	33
2.12	Correlation for the dry surface heat transfer factor - McQuiston	38
2.13	Correlation for the dry surface pressure drop factor - McQuiston	38
2.14	Correlation for the wet surface heat transfer factor - McQuiston	42
2.15	Correlation for the wet surface pressure drop factor - McQuiston	42

2.16	Typical variations of heat transfer coefficient and refrigerant temperature along the tube in a DX-coil	46
2.17	Variation of the in-tube local heat transfer coefficient, with outlet vapour fraction	48
2.18	Local heat transfer coefficients for R-12/ oil mixture in a horizontal tube, as measured by Worse-Schmidt	50
2.19	Effect of oil concentration on heat transfer for evaporation of R-12 in a horizontal tube	51
2.20	Average Nusselt number for incomplete evaporation - Pierre	58
2.21	Average Nusselt number for complete evaporation - Pierre	58
2.22	Correlation for two-phase pressure drop factor for oil free, boiling R-12 in straight tubes-Pierre	60
3.1	Cooling coil performance test measurement schematic diagram	66
3.2	Heat exchanger performance testing apparatus	71
3.3	Automatic air-side instrumentation layout	72
3.4	Air flow measurement nozzle	75
3.5	Heating and humidifying system schematic diagram	76
3.6	Refrigeration system schematic	78
3.7	Relative humidity sensor	83
3.8	Humidity sensor calibration data	84
3.9	Location of the air static pressure transducers	86
3.10	Refrigerant temperature sensor	87
3.11	Refrigerant pressure transducer	88
3.12	Tube surface temperature measurement	90

4.1	Typical test coil	94
4.2	Working fluid properties	98
4.3	Air, tube surface and refrigerant temperature variations along the tube circuit	98
4.4	Resistances to heat flow in typical finned tube coils	99
5.1	Air-side dry surface heat transfer factors, experimental data	116
5.2	Air-side dry surface pressure drop factors, experimental data	120
5.3	Air-side wet surface heat transfer factors, experimental data	124
5.4	Air-side wet surface pressure drop factor - experimental data	127
5.5	Refrigerant-side average boiling number - air-side dry surface tests	130
5.6	Refrigerant-side average boiling number, air-side wet surface tests	131
5.7	Refrigerant-side average Nusselt number, air-side dry surface tests	134
5.8	Refrigerant-side average Nusselt number, air-side wet surface tests	135
5.9	Refrigerant-side pressure drop factor - air-side dry surface tests	137
5.10	Refrigerant-side pressure drop factor - air-side wet surface tests	138
6.1	Comparison of the experimental and computed data - $j_{a,D}$	154
6.2	Comparison of the experimental and computed data - $f_{a,D}$	156
6.3	Comparison of the experimental and computed data - $j_{a,w}$	158

6.4	Comparison of the experimental and computed data - $f_{a,w}$	160
6.5	Comparison of the experimental and computed data - Nu_r	162
6.6	Comparison of the experimental and computed data - Nu_r	163
6.7	Comparison of the experimental and computed data - f_r	165
7.1	Typical temperature and enthalpy variations	171
7.2	Thermodynamic conditions of the working fluids in the heat exchanger	174
7.3	Thermodynamic conditions of the working fluids in the first row	175
7.4	Flow chart of the computer assisted design method	189

LIST OF TABLES

Table No.		Page No.
1.1	Actual energy consumption in Canada by sectors	2
1.2	Percentage change in the energy demand growth by sectors and by periods	2
2.1	Typical configurations for air cooling and dehumidifying coils	10
3.1	Nomenclature for measurements	68
3.2	Summary of the instrumentation specifications	80
4.1	Equations for the heat transfer surface and flow area calculations	100
5.1	Comparison of the experimental data - $j_{a,D}$	117
5.2	Comparison of the experimental data - $f_{a,D}$	121
5.3	Comparison of the experimental data - $j_{a,w}$	125
5.4	Comparison of the experimental data - $f_{a,w}$	128
5.5	Comparison of the dry and wet surface heat transfer factors	141
5.6	Comparison of the dry and wet surface pressure drop factors	143
6.1	Dimensionless groups used in the regression analysis	150
6.2	Comparison of the relative deviations of the computed data	152
7.1	Comparison of the experimental and computed performance data	154

CHAPTER - 1

INTRODUCTION

The actual consumption energy by sectors in Canada, for the period 1966 to 1983, is shown in Table-1.1 [1]. Total energy consumption increased by 62% during this period, and the increase in the comsumption for the residential and commercial sectors is the highest (68%) among the sectors considered. The oil embargo period (during the period 1973 to 75) may be the turning point for energy consumption and demand growth in the industrialized countries. Sudden reduction of the energy supply and steep increases in the cost of energy, forced the industrialized countries to implement various conservation measures and to evaluate consumption habits. As a result of the conservation measures implemented, and the economic recession following the energy crisis, drastic reductions in energy consumption growth were achieved. A comparison of energy consumption growth rates during the pre and post oil embargo periods (1966 to 75 and 1978 - 83 respectively) are shown in Table-1.2. In Canada, with the conservation measures implemented and the effects of the economic recession (during the post embargo period), the energy growth rate for the residential and commercial sectors is the highest during the post embargo period (6.3%), and even higher rates of increase in the demand growth may be expected, when economic recovery occurs.

TABLE - 1.1 ACTUAL ENERGY CONSUMPTION IN CANADA BY SECTORS [1] (TRILLION kJ)

SECTOR	YEAR				
	1966	1975	1978	1980	1983
1. Residential and Commercial	1400	1800	2209	2235	2347
2. Industrial	1246	1870	1907	1957	1912
3. Transport	987	1470	1656	1972	1615
TOTAL	3633	5140	5772	6164	5874

TABLE - 1.2 PERCENTAGE CHANGE IN THE ENERGY CONSUMPTION GROWTH BY SECTORS, AND BY PERIOD (COMPUTED FROM TABLE - 1)

SECTOR	Pre-oil Embargo Period 1966-75	Post oil Embargo Period 1978-83	Total Period 1966-83
1. Total Energy	41.5%	1.8%	61.6%
2. Residential and Commercial	28.6%	6.3%	67.6%
3. Industrial	50.1%	0.3%	53.5%
4. Transport	48.9%	-2.51%	63.62%

This high consumption growth rate may be attributed to the relatively high energy consumption for heating and cooling buildings, which is about 30% of the total energy consumption in Canada [2]. In order to reduce the energy consumption growth rate for heating and cooling buildings, improved methods for the design and operation of the indoor environmental control systems and components are required.

Cooling and dehumidifying coils are the main link between the space thermal loads (sensible and latent) contained in the air, and the mechanical systems which are expected to remove the excess energy from the space air to maintain comfort conditions. In consequence, improvements in their design are essential for development of energy efficient building indoor environmental control systems.

In this thesis, an analysis of the performance of direct expansion (DX) refrigerant air cooling and dehumidifying coils (for human comfort applications), and a method for their selection to minimize the air-side and the refrigerant-side pressure drop are presented.

Air cooling and dehumidification may be achieved either by chilled water coils (sensible heat transfer occuring on the coolant side), or by direct expansion refrigerant coils (DX-Coils), where the heat (sensible and latent) from the air is absorbed by the boiling refrigerant inside the tubes. In order to develop energy effective design and selection methods for air cooling and dehumidifying coils, correlations for prediction of the heat, mass and and momentum transfer factors for the

working fluids (air and refrigerant) are required. Extensive experimental studies have been conducted on the performance of chilled water coils (see Bibliography, items 1 to 40), and methods for their performance simulation have been established [3]. However, such studies on DX-Coils are very limited in the present published literature.

The existing correlations for prediction of the refrigerant side heat transfer and pressure drop factors, based on earlier experimental studies (Items 41 to 49 - Bibliography) on boiling refrigerants (oil free) in plain straight tubes, are not suitable for application to DX-Coils without correctional terms to account for the effects of the coil geometry and the actual flow conditions (with the presence of oil) occuring [4]. Hence, experimental studies are required to establish correlations for the refrigerant side heat transfer and pressure drop factors for DX-Coils.

Due to lack of methods for prediction of the performance of DX-Coils in the published literature, the existing methods for building energy requirement estimation (such as Ref. [5] and [6]), utilize manufacturer's catalogue data. This catalog data generally includes extrapolated and interpolated values, based on limited experimental data developed from certification tests [Performed by the Air conditioning and Refrigeration Institute (A.R.I.)]. The extrapolation and interpolation techniques used in the development of the catalogue data for cooling and dehumidifying coils, may result in over estimation (up

to + 20%) of the energy requirement (due to the coils) depending on the heat exchanger configuration and the operating conditions [7]. Hence, better methods for prediction of the performance of DX-Coils are required.

The sales (in North America) of unitary systems (cooling capacity in the range 18 to 36 kW), where mostly DX-Coils are used, have the highest annual growth rate (13.1%) for 1982, compared to the other packaged systems [8]. This high sales growth rate, coupled with the lack of published methods for energy effective design and selection of DX-Coils and lack of methods for prediction of the energy requirement due to the coils, are the main reasons for undertaking the present study.

The objectives of the present study are as follows:

1) To develop correlations for heat transfer and pressure drop factors for plate finned-tube, direct expansion, air cooling and dehumidifying coils, for comfort air conditioning applications.

2) To develop a method for selection of DX-Coils, to minimize energy consumption due to the coil in air conditioning systems.

A literature survey of the relevant studies is summarized in Chapter-2. A description of the test facility and the measurement systems used in the experimental study, is presented in Chapter-3. The experimental procedure and the test data reduction method, are presented in Chapter-4. An analysis of the experimental data and comparison with the relevant existing data, are summarized in Chapter-5. The correla-

tions for the heat transfer and pressure drop factors developed from the experimental data, and a comparison with the existing correlations, are presented in Chapter-6. The DX-Coil selection method developed is presented in Chapter-7. Finally, a summary of the conclusions from this study is presented in Chapter-8.

CHAPTER 2

LITERATURE SURVEY

CHAPTER 2

LITERATURE SURVEY

In this chapter, a brief description of the construction and operation of the direct expansion coils (DX-Coils) is presented. A review of the existing literature on the heat transfer and pressure drop phenomena in DX-Coils is then presented.

1. CONSTRUCTION OF DX-COILS:

DX-Coils used in comfort air conditioning applications may be described as air-to-refrigerant, compact, finned-tube, multiple-row heat exchangers. Multiple rows of finned tubes are used to provide the additional surface area required to increase the heat transfer rate per unit volume of the heat exchanger.

A pictorial view of a typical DX-Coil and its components are shown in Fig. 2.1. Typical variations of the configuration of the DX-Coil are shown in Table 2.1. Critical dimensions for smooth plate finned-tube coils are defined in Fig. 2.2.

To achieve close contact between the plate-fins and the tubes, hydraulic (or mechanical) pressure is applied through the tubes, prior to the installation of the tube-bends.

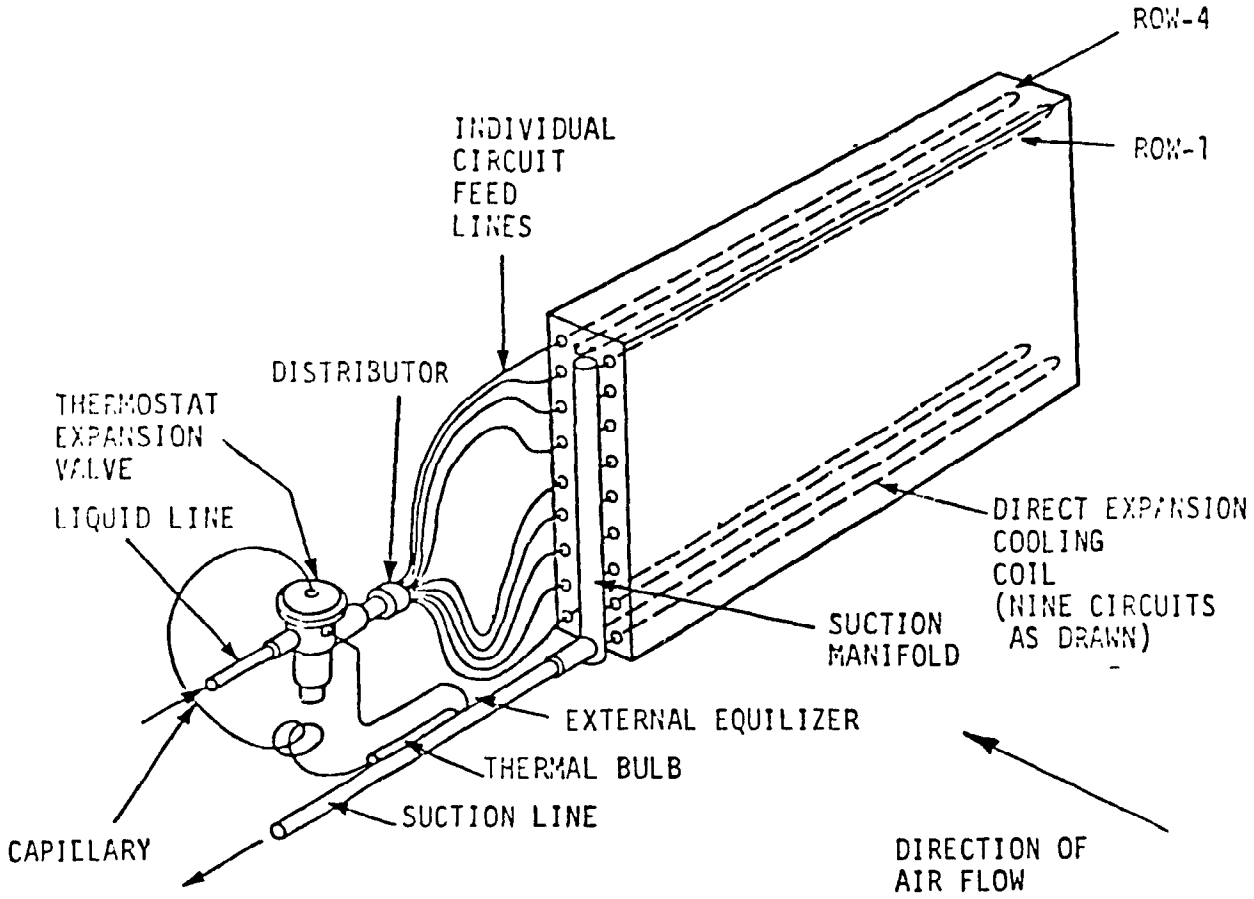

FIG. 2.1 PICTORIAL VIEW OF A TYPICAL 4-ROW DIRECT EXPANSION COIL

[FROM TRANE AIR CONDITIONING MANUAL - PUBLISHED BY, TRANE CO., 1972]

TABLE 2.1 Typical Configurations for Air Cooling and Dehumidifying Coils (for air conditioning applications) [32].

Fin materials:	copper or aluminum
Fin spacing:	1 to 8 fins/cm
Fin thickness (Y_f):	0.1 - 0.3 mm
collar length (L_c):	0.1 to 0.2 mm
Tube material:	copper
Tube Diameter (D_o):	0.8 to 2.5 cm
Tube transverse spacing (S_T):	2 to 6 cm
Tube longitudinal spacing (S_L):	2 to 6 cm
No. of tube rows (N_R):	3 to 8

FIN TYPE:

Continuous flat plate fins

Continuous configurated plate fins

Crimpled spiral fins

Smooth spiral fins

Individually fitted flat plate fins (with or without collar)

Individually fitted configurated plate fins (with or without collar)

Circular fins

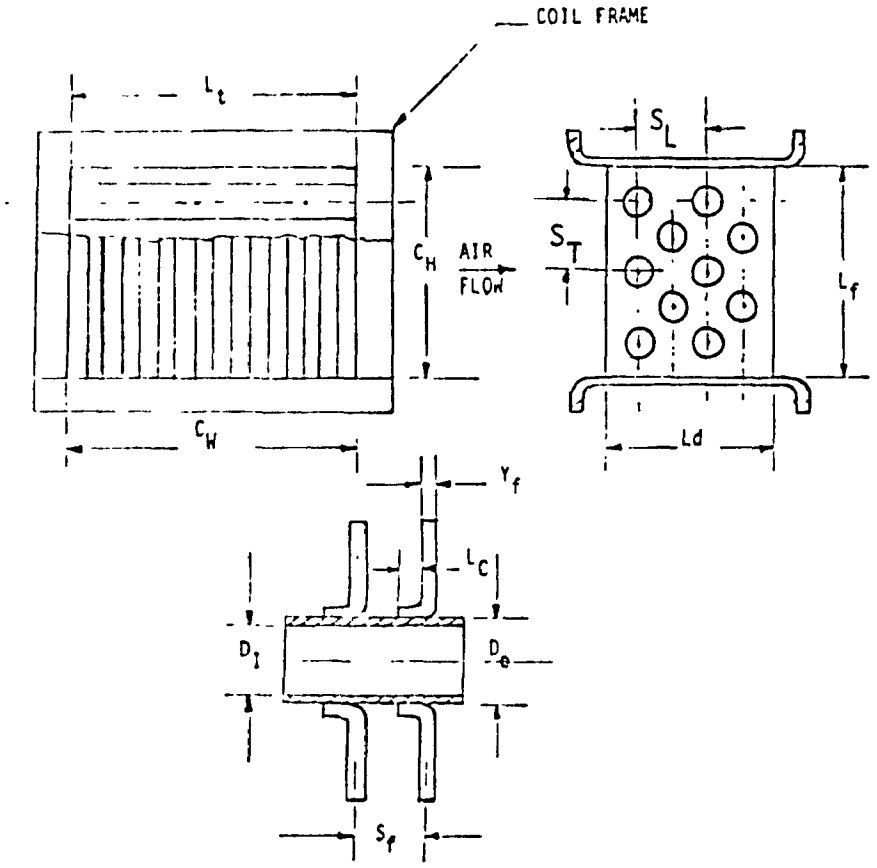

N_R - NO. OF ROWS

N_f - NO. OF FINS

N_T - NO. OF TUBES

N_{TR} - NO. OF TUBES PER ROW

$L_T = C_W$

FIG. 2.2 GEOMETRICAL PARAMETERS FOR DX-COILS

2. OPERATION OF DX-COILS

DX-Coils are used, either for sensible cooling, or for cooling and dehumidifying of moist air. A schematic plan view of a typical DX-Coil is shown in Fig. 2.3.

Air from the conditioned spaces in the building (sometimes mixed with some outdoor air), at the temperature (dry and wet bulb) and flow conditions dictated by the building thermal load, is circulated through the coil by a ventilation fan.

As shown in Fig. 2.1, the liquid refrigerant enters the coil through a thermostatic expansion valve, where the refigerant pressure is reduced to the operating pressure of the coil (see Fig. 2.6). The refrigerant leaving the expansion valve is usually at a low vapour quality (5 to 15%).

The refrigerant distributor (see Fig. 2.1) provides equal quantity of refrigerant to the tube circuits (in order to equalize the circuit load). The refrigerant evaporates in the tube circuits absorbing the heat from the circulating air, and leaves the coils in the vapourphase through the suction manifold to the suction line.

The expansion valve controls the rate of flow of refrigerant through the coil by a thermal-bulb located in the suction line, which senses the temperature of the refrigerant vapour leaving the coil. The expansion valve also maintains a minimum superheat (3 to 6°C) for the

refrigerant vapor leaving the DX-Coil (in order to prevent liquid refrigerant entering the compressor).

Typical flow arrangement of the working fluids (air and the refrigerant), and their temperature variations along the developed length of the finned-tubes of the coil, are shown in Fig. 2.3 and 2.4 respectively. The psychrometric representation of a typical cooling and dehumidifying process, (for a 5-row finned-tube DX-Coil) is shown in Fig. 2.5. In general, sensible heat transfer occurs mostly in the up stream rows (rows 1 and 2), and latent heat transfer is predominent in the down stream rows (rows 3 to 5) [9]. The heat, mass, and momentum transfer coefficients for the working fluids (air and the refrigerant) depend on the coil geometry and the fluid flow conditions existing in the flow channels, and are discussed in detail in the following sections. The pressure enthaply variations in a typical vapor compression refrigeration cycle (for DX-Coils) are shown in Fig. 2.6.

3. ENERGY REQUIREMENTS DUE TO DX-COILS:

DX-Coils contribute to the energy consumption of the air conditioning systems due to resistance to the air flow caused by the finned-tubes, and the two-phase refrigerant pressure drop in the tube circuits. In typical commercial building air conditioning systems, the power consumption due to the resistance to the air flow in DX-Coils, may be as high as 30% of the total fan energy consumption, depending on the coil configuration, the air flow Reynolds number, and the period of

operation [8]. The energy consumption due to the refrigerant pressure drop may account for up to 20% of that for the compressor, depending on the existing operating conditions [8]. Consequently, in order to develop energy effective selection methods for DX-Coils, techniques for prediction of the heat transfer rate and the pressure drop of the working fluids in these heat exchangers are required. A discussion of the existing literature on this subject, is presented in the following sections.

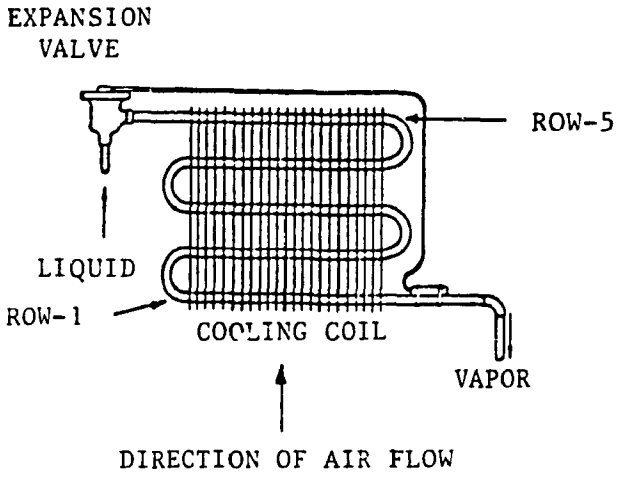

FIG. 2.3 SCHEMATIC PLAN VIEW OF A TYPICAL DX-COIL (5-ROWS)

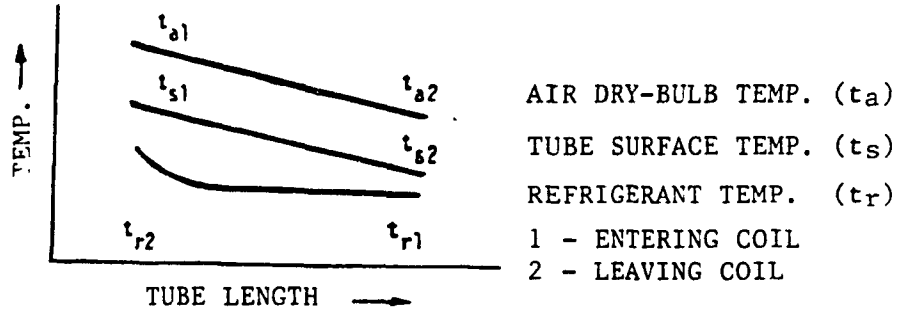

FIG. 2.4 TYPICAL FLUID AND SURFACE TEMPERATURE VARIATION ALONG TUBE

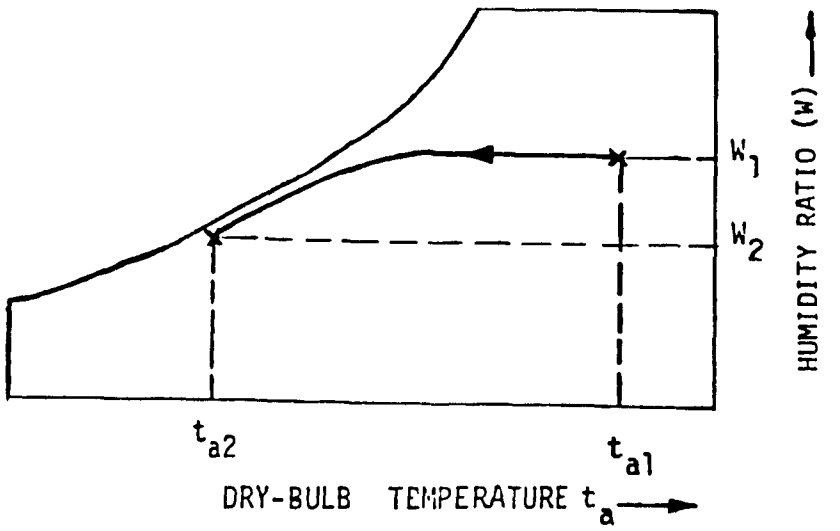

FIG. 2.5 TYPICAL PSYCHROMETRIC REPRESENTATION OF A COOLING AND DEHUMIDIFYING PROCESS

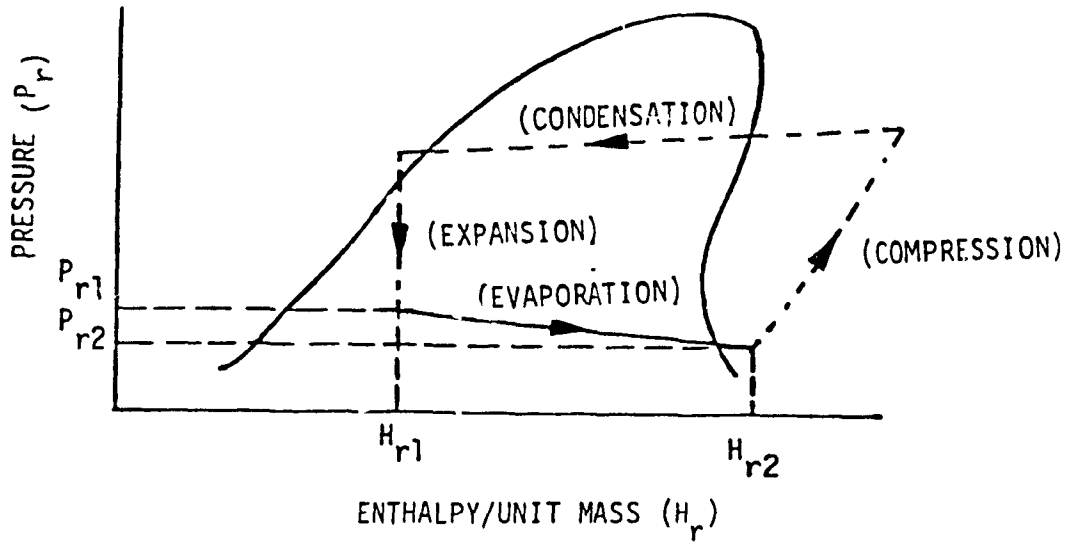

FIG. 2.6 PRESSURE - ENTHALPY VARIATIONS IN A TYPICAL VAPOR COMPRESSION REFRIGERATION SYSTEM.

4. HEAT TRANSFER AND PRESSURE DROP PROCESSES IN DX-COILS:

In this section, a review of the relevant existing studies on the heat transfer and pressure drop processes, for the air and the coolant sides of air cooling and dehumidifying coils, is presented.

Experimental studies on the performace of DX-Coils are almost non-existant in the present published literature. The heat, mass and momentum transfer processes for the air-side of DX-Coils may be expected to be similar to those for the chilled water coils, due to similarities in the heat exchanger geometries and the fluid flow conditions; however, considerable differences in these processes exist for the coolant-side, due to the two-phase flow conditions occuring in the refrigerant-side for DX-Coils.

The existing literature on the air-side performance of the cooling and dehumidifying coils is extensive, and at least two state-of-the-art surveys [10,11] on this subject have been published. The existing literature on the refrigerant-side heat transfer and pressure drop factors is limited to experimental and analytical studies on boiling refrigerants in plain (unfinned) straight tubes, which are not applicable to DX-Coils without modifications to account for the heat exchanger geometry [4].

This literature survey covers the following topics:

1) A brief review of the existing literature on the air-side heat

transfer and pressure drop processes in cooling and dehumidifying coils.

ii) A detailed discussion of the recent experimental studies [7,13, and 14] on the air-side performance of smooth plate finned-tube compact air cooling and dehumidifying heat exchangers (chilled water coils) for comfort air conditioning applications, which are related to the present study.

iii) A brief review of the existing methods [12] for the heat transfer and pressure drop factor prediction for boiling refrigerants (inside tubes).

iv) A detailed discussion of the existing experimental studies [15,16 and 17] on the boiling refrigerants inside tubes and tube-bends, which form the basis for the current methods for design of the refrigerant-side of DX-Coils.

4.1 Review of the Existing Air-Side Studies:

The existing studies on the air-side performance of chilled water heat exchangers are listed in the Bibliography (items 1 to 42). In the following section, a brief review is made of the studies on the air-side heat transfer and pressure drop coefficients, for finned-tube compact heat exchangers, for dry and wet contact surface conditions.

A. AIR-SIDE DRY SURFACE CONDITIONS:

The air flow patterns within the plate finned-tube surface, for the air-side dry surface conditions for typical air flow velocity range (1 to 4 m/s) occuring in the comfort air conditioning applications, may be described as "superimposition of the turbulence generated by the tubes, upon the laminar boundary layer on the fin surface" [18]. At low air flow velocities (< 1 m/s), a pair of standing vorticies are formed behind each tube. As the air flow velocity is increased, the standing vorticies break away from the tubes, and move towards the back of the coil (in the direction of the air flow), in an assymmetrical pattern. The velocity at which the break away occurs, depends on the finned-tube configuration. For typical coil configurations, where the tube diameter (D_o) is much higher (5 to 20 times) than the fin spacing, stable vorticies exist during the entire velocity range (1 to 4 m/s). During the dry surface conditions, sensible heat is transfered by convection, from the air, through the finned-tube surface, to the refrigerant. The heat transfer rate is dependent on the temperature differential between the fluid and the contact surface, and the convective heat transfer coefficient. The available information for the dry surface heat transfer is usually in the form of graphs or equations, representing the relationship between the average heat transfer factor ($j_{a,D}$) and the air flow Reynolds number (Re_a). The $j_{a,D}$ is expressed as follows:

$$j_{a,D} = St. (Pr)^{2/3} \qquad (2.1)$$

where

St - Stanton Number, evaluated at the Reynolds number (Re_a) with mass flux based on the minimum flow area ($G_{m,f}$)

Pr - Air Prandtl number

The Reynolds number (Re_a) is usually based on the coil hydraulic diammeter (D_h), as follows [19]:

$$Re_a = G_{m,f} D_h/\mu_a \qquad (2.2)$$

where:

$$D_h = 4 A_{m,f} L_d/A_o \qquad (2.3)$$

and

μ_a - air dynamic viscosity

$G_{m,f}$ - Air mass flux based on the minimum flow area

$A_{m,f}$ - Minimum flow area

A_o - Total finned-tube surface area

L_d - Depth of the plate fin, in the direction of air flow

Various other definitions for the Reynolds number are also used in the existing studies, and are discussed later in the appropriate sections.

From Eqn. 2.1, for comfort air conditioning applications (for given finned-tube geometry), since the changes in the Nusselt number (Nu) and Prandtl number (Pr) are small in comparison with those for the Reynolds number (Re_a), the average dry surface heat transfer factor ($J_{a,D}$) gener-

rally decreases when the air flow Reynolds number is increased [18].

The dry surface average pressure drop factor ($f_{a,D}$) for forced convection cross flow of air over finned-tube bundle may be expressed as follows [18]:

$$f_{a,D} = \Delta p_a[2\ (D_h/4L_d)/(G^2_{m,f}\ v_m)] - [(v_2-v_1)/v_m](1+\sigma^2)\ (D_h/4L_d) \quad (2.4)$$

where

$\Delta p_{a,d}$ - air pressure drop, for dry surface conditions

$G_{m,f}$, L_d and D_h - defined at Eqns. 2.2 and 2.3

v_m - air specific volume, at the mean conditions in the finned-tube section (air D.B and W.B temps.)

σ - ratio of the minimum flow area ($A_{m,f}$) to coil face area (A_F)

v_1 and v_2 - air specific volume at the entering and leaving conditions of the coil, respectively.

In the range of comfort air conditioning applications ($300 < Re_a < 1500$) the dry surface pressure drop factor ($f_{a,D}$) decreases when the air mass flux ($G_{m,f}$) is increased (for a given finned-tube configuration) [18].

B. AIR SIDE WET SURFACE CONDITIONS:

During air side wet surface conditions simultaneous sensible and latent heat transfer as well as moisture (mass) transfer occur. The transfer of the sensible heat is similar to that for the dry surface conditions. The latent portion of the heat transfer is dependent on the partial vapour pressure difference between the fluid and the tube surface temperature, and the mass transfer coefficient (h_d) [20].

When condensation occurs on the heat transfer surface, both temperature and humidity potentials exist. The dry-bulb temperature differential between the air and the contact surface is the potential for the sensible heat transfer. The difference between the surrounding air specific humidity and the specific humidity of saturated air at the wet surface temperature is the potential for the latent heat transfer. enthalpy potential method [21], combining the temperature and humidity potential, is generally used to determine the wet surface performance.

The thickness of the condensate film is usually of the same order of magnitude as the fin thickness (0.1 and 0.3 mm) [7]. The condensate film will result in a reduction in the minimum flow area ($A_{m,f}$) and the coil hydraulic diameter (D_h), while the minimum mass flux ($G_{m,f}$) increases (compared to the corresponding dry surface condition, for a given air flow velocity). It is difficult to measure the water film thickness; however, a uniform film thickness of 0.1mm may be assumed for typical smooth plate finned-tube compact heat exchangers, for the comfort air conditioning applications (7). In general, for a given air

flow Reynolds Number (Re_a) the average wet surface heat transfer factor ($j_{a,w}$) is higher than that for the corresponding dry surface condition ($J_{a,D}$) due to combined latent and sensible heat transfer. The wet surface heat transfer factor is generally expressed as a function of the corresponding $j_{a,D}$, when both dry and wet surface conditions exist simultaneously.

For the air-side wet surface conditions, both film and drop-wise conditions may exist simultaneously particularly at the part load conditions [7].

The wet surface average pressure drop factor ($f_{a,w}$) may be expressed by an equation similar to that for the corresponding dry surface case (Eqn. 2.4). For the wet surface conditions, the air pressure drop ($\Delta P_{a,w}$) is generally higher than that for the corresponding dry surface case due to the condensate film. Consequently, $f_{a,w}$ is generally higher than the corresponding $f_{a,D}$.

C. EFFECTS OF FIN SPACING AND TUBE ROWS ON THE AIR SIDE HEAT TRANSFER AND PRESSURE DROP COEFFICIENTS:

The effects of fin spacing and tube rows on the air-side dry surface heat transfer and pressure drop coefficients (for air heating coils) reported by Rich [18, 22] are summarized in this section.

Effects of the Fin Spacing:

The effects of fin spacing (S_L and S_T) on the air-side dry surface heat transfer and pressure factors (for a given number of tube rows, tube diameter and tube arrangement) were investigated by Rich [18]. Based on his experimental data [18], Rich concluded that the effect of the fin spacing may be correlated by using the Reynolds number ($Re_{a,L} = G_{m,f} S_L/\mu_a$, based on the longitudinal spacing (S_L). He proposed that the alternating growth and decay of the laminar boundary layer on the fin surface (as the air passes through each tube row) can be better represented by use of Reynolds number based on the tube longitudinal spacing ($Re_{a,L}$) than that based on the conventional coil hydraulic diameter (Eqn. 2.2). Based on his test results, he also concluded that for a given $G_{m,f}$, the dry surface heat transfer factor ($J_{a,D}$) is independent of the fin density (for $1 < P_s < 8$ fins/cm), and the corresponding pressure drop factor ($f_{a,D}$) is independent of the fin density for ($p_s < 5$ fins/cm). However, he reported that these conclusions should be validated for coil configurations other than those considered in his study [18]. The results from this study are shown in Fig. 2.7.

B. **Effect of the Tube Rows:**

Rich [22] also investigated the effects of the number of tube rows (for given fin spacing, tube diameter, S_L and S_T) on the dry surface heat transfer factor. He concluded that the average dry surface heat transfer factor ($j_{a,D}$) for deep row coils ($N_R > 6$), may be higher or lower than that for the shallow coils ($N_R < 6$), depending on the air flow Reynolds number ($Re_{a,l}$). He also concluded that the row effect is greatest at low Reynolds number ($Re_{a,l} < 5000$), and becomes neglible at high Reynolds number ($Re_{a,l} > 15000$). This implies that in the normal operating range ($10000 < Re_{a,l} < 20000$) for comfort air conditioning applications, the row effect on the dry surface heat transfer factor ($j_{a,D}$) is negligible. This conclusion is in agreement with similar study conducted by Iuve [23]. Rich did not propose a correlation for the row effect on $j_{a,D}$, and his test results are shown in Fig. 2.8.

A detailed discussion of the effects of coil geometrical parameters and the fluid flow parameters on the air side dry and wet surface heat transfer and pressure drop factors, is presented in the following section.

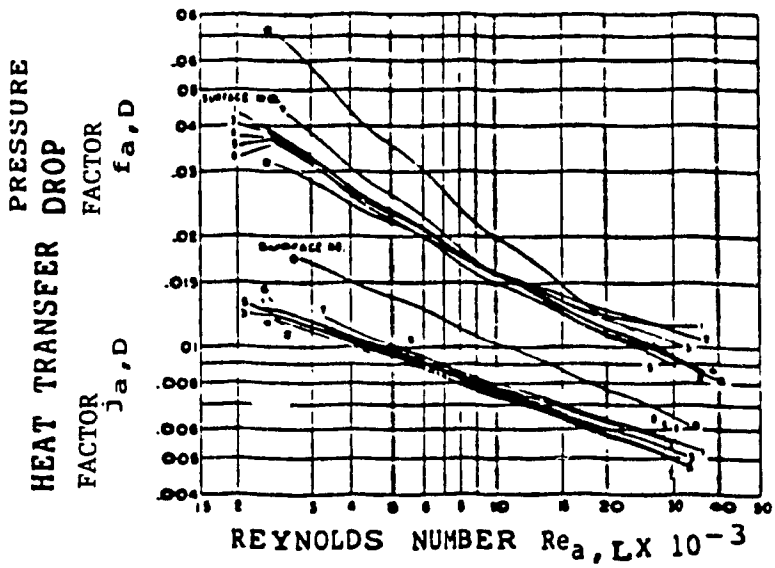

FIG. 2.7 **FIN EFFECTS ON HEAT TRANSFER AND PRESSURE DROP** FACTORS (18)
(AIR-SIDE DRY SURFACE)

COIL GEOMETRIC PARAMETERS [18 AND 22]

FIXED PARAMETERS

S_T = 3.2 cm

S_L = 2.8cm

D_o = 1.3cm

Y_f = 0.15cm

FIG 2.7 SURFACE No.	FINS/cm	FIG 2.8 COIL No.	TUBE ROWS
0	0	1	1
1	1.2	2	2
2	1.7	3	3
3	2.6	4	4
4	3.0	5	5
5	3.6	6	6
6	4.6		
7	5.7		
8	8.1		

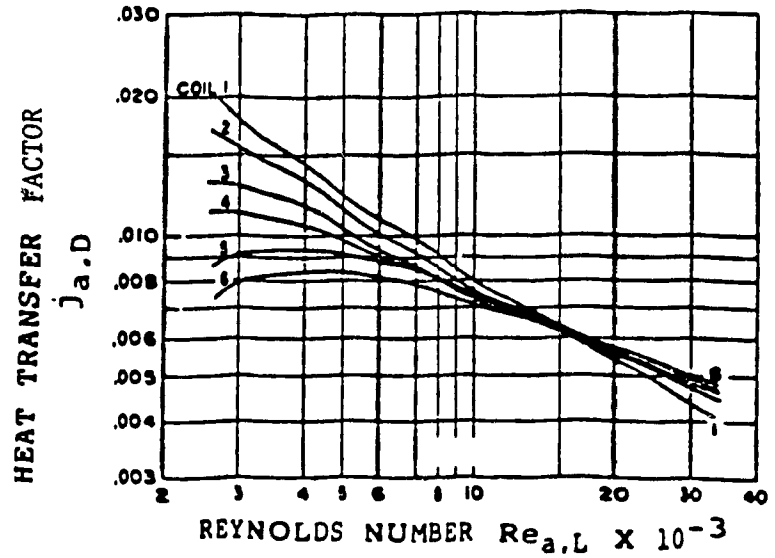

FIG. 2.8 ROW EFFECTS ON THE HEAT TRANSFER FACTOR (22)
(AIR-SIDE DRY SURFACE)

4.2 DISCUSSION OF THE RECENT STUDIES ON THE AIR-SIDE PERFORMANCE:

In this section a discussion of the recent studies [7, 13, 14] on the air-side performance is presented. The experimental data and the correlations for the heat transfer and pressure drop coefficients developed from these studies are compared with the experimental data from the present study (see Chapter-5).

Elmahdy [7] investigated the air-side heat transfer coefficient in multi-row plate finned-tube compact heat exchangers, during cooling and dehumidifying process. His experimental studies were conducted on a 8-row, 4.7 fins/cm (flat plate fins) chilled water coil. The specifications of the tested heat exchanger are presented in Appendix-1. Elmahdy proposed that the air-side dry surface heat transfer factor ($j_{a,D}$) may be expressd in a generalized form as follows:

$$j_{a,D} = C_1 \, Re_a^{C_2} \qquad (2.5)$$

were:

C_1 and C_2 - constants for a given coil, determined from experimental data.

Re_a - Defined at Eqn. 2.2

He proposed that the coefficients C_1 or C_2 are dependent on the following non-dimensional coil geometric parameters, based on the earlier studies:

1) Fin spacing (s_f) / equivalent fin height (F_h)

2) Fin tip equivalent diameter (F_d) / tube transverse spacing (S_T)

3) Fin thickness (Y_f) / coil hydraulic diameter (D_h)

4) Fin tip equivalent diameter (F_d) / tube logitudial spacing (S_L)

5) Fin thickness (Y_f) / fin spacing (S_f)

6) Tube diameter (D_o) / fin tip equivalent diameter (F_d)

7) Fin thickness (Y_f) / fin equivalent height (F_h)

8) Coil minimum flow area ($A_{m,f}$) / coil face area A_F

The methods used for the calculation of F_h and F_d for continuous fins were presented in Ref. [7].

Elmhady proposed the following formulation for C_1 (or C_2)

$$C = a_o (A_{m,f}/A_F)^{a_1} (S_f/F_h)^{a_2} (F_d/S_T)^{a_3} (Y_f/D_h)^{a_4} (F_d/S_L)^{a_5} \times (Y_f/S_f)^{a_6} (D_o/F_d)^{a_7} (Y_f/F_h)^{a_8} \quad (2.6)$$

By regression analysis of the experimental data and the non-dimensional coil geometric groups for 20 configurations from References [18], [19] and [25], Elmahdy proposed the following correlations for C_1 and C_2:

$$C_1 = 0.159 (Y_f/D_h)^{-0.065} (Y_f/F_h)^{0.141} \quad (2.7)$$

$$C_2 = 0.323 (S_f/F_h)^{0.049} (F_d/S_L)^{0.549} (Y_f/S_f)^{-0.028} \quad (2.8)$$

Eqns. 2.7 and 2.8 are limited to the range of the non-dimensional groups shown in Table 2.2.

Table 2.2 RANGE OF DIMENSIONLESS GROUPS CONSIDERED IN REF. [7].

	Y_f/D_h	Y_f/F_h	Y_f/S_f	S_f/F_h	F_d/S_L
MIN.	0.03	0.01	0.04	0.15	0.87
MAX.	0.33	0.45	0.50	0.91	1.27

From his experimental data [7], Elmahdy proposed the following correlation for the air-side dry surface heat transfer factor ($j_{a,D}$) [for the coil tested]:

$$j_{a,D} = 0.101 \quad Re_a^{-0.369} \qquad (2.8A)$$

that is for his test coil, $C_1 = 0.101$ and $C_2 = -0.369$

He reported about 5% deviation for the computed data. His test results, shown in Fig. 2.9, indicate that $j_{a,D}$ is a decreasing function of Re_a, and is dependent on the coil geometry. The relative effects of the coil geometric groups on $j_{a,D}$ were not presented in Ref. [7]. The latter studies [13] indicate that the tube diameter (D_o) and the transverse spacing (S_T) have a significant effect on the $j_{a,D}$ (for a given given air flow Reynolds number).

For the air-side wet surface conditions, Elmahdy assumed a uniform condensate film thickness (0.1mm), and from the enthalpy potential

difference method [20], he computed the average heat transfer factor ($J_{a,w}$). Due to lack of published experimental data for the $j_{a,w}$ (at the time of his study), he proposed a correlation for the $j_{a,w}$ based on his his own data as follows [7]:

$$J_{a,w} = j_{a,D} \, (C_J) \tag{2.9}$$

where

$$(C_J) = 1.425 - 0.51 \, (Re_a/1000) + 0.263 \, (Re_a/1000)^2 \tag{2.10}$$

Re_a - Defined at Eqn. 2.2

$J_{a,D}$ - Defined at Eqn. 2.8

For the coil considered in his study (configuration parameters defined in Appendix-1) he reported the following correlation:

$$J_{a,w} = 0.22 \quad Re_a^{-0.46} \tag{2.10 A}$$

The experimental data from his wet surface tests are shown in Fig. 2.10. Eqn. 2.9 implies that, for a given Reynolds Number (Re_a), the $J_{a,w}$ is dependent on the corresponding $J_{a,D}$. However, the later studies [13] indicate that the condensate mass transfer factor and the fin spacing may also have an effect on the $J_{a,w}$. Hence, Eqn. 2.9 has to be validated by comparison with other experimental data. A comparison of the dry and wet surface heat transfer coefficients reported by Elmahdy [7] are shown in Fig. 2.11 which indicates that the $J_{a,w}$ is higher than the $J_{a,D}$ (for a given Re_a), and the difference between the two ($J_{a,w} - J_{a,D}$) decreases when the Re_a is increased.

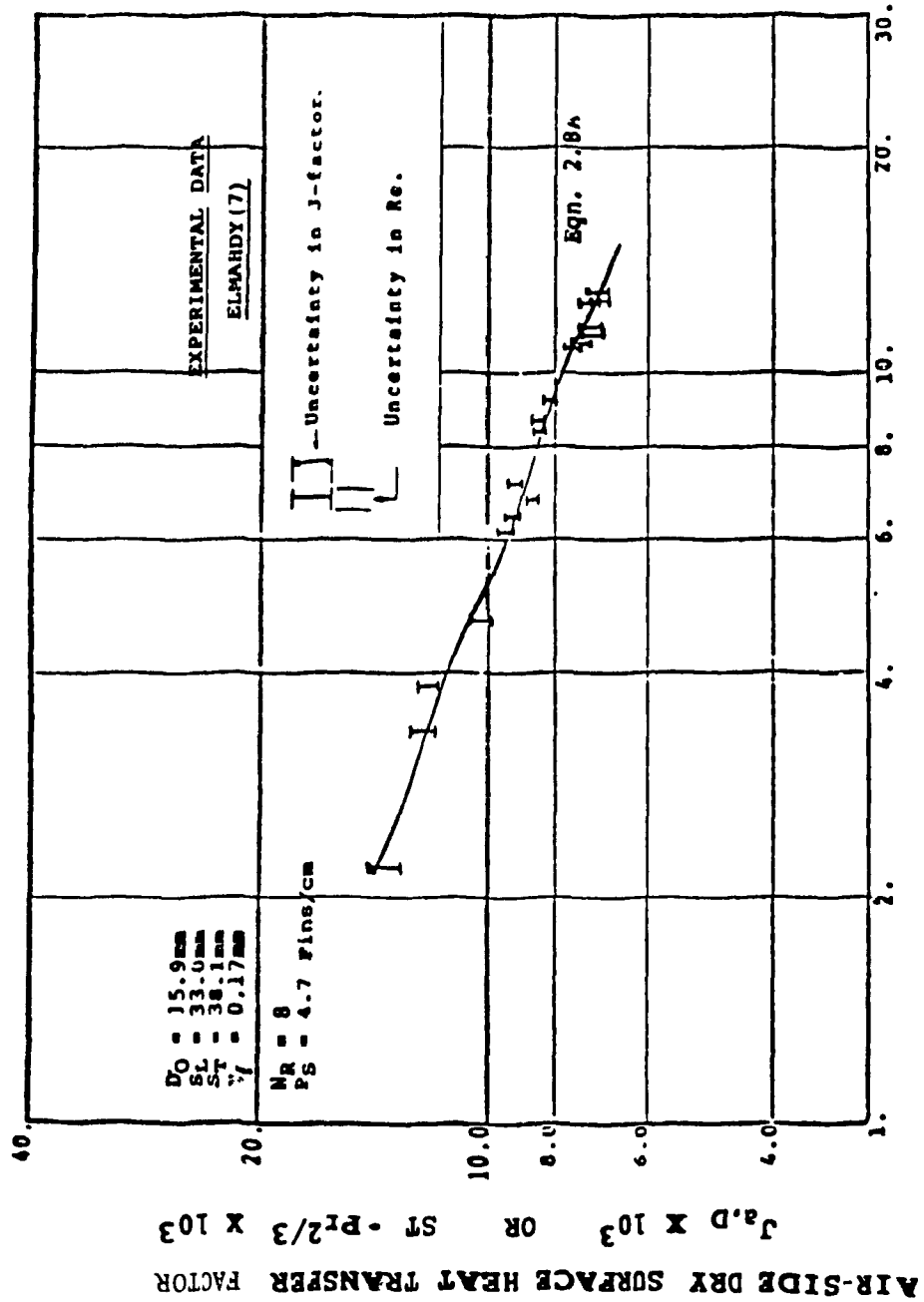

FIG. 2.9. CORRELATION FOR THE AIR-SIDE DRY SURFACE HEAT TRANSFER FACTOR, ELMAHDY (7)

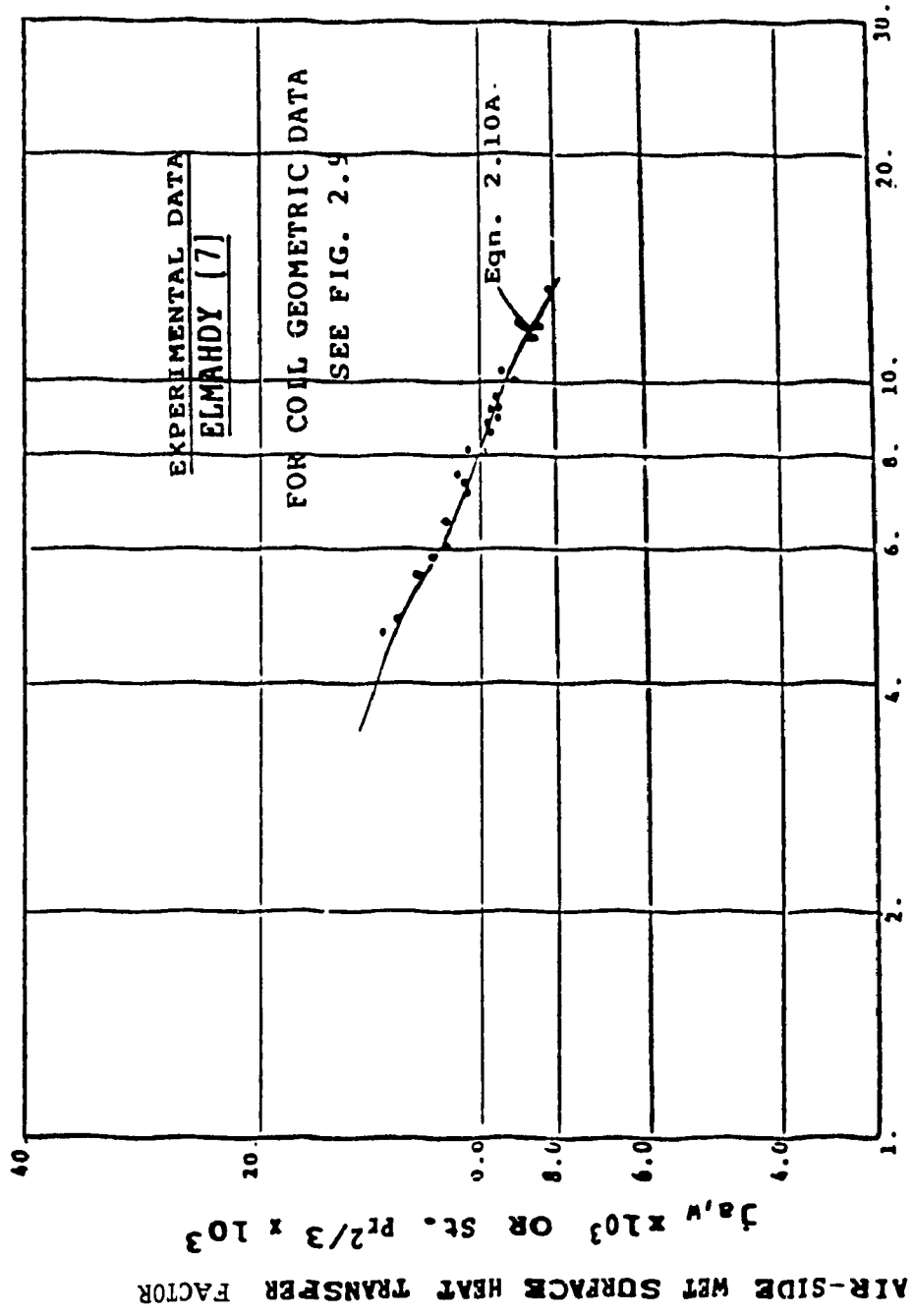

FIG. 2.10 CORRELATION FOR THE AIR-SIDE WET SURFACE HEAT TRANSFER FACTOR, ELMAHDY (7)

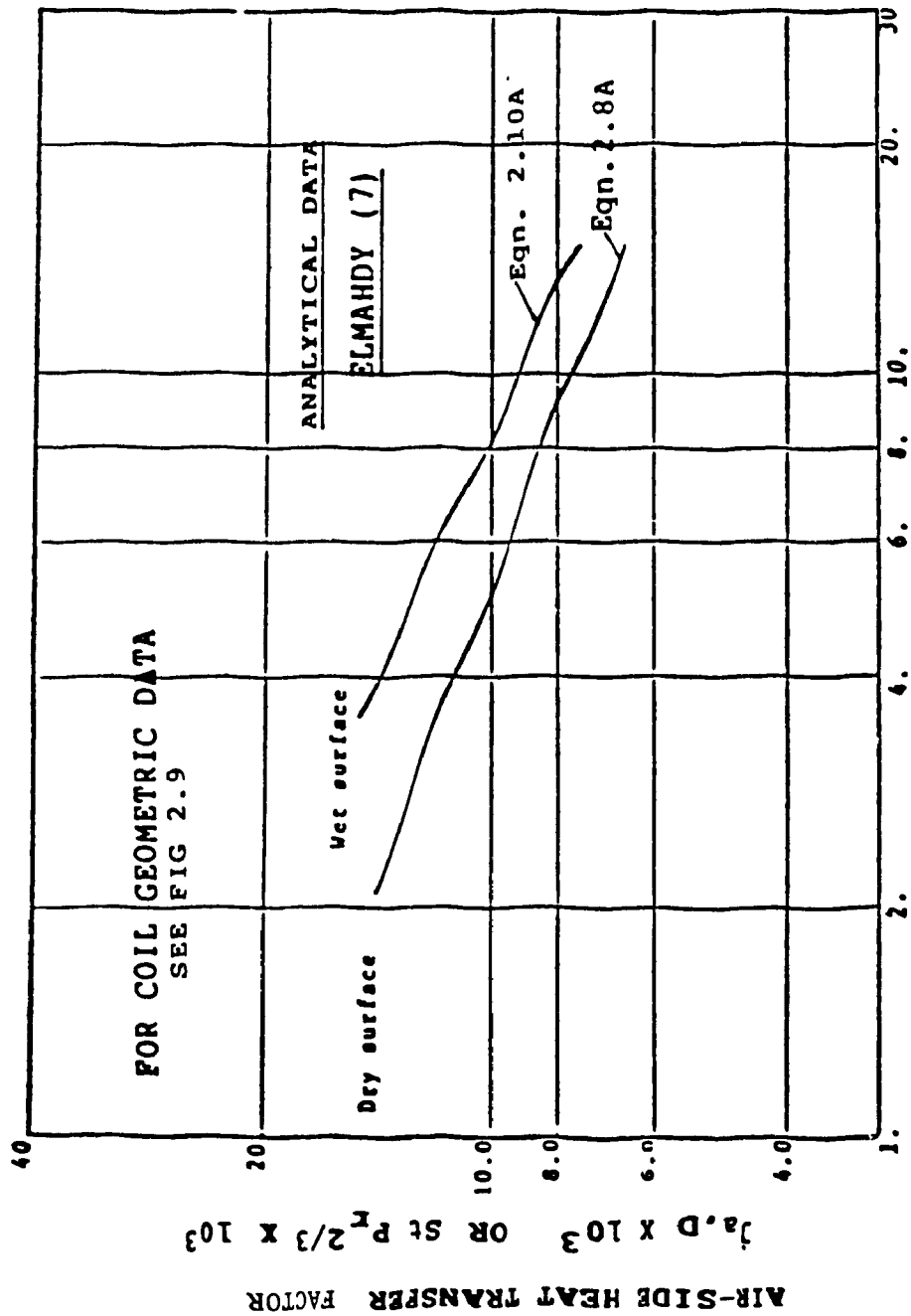

FIG.2.11. COMPARISON OF THE AIR-SIDE WET AND DRY SURFACE

HEAT TRANSFER FACTOR CORRELATIONS, ELMAHDY (7)

McQuiston [13] conducted experimental studies on five (5) smooth plate finned-tube heat exchangers with varied fin spacing (1.0 to 5.5 fins/cm) to investigate the heat, mass and momentum transfer. Based on the existing studies [18, 19, 20, 22, 24, and 26] conducted, McQuiston [14] proposed that the predominant parameters in the air-side dry surface heat transfer prediction are as follows:

A) The air flow Reynolds number ($Re_{a,D}$) based on the tube diameter, expressed as:

$$Re_{a,D} = G_{m,f} \; D_o/\mu_a \qquad (2.11)$$

$G_{m,f}$ and a - defined at Eqn. 2.2

D_o = tube diameter

B) The ratio of the total surface area (A_o) to the tube (primary) surface area (A_p), expressed as follows:

$$A_o/A_p = 4 \; S_L \; S_T \; A_{m,f} \; / \; D_h \; D_o \; A_F \qquad (2.12)$$

where

$A_{m,f}$, A_o, and D_n - defined at Eqn. 2.3

A_F - Coil face area

S_L - Tube longitudinal spacing

S_T - Tube transverse spacing

He noted that the Eqn. 2.12 contains "all the significant coil geometric parameters that have an influence on the dry surface heat

transfer factor, excepting the number of tube rows (N_R)". Based on the experimental data from Ref. [22], he proposed a correlation for the row effects, as follows:

$$J_{a,D,N} / J_{a,D,1} = 1 - 1280\ (N_R)\ (Re_{a,L})^{-1.2} \qquad (2.13)$$

valid in the range $3000 < Re_{a,L} < 15000$, for the coil configurations tested in Ref. [20].

where

$$Re_{a,L} = G_{m,f}\ S_L / \mu_a \qquad (2.14)$$

and

S_L - tube logitudinal spacing

$J_{a,D,N}$ and $J_{a,D,1}$ - dry surface heat tranfer factor for 1 row and N-rows, respectively.

However, as stated earlier, in the normal range for air conditioning applications ($10000 < Re_{a,L} < 20000$), the row effect on the dry surface heat ransfer factor is negligible (< 8%). McQuiston [14] proposed a correlation for the dry surface heat average transfer factor ($J_{a,D}$), as follows:

$$J_{a,D} = 0.0014 + 0.2628\ (JP) \qquad (2.15)$$

valid in the range $1000 < Re_{a,D} < 4000$

where

$$(JP) = Re_{a,D}^{-0.4}\ \ (Ao/Ap)^{0.15} \qquad (2.16)$$

Ao/Ap - defined at Eqn. 2.12

$Re_{a,D}$ - defined at Eqn. 2.11

He reported that ninety percent (90%) of the experimental data from Refs. [13], [19], and [12] agreed within $\pm$ 10% of the mean value (see Fig. 2.12). McQuiston [14], also proposed that the dry surface pressure drop factor ($f_{a,D}$) is influenced by the following non-dimensional coil geometric groups:

a) $F_1 = D_o/2R' = (Ao/Ap) / (S_T - D_o) P_s + 1$ (2.17)

where

R' - derived coil hydraulic radius,

P_s - Fin pitch

b) $F_2 = (S_T - D_o) P_s / [4 (1 - P_s Y_f)]$ (2.18)

where

Y_f - fin thickness

S_T - tube transverse spacing

c) $F_3 = (S_T/2R') - 1$ (2.18A)

He proposed a correlation for the air-side dry surface factor ($f_{a,D}$) as follows:

$$f_{a,D} = 4.904 \times 10^{-3} + 1.382 (FP)^2 \quad (2.19)$$

valid in the range $1000 < Re_{a,D} < 4000$

where

$$(FP) = (F_1)^{0.25} (F_2)^{-0.4} (F_3)^{-0.5} Re_{a,D}^{-0.25} \qquad (2.20)$$

Explanation of the effects of these derived parameters (F_1, F_2, and F_3) on $f_{a,D}$, was not offered by McQuiston. He reported an error of $\pm$ 35% for Eqn. 2.19 (Based on the results from Ref. [13, 18 and 19]).

He also observed that the tube transverse spacing (S_T) and the tube diameter (D_o) are significant parameters that affect $J_{a,D}$ and that the larger error ($\pm$ 35% from the mean) for Eqn. 2.19 is due to the differences in the surface roughness for the heat exchangers considered in the studies compared. His results for the dry surface pressure drop factor ($f_{a,D}$) are shown in Fig. 2.13.

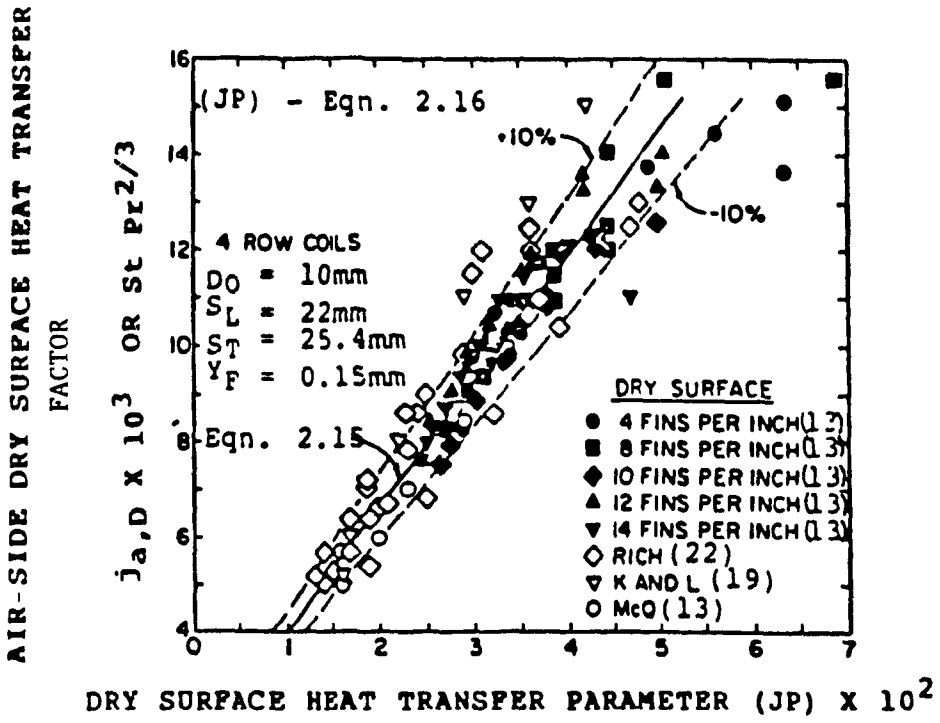

FIG.2.12. CORRELATION FOR THE DRY SURFACE HEAT TRANSFER FACTOR, McQUISTON (14)

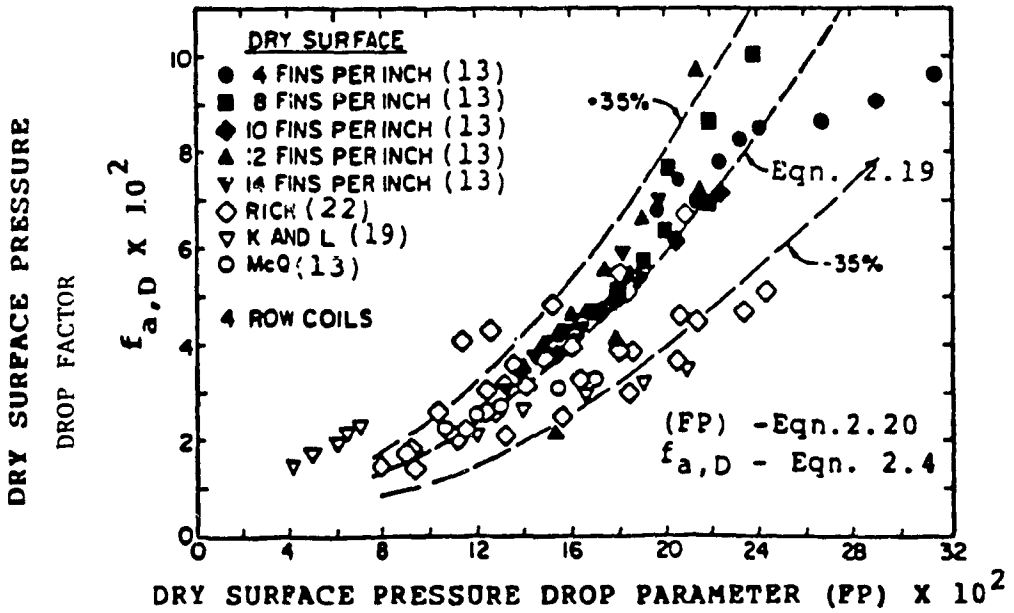

FIG. 2.13. CORRELATION FOR THE DRY SURFACE PRESSURE DROP FACTOR, McQUISTON (14)

For the air-side wet surface conditions, McQuiston [14] proposed that the heat transfer ($J_{a,w}$) and pressure drop ($f_{a,w}$) factors are influenced by the following parameters:

1) Air flow Reynolds number based on the fin spacing ($Re_{a,s}$), defined as follows:

$$Re_{a,s} = G_{m.f} \; S_f/\mu_a$$

where

$G_{m,f}$ and μ_a - defined at Eqn. 2.2

S_f - fin spacing

2) Ratio of the fin spacing to the distance between the fins (F_s), expressed as follows:

$$F_S = S_f / (S_f - Y_f) \qquad (2.22)$$

McQuiston [14], proposed correlations for the wet surface heat transfer and pressure drop factors, (for a given air flow Reynolds number), as follows:

$$J_{a,w} = f\,[(JP), J(S)] \qquad (2.23)$$

$$f_{a,w} = f\,[(FP), F(S)] \qquad (2.24)$$

where

(JP) - Sensible heat transfer parameter, defined at Eqn. 2.15

J(S) - Corresponding latent heat transfer parameter (defined at Eqn. 2.25)

(FP) - Dry surface pressure drop parameter, defined at eqn. 2.19.

F(S) - Corresponding wet surface pressure drop parameter defined at Eqn. 2.26)

McQuistion, determined the parameters J(S) and F(S), for film-wise conditions, from his experimental data, as follows:

$$J(S) = [0.95 + 0.4 \times 10^{-5} \, Re_{a,s}^{1.25}] \, F_s^{2} \qquad (2.25)$$

$$F(S) = [0.6 + Re_{a,s}^{-0.15}] \, F_s^{-3} \qquad (2.26)$$

Finally, McQuistion [14] proposed the following generalized correlation for the heat transfer (j_a) and pressure drop (f_a) factors for both the air-side dry and wet surface conditions:

$$j_a = 0.0014 + 0.2618 \, (JP) \, J(S) \qquad (2.27)$$

$$f_a = 4.094 \times 10^{-3} + 1.382 \, [(FP)F(S)]^{2} \qquad (2.28)$$

where the parameters J(S) and F(S) are equal to one for the dry surface conditions, and are defined by eqns. 2.25 and 2.26 (respectively) for the wet surface conditions. His results are shown in Figs. 2.14 and 2.15. McQuiston reported that the $j_{a,w}$ may be predicted within about $\pm$ 10 percent uncertainty, and the corresponding pressure drop factor ($f_{a,w}$) may be predicted within $\pm$ 35 percent uncertainty; he attributed the higher uncertainty for the predicted

wet surface pressure drop factor to the "extreme interaction between the air and the condensate streams for high fin densities 5 (>5 Fins/cm)"; however, no specific explanation for this phenomenon was offered.

In conclusion, the effects of some of the geometric parameters [such as fin spacing (S_f)] on the heat transfer and pressure drop factors may be more significant for the wet surface conditions,compared to tne corresponding dry surface condition, due to the condensate film. Hence, correlations for prediction of the average heat transfer and pressure drop factors should account for these effects by introduction of the appropriate parameters [such as J(S) and F(S)].

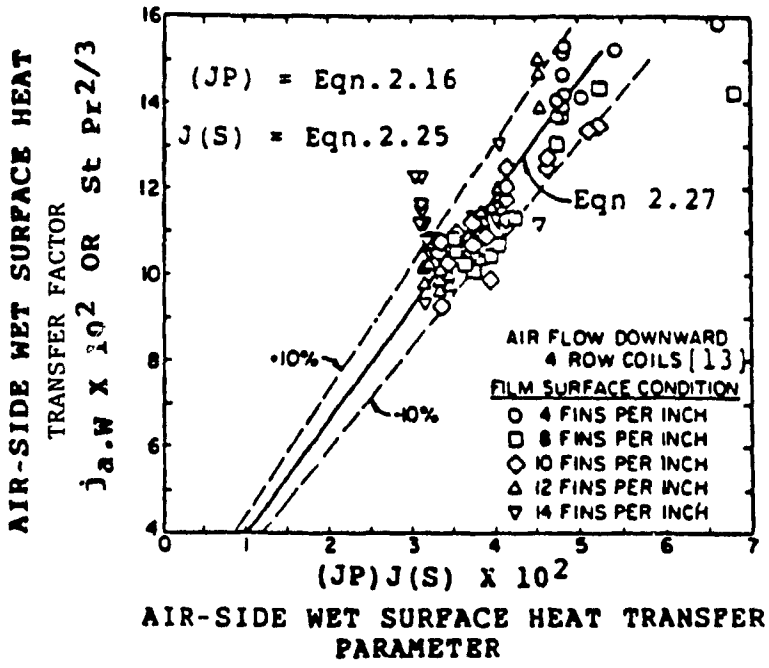

FIG. 2.14. CORRELATION FOR THE AIR-SIDE WET SURFACE HEAT TRANSFER FACTOR, McQUISTON (14)

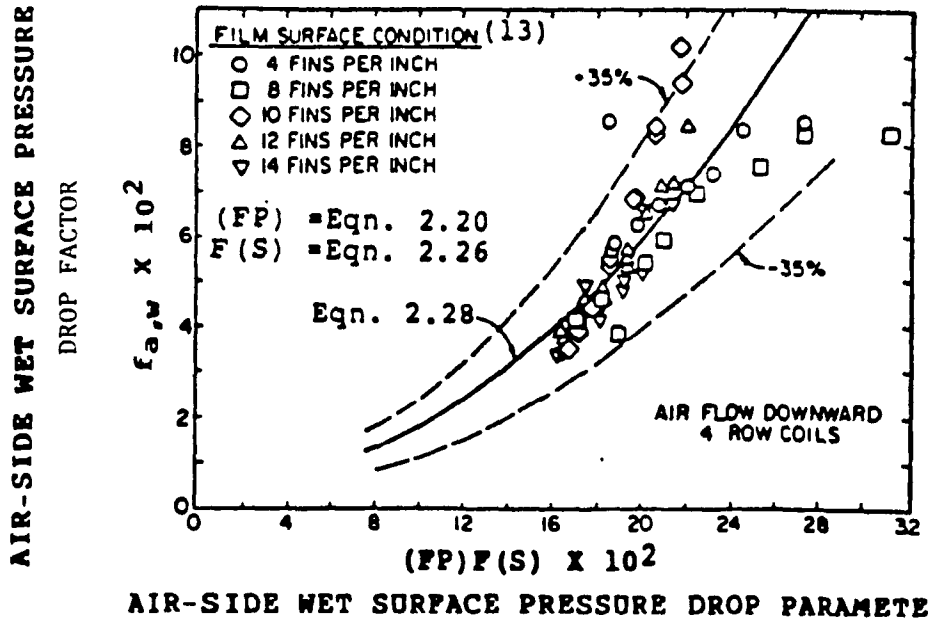

FIG. 2.15. CORRELATION FOR THE AIR-SIDE WET SURFACE PRESSURE DROP FACTOR, McQUISTON (14)

4.3 SUMMARY OF THE EXISTING LITERATURE ON THE AIR-SIDE PERFORMANCE

A summary of the existing literature on the air-side performance of finned-tube air cooling and dehumidifying heat exchangers, and the limitations of the existing correlation for prediction of the air-side heat transfer and pressure drop factors, are presented in this section. The findings from the relevant existing air-side studies may be summarized as follows:

i) The non-dimensional heat transfer and pressure drop factors (j and f factors) for smooth plate finned-tube coils may depend on the following heat exchanger dimensional parameters, and the fluid flow related parameters:

A) **Heat Exchanger Dimensional Parameters (see Fig. 2.2)**

- i) Fin spacing (S_f)
- ii) Fin thickness (Y_f)
- iii) Plate fin depth (L_a)
- iv) Tube logitudinal spacing (S_L)
- v) Tube transverse spacing (S_T)
- vi) Tube diameter (D_o)

B) **Fluid Flow Parameters**

- i) Air flow Reynolds number (Re_a, $Re_{a,D}$, $Re_{a,L}$ or $Re_{a,s}$)
- ii) Type of condensation (film or drop wise)
- iii) The condensate mass transfer rate.

2) The non-dimensional parameter Ao/Ap (Eqn. 2.12 - which includes most of the coil dimensional parameters) and the air flow Reynolds number are significant parameters in the correlations for prediction of the dry surface heat transfer and the pressure drop factors.

3) The effect of the number of rows (for a given fin spacing) on the dry surface heat transfer coefficient (for comfort air conditioning applications) is insignificant.

4) For a given air flow Reynolds number, the wet surface heat transfer and pressure drop factors ($j_{a,w}$ and $f_{a,w}$) are dependent on the corresponding dry surface factors ($j_{a,D}$ and $f_{a,D}$).

5) The fin spacing may have a significant effect on the wet surface heat transfer and pressure drop factors, due to the condensate film on the contact surface.

6) For a given fin and tube spacing (S_f, S_T, S_L, D_o and Y_f), the dry and wet surface heat transfer and pressure drop factors generally decrease when the air flow Reynolds number is increased.

Limitations of the Existing Air-Side Studies:

1) The effects of fin spacing and tube rows on the wet surface average heat transfer and pressure drop factors have not been fully investigated in the existing studies.

2) The existing correlations for the average pressure drop factor prediction (Eqn. 2.19 and 2.27) have relatively high errors (± 35%), and the use of these correlations for prediction of the energy requirements may result in higher errors. Therefore, in order to develop energy effective methods for DX-Coil design, correlations for prediction of the air-side average heat transfer and pressure drop factors are required in a form convenient for assessment of the effects of significant coil geometric parameters (such as fin spacing and the tube spacing).

4.4 REVIEW OF THE EXISTING METHODS FOR PREDICTION OF THE HEAT TRANSFER AND PRESSURE DROP FACTORS FOR BOILING REFRIGERANTS

Correlations for prediction of the refrigerant-side heat transfer and pressure drop factors are required for the design of DX-coils. However, formulation of generalized correlations are difficult due to changing two-phase flow conditions and the presence of lubrication oil transported from the compressor to the coil. The existing correlations for the prediction of the refrigerant-side heat transfer and pressure drop factor (Bibliography - 41 to 56) are limited to applications for boiling refrigerants in plain (un-finned) tubes and tube-bends.

Anderson et. Al [4], compared their experimental data for the average heat transfer coefficient in straight tubes, with the computed

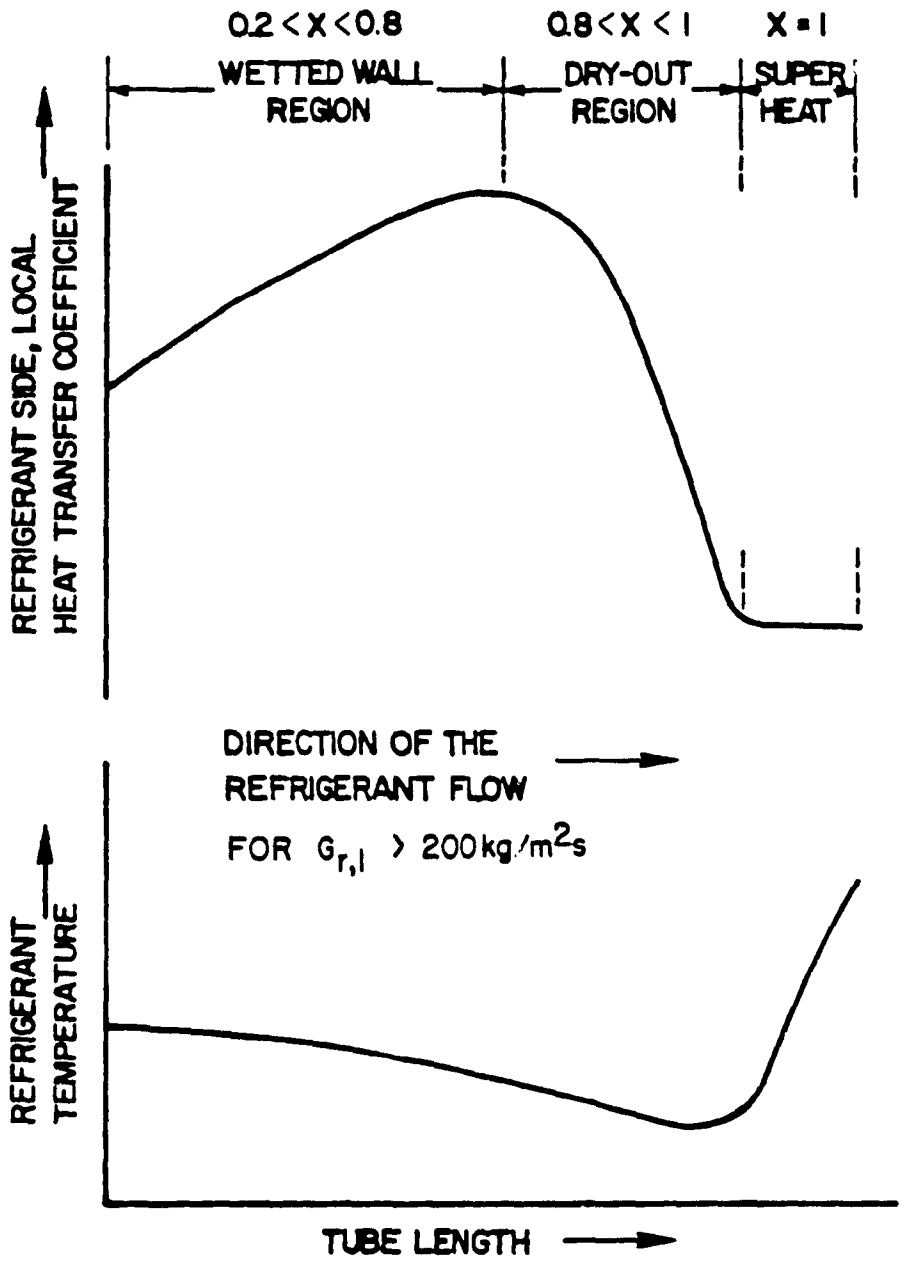

FIG 2.16 TYPICAL VARIATION OF HEAT TRANSFER COEFFICIENT AND REFRIGERANT TEMPERATURE ALONG THE TUBE LENGTH IN A DX-COIL

data from the correlations reported in the earlier studies (items to 41 to 45 - bibliography). They concluded that "None of the existing correlations are satisfactory for prediction of the average heat transfer factor for DX-Coils, due to the wide range of refrigerant mass flow rates and heat exchanger geometries used in DX-Coils". However, they added that the correlations proposed by Pierre [15] provided most satisfactory results among the correlations compared; a detailed discussion of the study by Pierre [15] is presented in section 4.6 (of this chapter). Rich and Chaddock [12] proposed that the flow regimes occuring along the tube circuit (in DX-Coils) may cause variations in the local heat transfer coefficient, depending on the liquid refrigerant mass flux ($G_{r,L}$). Fig. 2.16 shows typical variations of the local heat transfer coefficient (n_r) and the refrigerant temperature (t_r) for high refrigerant mass flux ($G_{r,L} > 200$ kg/m^{2}s) as proposed by Rich and Chaddock. Based on Fig. 2.16, in the up stream side of the refrigerant flow (wet-wall region) the local heat transfer coefficient gradually increases, due to decreasing refrigerant film thickness on the inside tube wall, and reaches a maximum value, typically at a local vapour fraction of about 80%. At this stage, the wall "Dry-out" begins, which considerably reduces the local heat transfer coefficient. In the downstream side of the refrigerant flow in the tube, the heat transfer coefficient variation is stabilized, being equal to that for 'pure' refrigerant in the 'superheat' vapour region.

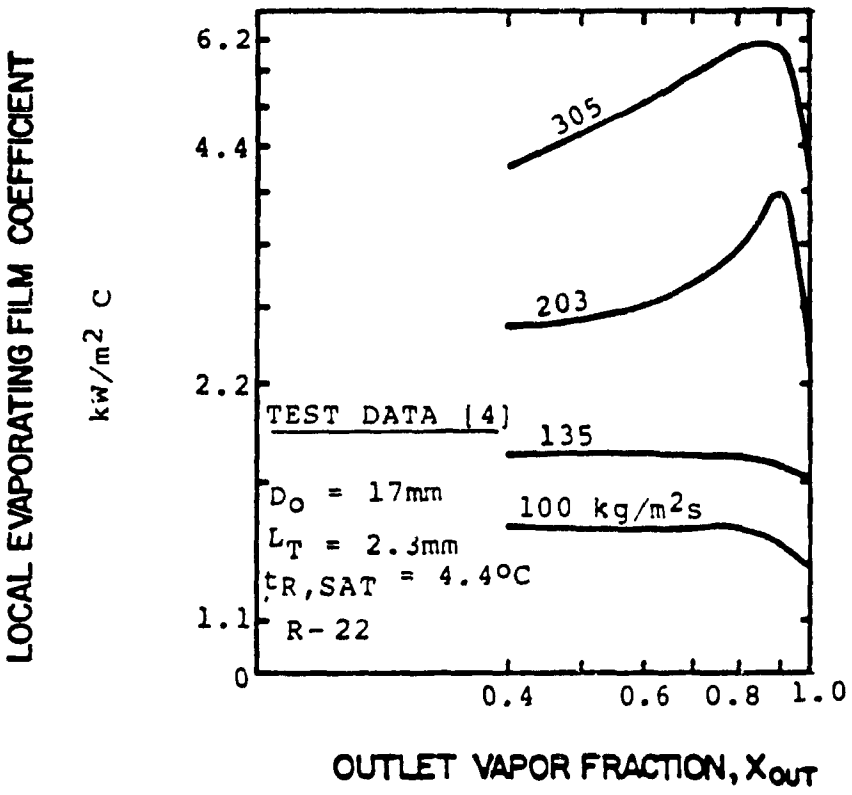

FIG. 2.17 VARIATION OF THE IN-TUBE LOCAL HEAT TRANSFER COEFFICIENT, WITH OUT-LET VAPOUR FRACTION [4]

Anderson [4] presented the variations of the experimental heat transfer coefficient (h_r) with the outlet vapour fraction (x_{out}), for different refrigerant mass flux ($G_{r,l}$), (see Fig. 2.17). While the local heat transfer coefficient varies considerably for high refrigerant mass flux ($G_{r,l} > 200$ kg/m^{2}s), for low mass flux ($G_{r,l} < 130$ kg / m^{2}s) the local heat transfer coefficient is found to remain reasonably constant. Hence, for boiling refrigerants inside tubes, the heat transfer coefficient may be represented by a single average value, for low refrigerant liquid mass flux. Similar studies on the variations of the local pressure drop coefficient are not available in the existing literature. A discussion of the studies by Pierre [15 and 17] on the prediction of the refrigerant-side average two-phase heat transfer and pressure drop coefficients for forced convection flow in straight (plain) tubes and tube-bends (unheated), are presented in Section 4.6 (of this chapter).

A discussion of the existing literature on the effects of oil on the heat transfer and pressure drop coefficients for the refrigerant flow inside straight tubes, is presented in the following section.

4.5 EFFECTS OF OIL-REFRIGERANT MIXTURE ON THE HEAT TRANSFER AND PRESSURE DROP COEFFICIENTS.

Presence of lubricating oil, transported fr . the compressor into the evaporator, is known to have an influence on the heat transfer and pressure drop coefficients.

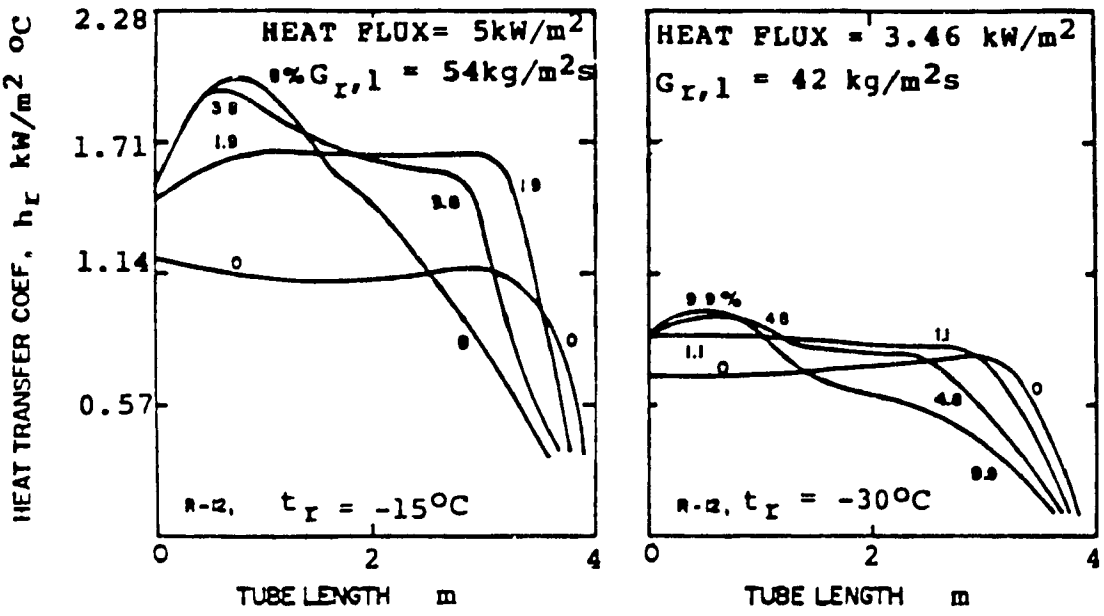

FIG. 2.18 LOCAL HEAT TRANSFER COEFFICIENTS FOR R-12/OIL MIXTURES IN A HORIZONTAL TUBE AS MEASURED BY WORSOE-SCHMIDT (PERCENTAGES SHOWN ARE WEIGHT PERCENT OIL IN THE MIXTURE) [28]

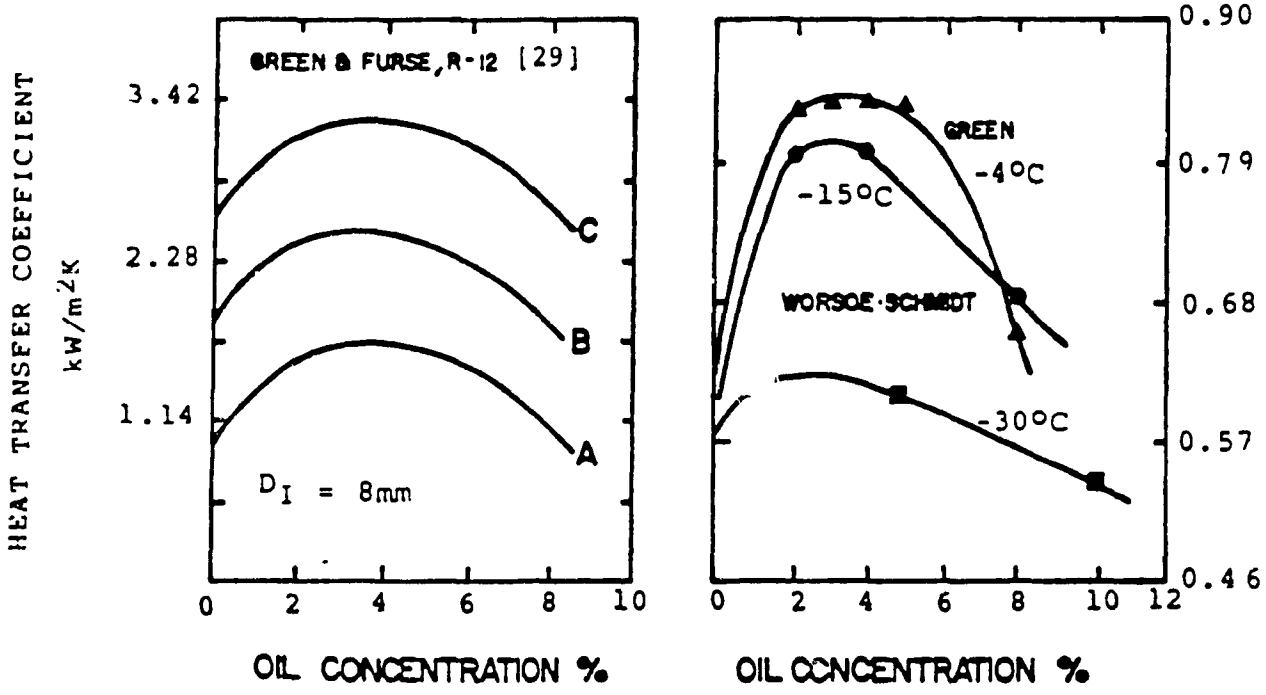

FIG 2.19 EFFECT OF OIL CONCENTRATION ON HEAT TRANSFER FOR EVAPORATION OF R-12 IN A HORIZONTAL TUBE

In this section, a discussion of the existing literature on the effects of lubricating oil on the heat transfer and pressure drop in DX-Coils, is presented.

Refrigerants commonly used in direct expansion coils (for air cooling and dehumidifying applications) are highly miscible in lubricating oils; While the solubility of R-22 and R-502 in lubricating oils is very high at elevated temperatures, the solubility of R-11 and R-12, at a given temperature, depends on the operating pressure [27].

Worsoe-Schmidt [28] conducted experimental studies on the effect of oil on evaporating R-12 inside tubes; these tests were conducted at mass flux of about 54 kg/m^2s. His results are shown in Fig. 2.18. The increase (about 50%) of the heat transfer coefficient in the leading section with the addition of oil (8% by weight), is attributed to tube-wall wetting, starting almost at the beginning of the evaporator; based on his results (Fig. 2.18), this effect (increase in the heat transfer coefficient) appears to be more significant at -15°C evaporator temperature compared to that at -30°C. In both cases (-15°C and -30°C evaporator temperatures), the development of oil-rich film towards the end of the evaporator for low liquid refrigerant mass flux ($G_{r,l}$ < 60 kg/m^2s) resulted in reduction of the heat transfer coefficient.

Green and Furse [29] investigated the effects of oil on the heat transfer for evaporation of R-12 (in tubes). Their results are shown in Fig. 2.19 which confirms the increase of the heat transfer coefficient

with the addition of oil due to tube wall wetting. The curves A, B andC in Fig. 2.19 represent increasing order of the mass flow rate, from A to C; specific values for the mass flow rates were not indicated in this publication. Chaddock [30] summarized the findings of a unpublished study on the effects of oil on the DX-coil performance as follows:

- In typical commercial refrigeration systems containing 0.5 to 2% by weight of oil, the variation of oil content will have an insignificant effect on the evaporator performance; however, the performance is different for the oil free case.

- The presence of oil tends to promote an annular flow pattern (tube wall-wetting), and also tends to increase the pressure drop.

- At low vapour velocities (not defined in Ref. [30]), oil in small quantities will influence the flow pattern, and this may result in an increase in the heat transfer coefficient compared to the oil-free operation.

- In the region of high vapour velocity (not defined in Ref. [30]), oil tends to inhibit wall dry-out resulting in an increase in the heat transfer coefficient. Oil also tends to increase the heat transfer coefficient in the superheat region. The magnitude of this effect can range up to 50%.

- For in-tube evaporation, the influence of oil on the nucleate boiling component of the heat transfer coefficient is insignificant when the oil content is below 2% by weight.

- At temperatures below the critical solution temperature [27] of the refrigerant-oil mixtures for R-22/oil mixtures, the partial miscibility characteristic (at this temperature,) tends to keep the refrigerant properties closer to the 'pure' refrigerant, and thereby do not influence the flow pattern or the heat transfer characteristics.

The discussion presented above illustrates the effect of oil on the heat transfer and pressure drop in DX-coils. In the present study, experimental data were developed with the presence of about 2% by weight of oil which is representative of typical DX-coil operating conditions. Empirical correlations for the heat transfer and pressure drop factors are then developed from the experimental data.

4.6 DISCUSSION OF THE EXPERIMENTAL STUDIES ON THE BOILING REFRIGERANTS CONDUCTED BY PIERRE [15, 16, and 17].

Pierre [15, 16 and 17] investigated the heat transfer and pressure drop phenomenon for boiling refrigerants (R-11 and R-12 - oil free) in plain straight tubes ($4 < L_T < 9.5$m, $12 < D_I < 18$mm), and the pressure drop in the tube-bends (unheated). Based on his experimental data, Pierre [13] proposed a generalized correlation for the average Nusselt

number (Nu_r) as follows:

$$Nu_r = a\,[Re^2_{r,l}\ K_f]^n \qquad (2.29)$$

valid in the range $10^9 < (Re^2_{r,l}\ K_f) < 0.7 \times 10^{12}$

where

$$Nu_r = h_r D_I/K_{r,l} \qquad (2.30)$$

$$Re_{r,l} = G_{r,l}\ D_I/\mu_{r,l} \qquad (2.31)$$

$$K_f = J\,(\Delta x)\,H_{fg}/L_t \qquad (2.32)$$

and

$a = 0.0009$, $n = 0.5$ (from experimental data [13])

For incomplete evaporation of the refrigerant in the tube

($x_{out} < 0.9$)

$a = 0.00062$, $n = 0.4$ (from experimental data [13])

for complete evaporation ($x_{out} > 0.9$)

Nu_r - Refrigerant-side average Nusselt number

$Re_{r,l}$ - Refrigerant liquid flow Reynolds number

K_f - Refrigerant boiling number

h_r - Average heat transfer coefficient for the boiling refrigerant.

$G_{r,l}$ - Refrigerant liquid mass flux

D_i - Tube inside diameter

$\mu_{r,l}$ - Refrigerant liquid dynamic viscosity

$K_{r,l}$ - Refrigerant liquid thermal conductivity

J - Mechanical equivalent of heat (=1 N.m/W.hr.)

h_{fg} - Latent heat of vaporization

L_T - Tube length

Δx - Change in the refrigerant vapour fraction.

$(Re^2_{r,l}\ K_f)$ - Refrigerant-side heat transfer parameter.

The correlation (Eqns. 2.29) indicates that the average Nusselt number for (oil-free) boiling refrigerants in straight tubes, is a increasing function of the refrigerant-side heat transfer parameter $(Re^2_{r,l}\ K_f)$, where the boiling number (K_f) is based on the vapour quality change per unit length $[(\Delta x)/L_T]$. The experimental data (from Ref. [15]), are shown in Figs. 2.20 and 2.21. The decrease in the constant and the exponents of the heat transfer parameter $(Re^2_{r,l}\ K_f)$ for complete evaporation indicates 'suppressed turbulence' effect due to film boiling at higher exit vapour qualities (x_{out} 0.9) and the existance of the tube 'Dry out' (which reduce the average Nusselt number) [15].

Equations 2.29 to 2.32 imply that the average Nusselt number is dependent on the change in the vapour fraction (Δx), and the corresponding refrigerant flow Reynolds number (for given tube length).

However, Anderson [4] found that the refrigerant Nusselt number is also dependent on the outlet vapour fraction (x_{out}) and the corresponding mass flux ($G_{r,l}$) (see Fig. 2.17); in consequence, he proposed that eqns. 2.29 and 2.30 should be modified to include additional parameters to account for these effects. He also suggested that for compact finned tube coils, the surface area ratio (A_o/A_I) may have an influence on the average Nusselt number; however, due to lack of experimental data for DX-coils, no specific modifications were proposed (in Ref. [4]). In addition, the effect of the lubricating oil on the average Nusselt number is not considered in Eqn. 2.29.

For the pressure drop factor (f_r) in straight tubes, Pierre [10] proposed the following correlation:

$$f_r = [\Delta p_r/(\Delta P)] + \Delta X \tag{2.33}$$

where

$$\Delta X = (x_2 - x_1)\, D_I/x_m L_T \tag{2.34}$$

$$x_m = (x_1 + x_2)/2 \tag{2.35}$$

$$(\Delta P) = G_{r,l}^2\, x_m\, V_m\, L_T/D_I \tag{2.36}$$

and

Δp_r - Refrigerant pressure drop

x_1, x_2 and x_m - Vapour quality at entrance, exit, and mean values respectively

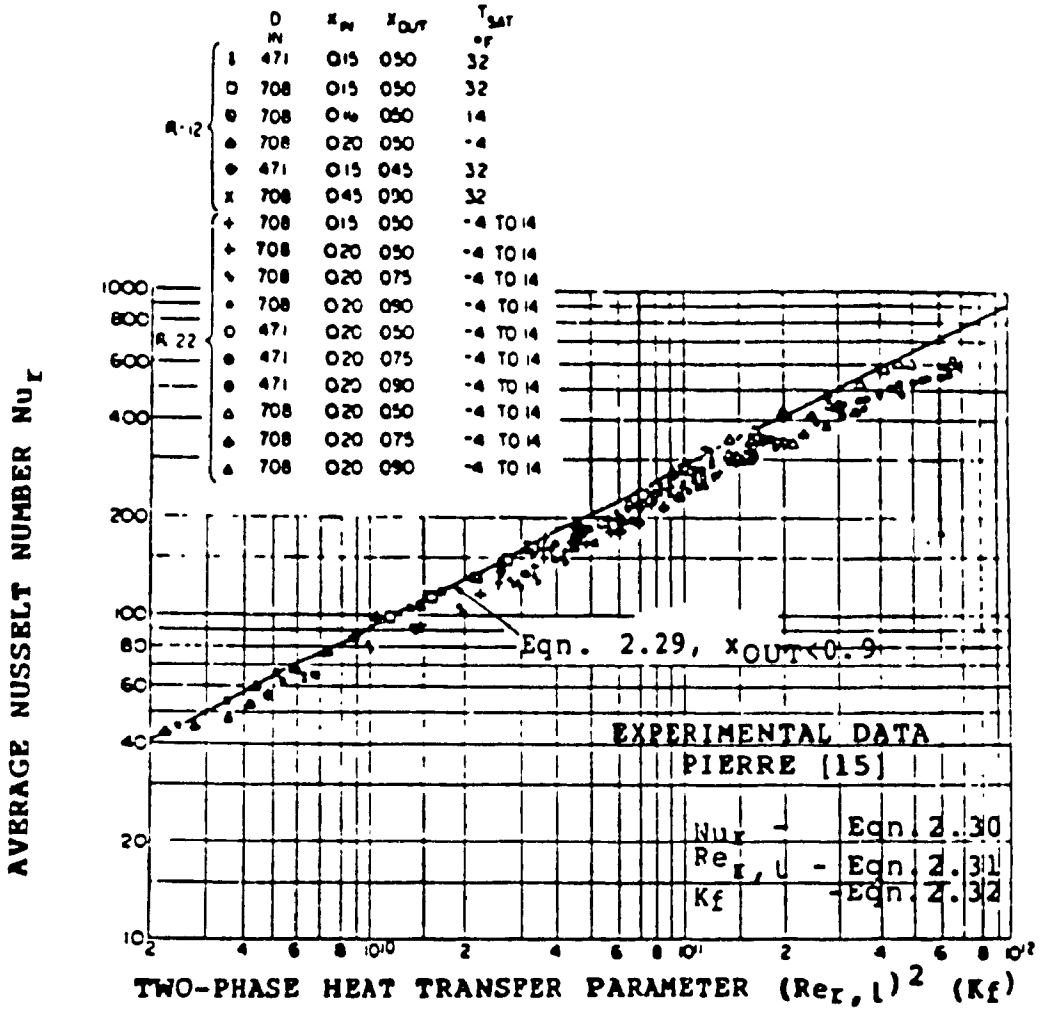

FIG.2.20. AVERAGE NUSSELT NUMBER FOR INCOMPLETE EVAPORATION [15]

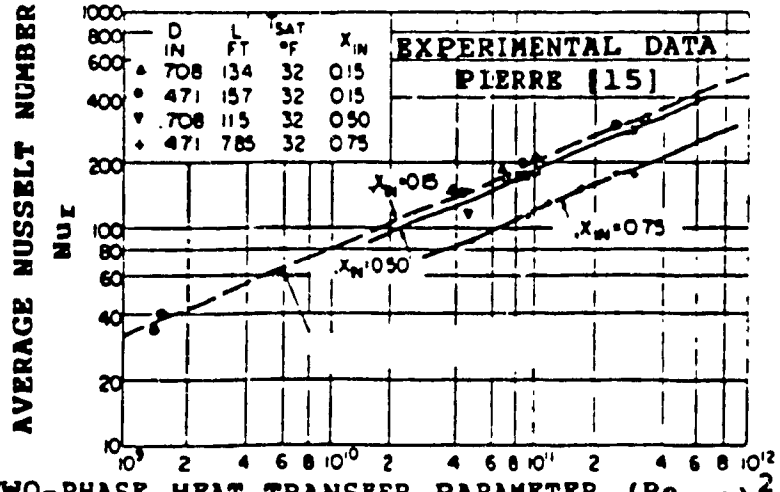

FIG. 2.21 AVERAGE NUSSELT NUMBER FOR COMPLETE EVAPORATION [15]

$G_{r,l}$ - Refrigerant mass flux

V_m - Refrigerant vapour, mean specific volume

L_T - Tube length

D_I - Tube inside diameter

In this correlation (Eqn. 2.33), Pierre [16] assumed that the velocities of the liquid and vapour phases are identical (homogeneous liquid vapour mixture). He also assumed that the flow resistance is due to friction generated from the shear force on the wet wall of the tube, and is a function of the square of the liquid vapour mixture velocity. His experimental data shown in Fig. 2.22, indicate that the average two phase pressure drop factor (f_r) is a function of the ratio of the liquid flow Reynolds number ($Re_{r,l}$) to the corresponding boiling number (K_f). In addition, when the $Re_{r,l}/K_f > 1$, Pierre proposed that the average two-phase pressure drop factor behaves similar to that for single phase turbulent flow. He also proposed that transition from laminar to turbulent flow occurs in the region when the ratio ($Re_{r,l}/K_f$) is about one. In the turbulent region ($Re_{r,l}/K_f$) > 1, which is predominent in typical typical DX-coils, the average two-phase pressure factor (f_f) may remain reasonably constant (in the range $1 < Re_{r,l}/K_f < 4$). Based on his experimental data, Pierre [16] proposed an empirical correlation for the average two-phase pressure drop factor (f_f) as follows:

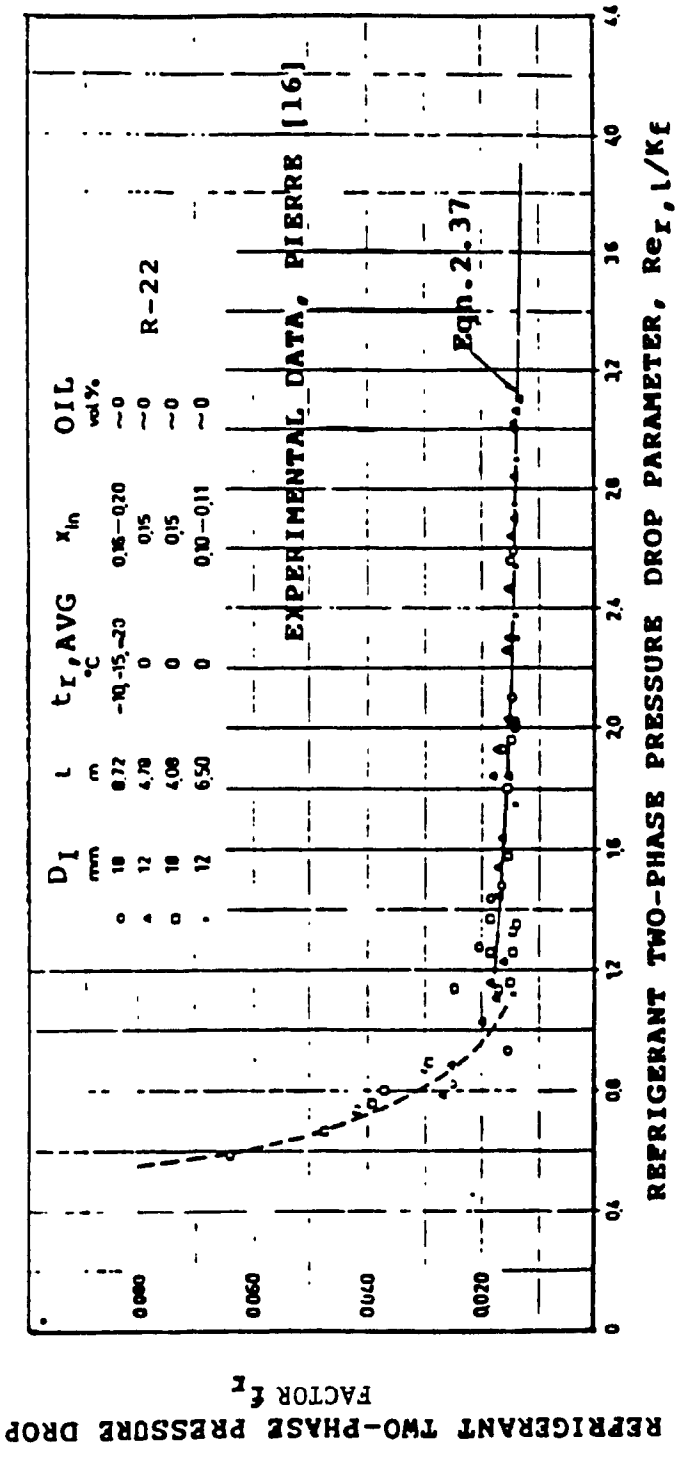

FIG. 2.22. CORRELATION FOR TWO-PHASE PRESSURE DROP FACTOR FOR (OIL FREE) BOILING R-22 IN STRAIGHT PLAIN TUBES, PIERRE [16]

For oil-free refrigerant flow:

$$f_r = 0.0185 \quad (K_f/Re_{r,l})^{0.25} \qquad (2.37)$$

valid for $(Re_{r,l}/K_f) > 1$

For the case, when 6 to 12% by volume of oil is present:

$$f_r = 0.053 \quad (K_f/Re_{r,l})^{0.25} \qquad (2.38)$$

valid for $(Re_{r,l}/K_f) > 2$

Pierre [16] reported that the presence of oil (6 to 7% by volume) approximately doubled the average two-phase pressure drop factor (for a given $Re_{r,l}/K_f$).

Refrigerant pressure drop in DX-coils occurs in the straight tubes (heated by the air), and the tube-bends (usually located outside the air stream). The refrigerant pressure drop in the tube-bends may be of the same magnitude as that for the straight tube portion of the refrigerant circuit depending on the circuit configuration [17]. Assuming a constant vapour fraction in the tube-bends (unheated) and a constant flow velocity for the liquid-vapour mixture, Pierre [17] proposed a correlation for the return-bend pressure drop ($\Delta P_{r,RB}$), as follows:

$$\Delta P_{r,RB} = \Delta P_{r,a} + \Delta P_{r,f} \qquad (2.39)$$

where

$$\Delta P_{r,RB} = f_{r,RB} \; (G^2_{r,l} \quad V_m)/2 \qquad (2.40)$$

$$\Delta P_{r,a} = f_{r,a} \ (G^2_{r,l} \ V_m)/2 \tag{2.41}$$

$$\Delta P_{r,f} = f_{r,f} \ (G^2_{r,l} \ V_m)/2 \tag{2.42}$$

$$f_{r,RB} = f_{r,a} + f_{r,f} \tag{2.43}$$

and

$\Delta P_{r,a}$, and $f_{r,a}$ - Pressure drop due to flow directional change and the corresponding pressure drop factor

$\Delta P_{r,f}$ and $f_{r,f}$ - Pressure drop due to friction and the corresponding pressure drop factor

$f_{r,RB}$ - Total pressure drop factor in the return-bend

$G_{r,l}$ - Liquid refrigerant mass flux

V_m - Refrigerant mean specific volume

From his experimental data, Pierre [17] proposed a generalized correlation for the return-bend two-phase pressure drop ($\Delta P_{r,RB}$) as follows:

$$\Delta P_{r,RB} = (N_{RB}) \ (f_{r,RB}) \ (G^2_{r,l}) \ V_m/2 \tag{2.44}$$

where

N_{RB} - Number of return-bends in the refrigerant circuit

$f_{r,RB}$ - Return-bend average refrigerant pressure drop factor is about 0.015 for oil-free flow, and is about 0.035 when 2 to 12% by volume of oil is present, for typical return-bend configurations found in DX-coils.

4.7 SUMMARY OF THE EXISTING STUDIES ON THE REFRIGERANT SIDE HEAT TRANSFER AND PRESSURE DROP FACTOR PREDICTION:

A) The local heat transfer coefficient (h_r) for boiling refrigerant inside straight tubes at high liquid refrigerant mass flux ($G_{r,l} > 200$ kg/m^{2}s) varies along the tube circuit length due to changing two-phase flow conditions; however, for lower mass flux ($G_{r,l} < 130$ kg/m^{2}s), these variations are minimal.

B) The refrigerant-side average Nusselt Number (Nu_r) is an increasing function of the heat transfer parameter ($Re^2_{r,l}\ K_f$), for two-phase oil-free turbulent flow ($Re_{r,l}/K_f) > 1$ in straight horizontal tubes.

C) The average two-phase pressure drop factor (f_r) (in straight horizontal tubes) is a decreasing function of the presssure drop parameter ($Re_{r,l}/K_f$).

D) For boiling refrigerant (R-11 and R-12) in straight horizontal tubes, the presence of oil (about 2 to 6% by volume) tends to increase the heat transfer and pressure drop factors. The existing correlations for prediction of the heat transfer and pressure drop factors [eqns. 2.29 and 2.33] are based on the experimental studies on boiling refrigerants in straight unfinned-tubes. These correlations are not applicable to DX-coils, without correctional terms to account for the effects of the coil geometry [4].

CHAPTER 3

DESCRIPTION OF THE TEST FACILITY AND THE MEASUREMENT SYSTEM

CHAPTER 3

DESCRIPTION OF THE TEST FACILITY AND THE MEASUREMENT SYSTEM

In order to determine the heat transfer and the pressure drop coefficients for the working fluids (air and the refrigerant), experimental studies were conducted on the test facility at the Centre for Building Studies of Concordia University, Montreal, designed and built in accordance with ASHRAE Standard 33-78 [31] and A.R.I. Standard 410-72 [32]. In this chapter, a detailed description of the test facility, and the measurement systems, are presented.

A schematic layout of the test apparatus is shown in Fig. 3.1, and the corresponding measurement nomenclature is shown in Table 3.1. Details of the measurement methods are presented in sections 3.3 to 3.7.

1. OPERATION OF THE TEST APPARATUS:

The air-circuit consists of a closed-loop air circulation system, driven by a variable air volume fan (fig. 3.1 item 1). The incoming air is cooled and dehumidified by the test coil (item 2). The air is then passed through the mixing chamber (item 3) where mixing is achieved by the baffle plates, and is circulated through the nozzle section (item 4) where the air volume flow rate is measured. The air is then passed over a finned-tube hot-water heating coil (item 5) and a steam humidifier (item 6) to maintain constant air intake conditions. Finally the air is circulated through the fan (item 1), the intake chamber (item 7) fitted with an air straightening section, and through the test coil.

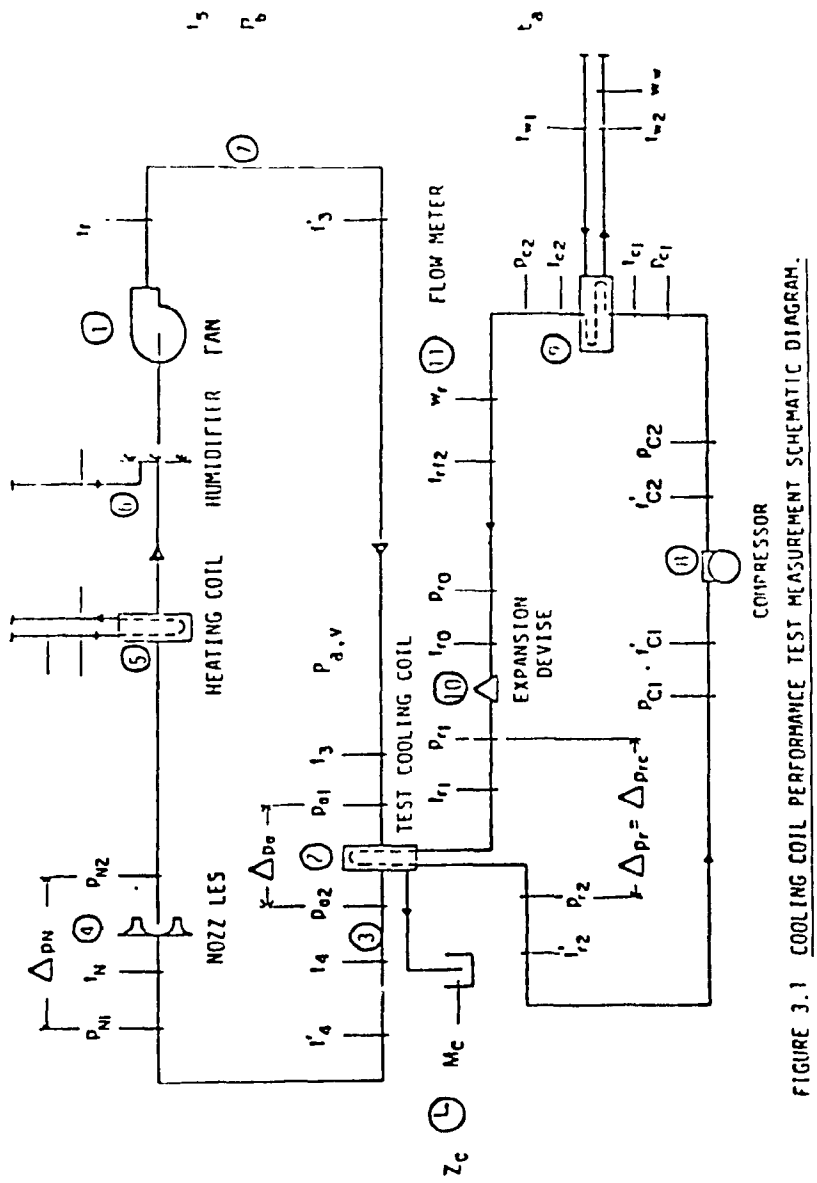

FIGURE 3.1 COOLING COIL PERFORMANCE TEST MEASUREMENT SCHEMATIC DIAGRAM.

The air-circuit is built in separate sections, bolted together with sealing gaskets.

The refrigerant circuit consists of, a 6-cylinder reciprocating compressor (item 8), the test coil serving as the evaporator, and a water cooled condenser (item 9). The evaporator is fitted with a thermostatic expansion valve (item 10) to provide the required flow rate, and to control the super heat of refrigerant vapour leaving the test coil within the required limits (2-8°C). A rotameter (item 11) is used to measure the liquid refrigerant flow rate in the liquid line. The refrigeration flow control is achieved by a combination of cylinder un-loading and hot gas by-pass methods [31].

Major equipment specifications are shown in Appendix - 2.

TABLE 3.1 - NOMENCLATURE FOR MEASUREMENTS
(For Fig. 3.1)

S. no.	Notation	Description	Remarks
		1. Air-Side Measurements	
1.	t_3	Entering air D.B. temp.	Average of 12 Measurements
2.	t_3'	Entering air W.B. temp.	Aspirator type wetted thermo-couple
3.	t_4	Leaving air D.B. temp.	Average of 9 measurements
4.	t_4'	Leaving air W.B. temp.	Aspirator type wetted thermo-couple
5.	t_5	Ambient air D.B. temp. surrounding test coil	Average of 4 measurements
6.	P_{a1}	Air static pressure entering coil	Average of 4 measurements
7.	P_{a2}	Air static pressure leaving coil	Average of 4 measurements
8.	P_{N1}	Air static pressure entering nozzle section	Average of 4 measurements
9.	P_{N2}	Air static pressure leaving nozzle section	Average of 4 measurements
10.	P_b	Ambient barometric pressure	
11.	t_a	Ambient temp. surrounding condenser	Average of 3 measurements
12.	$P_{a,v}$.	Air velocity pressure at coil face by pitot-tube traverse method	Average of 32 measurements.

Table 3.1 Cont'd:

S. no.	Notation	Description	Remarks
		2. Refrigerant-Side Measurement	
13.	$t_{r,0}$	Refrig. temp. entering expansion valve	
14.	$P_{r,0}$	Refrig. press entering expansion	
15.	$t_{r,1}$	Refrig. temp. entering coil	
16.	P_r	Refrig. press. entering coil	
17.	t_{r2}	Refrig. temp. leaving coil	
18.	P_{r2}	Refrig. press. leaving coil	
19.	t_{c1}'	Refrig. temp. entering compressor	
20.	P_{c1}'	Refrig. press. entering compressor	
21.	t_{c2}'	Refrig. temp. leaving compressor	
22.	P_{c2}'	Refrig. press. leaving compressor	
23.	t_{c1}	Refrig. temp. entering condenser	
24.	P_{c1}	Refrig. press. entering condenser	
25.	t_{c2}	Refrig. temp. leaving	
26.	P_{c2}	Refrig. press. leaving condenser	
27.	W_r	Refrigerant liquid flow rate	
28.	t_{rf2}	Refrig. temp. leaving flow meter	
29.	t_{w1}	Condenser water entering temp.	

Table 3.1 - Cont'd:

S. No.	Notation	Description	Remarks
30.	t_{w2}	Condenser water leaving temp.	
31.	W_w	Condenser water flow rate	
32.	Z_c	Test time	
33.	M_c	Condensate flow rate	

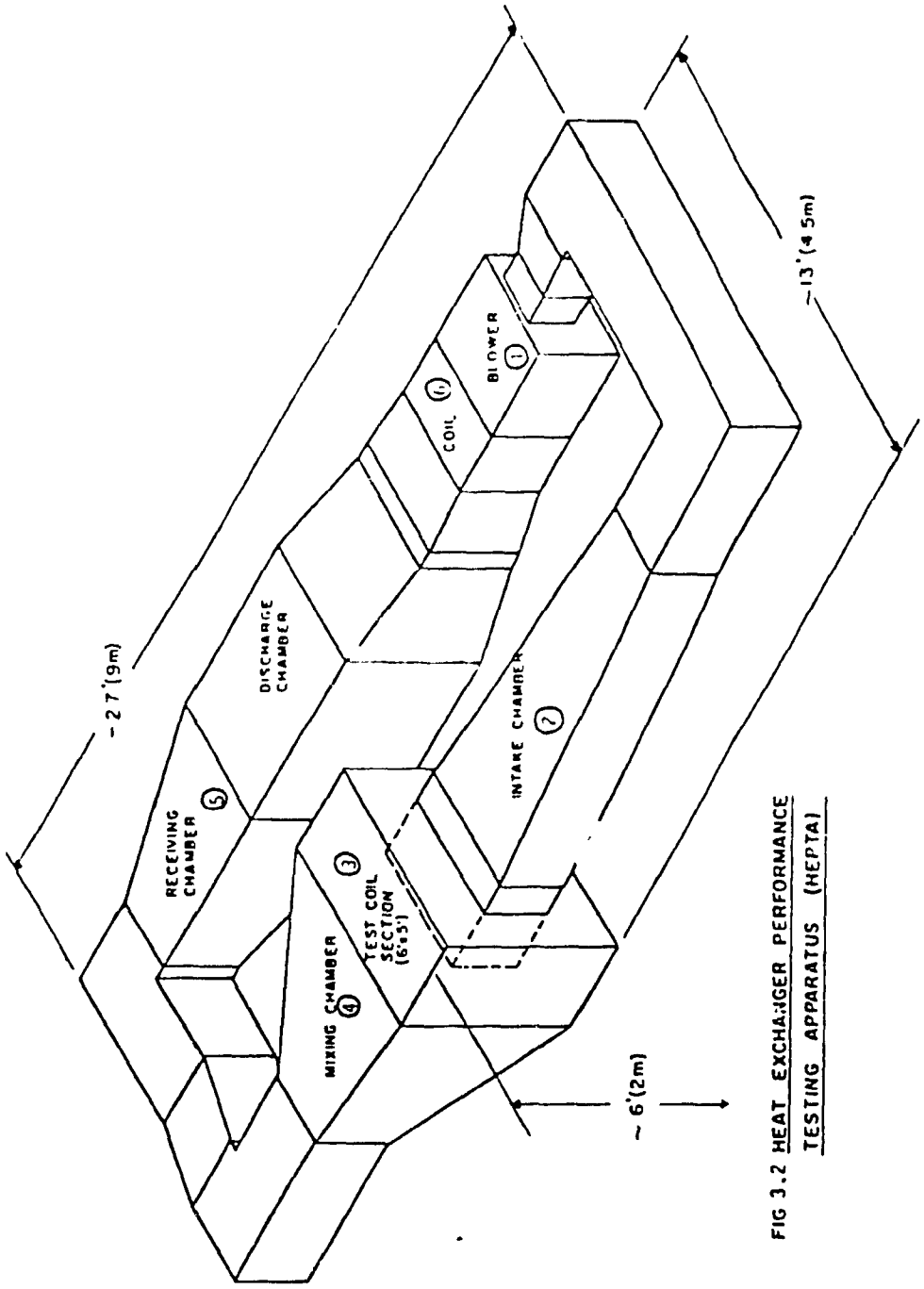

FIG 3.2 HEAT EXCHANGER PERFORMANCE TESTING APPARATUS (HEPTA)

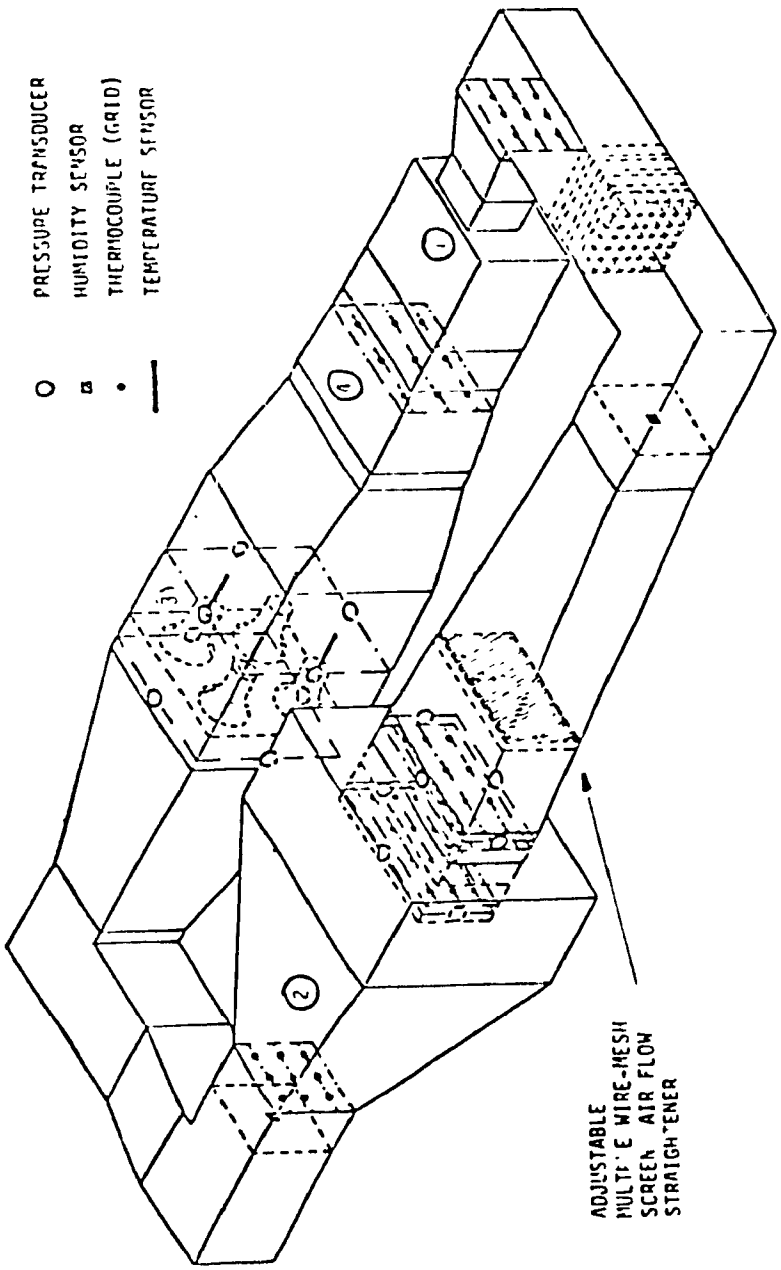

FIGURE 3.3 HEAT EXCHANGER PERFORMANCE TEST APPARATUS. AUTOMATIC AIR SIDE INSTRUMENTATION LAYOUT (COOLING COIL PERFORMANCE TEST).

2 COMPONENT DESCRIPTION

2.1 FAN: (Fig. 3.2, item 1)

The centrifugal fan air volume variation is achieved by a manually controlled, horizontal-slide, front face damper. The fan is pulley driven by an electric motor, and is connected to the air-loop by rectangular flexible ducts to minimize transfer of fan vibration. The fan itself is mounted on a coil-spring platform to minimize vibrations.

2.2 Intake Chamber: (Fig. 3.2, item 2)

The rectangular duct section is insulated on the inside surface with foil protected, 25 mm (1 in.) thick, rigid polyurethane insulation with a rated heat transfer coefficient of 37.14 $W/m^2.°C$. To provide smooth turning for the air flow through the bends, "AERO-FOIL" turning vanes are fitted at the four corners of the test apparatus. The air flow straightener consists of a series of adjustable wire-mesh screens fitted inside the duct section. The intake chamber also serves as the transition section, and is built in accordance with ASHRAE Standard 33-78 [31].

2.3 Test Coils: (Fig. 3.2 item 3)

A description of the test coil is presented in Chapter-4, section 1. The coils are installed in the test section through the door provided in the mixing chamber. A 35.56 cm wide rectangular sheet metal duct section is bolted to both faces of the coil to allow for the insta-

llation of the copper-constantan thermocouple grids (see Fig. 3.3) and the air static pressure transducers (see Fig. 5.9). The coil frame is equipped with condensate drainage channels and a collector for the measurement of condensate flow rate.

2.4 Mixing Chamber: (Fig. 3.2, item 4)

The mixing chamber is provided with baffles to provide mixing of cooled and dehumidified air leaving the coil, and a thermocouple grid is installed at the end of this section. A wet-bulb temperature sensor and automatic relative humidity sensor (see section 3.3.4) are also fitted in this section.

2.5 Nozzle Section: (Fig. 3.3, item 3)

Four nozzles, constructed in accordance with section 5.1.6 of the ASHRAE Standard 33-78, are mounted on a sheet metal plate (see Fig. 3.4). For the nozzle leaving (high velocity) air temperature measurement, long-contact-surface temperature sensors are installed at the centre of each of the nozzle leaving ends (see Table 3.2).

2.6 Re-heat Coil: (Fig. 3.2, item 6)

To maintain constant inlet air dry-bulb temperature, a 4-row, 14 fins/inch, hot water heating coil is installed in the air loop. The hot water flow rate is controlled manually by a hand valve located at the water inlet to the coil. The hot water temperature is controlled by

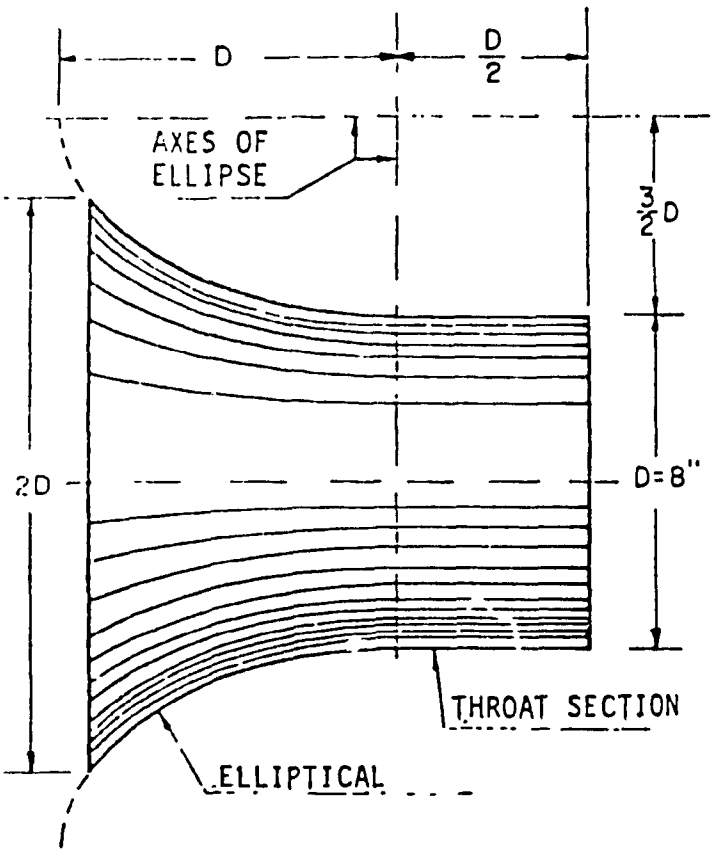

FIGURE 3.4 AIR FLOW MEASUREMENT NOZZLE
ASHRAE STANDARD 33-78 SECTION 5.1.6

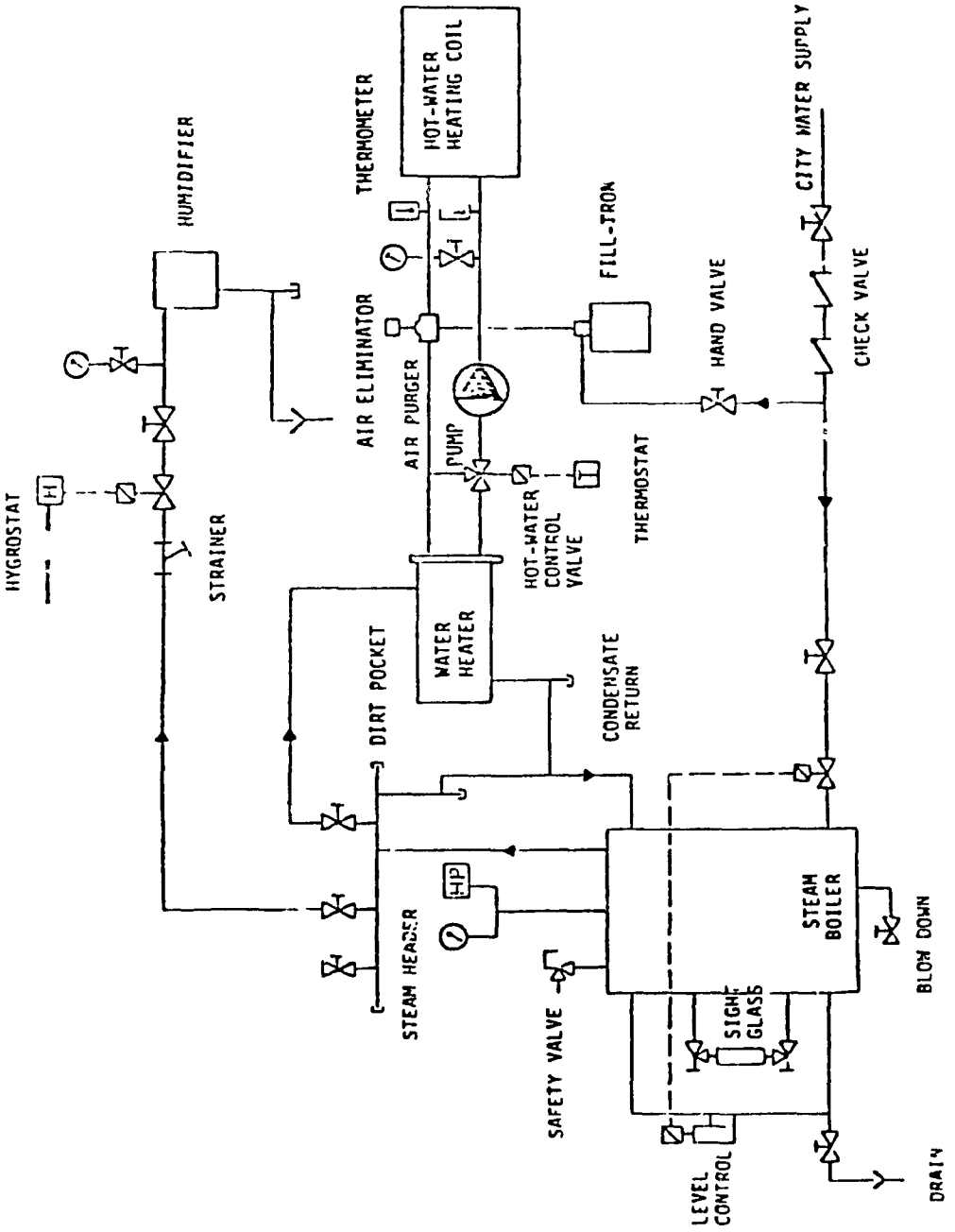

FIG. 3.5 HEATING & HUMIDIFYING SYSTEM SCHEMATIC DIAGRAM

a thermostatically controlled mixing valve in the hot water system (see Fig. 3.5).

2.7 Humidifier

To maintain constant inlet air humidity, a steam injector is provided in the air-loop, controlled by a humidistat. The steam is provided by a hot water/steam boiler (see Fig. 3.5).

2.8 Refrigeration system (Fig. 3.6)

A six cylinder reciprocating refrigerant vapour compressor is used to provide the refrigerant flow required for the test coil. The compressor is equipped with multi-stage cylinder unloading system for the control of the cooling capacity. A condenser water flow measurement sensor, and two well-type immersion thermometers to measure inlet and outlet water temperatures, are installed in this system. A series of thermostatic expansion valves, sized in accordance with the estimated coil capacity, are used to provide the refrigerant flow and superheat control.

3 AIR-SIDE MEASUREMENTS

A summary of the measurements and instrumentation used in this study are shown in Table 3.2. Error analysis of major measurements is presented in Appendix 7.

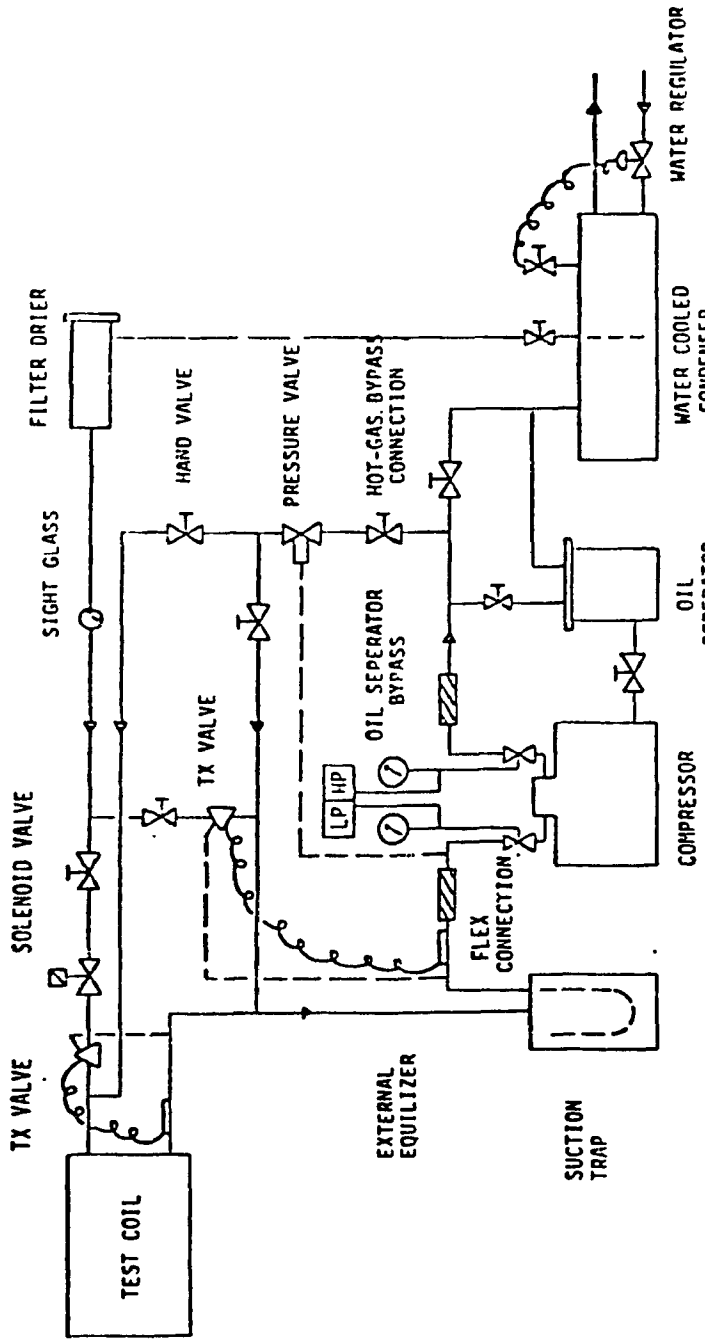

FIG. 3.6 REFRIGERATION SYSTEM SCHEMATIC

3.1 Dry-Bulb Temperature Measurement

Air temperature measurements are taken before the coil face in the intake chamber (see Fig. 3.1) for the entering air, and at the end of the mixing chamber for the leaving air. At both sections, a grid of copper-constantan, radiation shielded thermocouples are installed. The thermocouple end sections are connected to the reference junction of the automatic data acquisition system, which provided a uniform temperature for all the terminating points. A temperature sensing diode in the data acquisition system provides the air dry-bulb temperature measurement; the thermocouple output linearization is performed digitally [based on N.B.S. monograph #125 stored in the hardware of the data acquisition system (see section 3.7)].

TABLE 3.2 - SUMMARY OF THE INSTRUMENTATION SPECIFICATIONS

ITEM	NO. OF MEASUREMENT POINTS	TYPE OF MEASURING INSTRUMENT	RANGE OF OPERATION	ACCURACY REQUIRED BY STANDARD	DATA COLLECTION auto.	DATA COLLECTION non auto	COMMENTS
TEMPERATURE							
Air dry bulb temp.	50	Shielded Copper-constant. thermocouple	-450 to + 700°F	+ 0.1°F	x		High velocity
Air dry bulb temp. at nozzles	4	Shielded Copper-constant-thermocouple, 24" PROBE	-450 to + 700°F	+ 1°F	x		
Refrigerant temp.	2	RDT platinum resistance thermometer	0 to + 100°C	+ 0.5°F	x		
Condenser water temp.	2	Remote bulb immersion thermometer	+40 to + 220°F	+ 0.5°F		x	
Hot water temp.	2	Remote bulb immersion thermometer	+40 to + 220°F	+ 0.5°F		x	
HUMIDITY							
Air relative humidity	2	Hygromechanical actuated strain Gauge beam sensor	-40 to + 250°F	--	x		"HY-CAL" Special purpose sensor
PRESSURE							
Air static pressure	16	Strain gauge pressure sensor	0-20" W.G.	1% of value (0.005"W.G)	x		
Refrigerant pressure	2	Strain gauge pressure sensor	0-300 PSI	+ 5% ABS.	x		
TEMPERATURE & PRESSURE							
Refrigerant temperature and pressure	5	Standard refrigeration gauge	30VAC-300PSI -40 to + 120°F	--		x	Control function only
FLOW							
Refrigerant flow	1	Annular averaging Velocity heat sensor	0-30 GPM	+ 2% of value		x	"ANNUBAR"
Condenser water flow	1	Annular averaging Velocity heat sensor	0-30 GPM	+ 1% of value		x	"ANNUBAR"
Hot water flow	1	Annular averaging Velocity heat sensor	0-30 GPM	+ 1% of value		x	"ANNUBAR"

3.2 Air Wet-Bulb Temperature

Wet-bulb temperatures for coil entering and leaving air are measured by an aspirator-type, wetted-thermocouple junction (see Fig. 3.1). At both sections (entering and leaving), air is drawn by a fan through a 50.4 mm dia. tubing, and is 'blown' over a thermocouple junction wetted by a wick. The measured air velocity over the sensor averaged 20.3 m/s, which was within limits recommended by the ASHRAE Standard 33-78. The measured wet-bulb temperature is then checked (for each test) against the wet-bulb temperature calculated from the direct relative humidity measurement obtained from the automatic relative humidity sensor described in section 3.4.

3.3 Air Flow Rate

Air flow rate is measured by nozzles constructed in accordance with the ASHRAE Standard 33-78, section 5.1.6 (see Figs. 3.1 and 3.3). The nozzle section consists of four nozzles fitted on a plate. Air from the receiving chamber is allowed to flow through a selected number of nozzles (depending on the air flow rate) into the discharge chamber. The throat velocity at the smaller end of the nozzles is maintained at value greater than 15.24 m/s for all tests. The nozzle tip air dry-bulb temperature is measured by large-contact-surface temperature sensors, designed for the temperature measurement of high velocity air. The air-static pressure at the entering and leaving sections of the nozzles

are measured by air pressure transducers located at the center of each of the four walls of the receiving and discharge chambers, as shown in Fig. 3.3; from this data, the air flow rate is calculated in accordance with the procedures outlined in the ASHRAE Standard 33-78, section 9.1.1.

The air flow rate is also calculated from the average air face velocity measurement at the coil by pitot-tube-traverse method.

3.4 Relative Humidity: (Fig. 3.7)

The coil entering and leaving air relative humidities are measured by automatic sensors (commercially available) consisting of a special humidity sensitive cellulose crystalline strip mounted at the end of a "beam". The cellulose strip reacts to humidity changes, similar to a bimetallic strip reacting to temperature. A pair of solid state strain gauges attached to the "beam" measure the bending strain which is proportional to the relative humidity of the contact air. The output ends of the sensor are connected to a transmitter with a zero-span adjustment which is set at the desired range.

The humidity sensors are tested and calibrated by the manufacturer, at the National Research Council (N.R.C) Laboratories, in Ottawa, Canada, prior to use in experimental studies. (See Fig. 3.8).

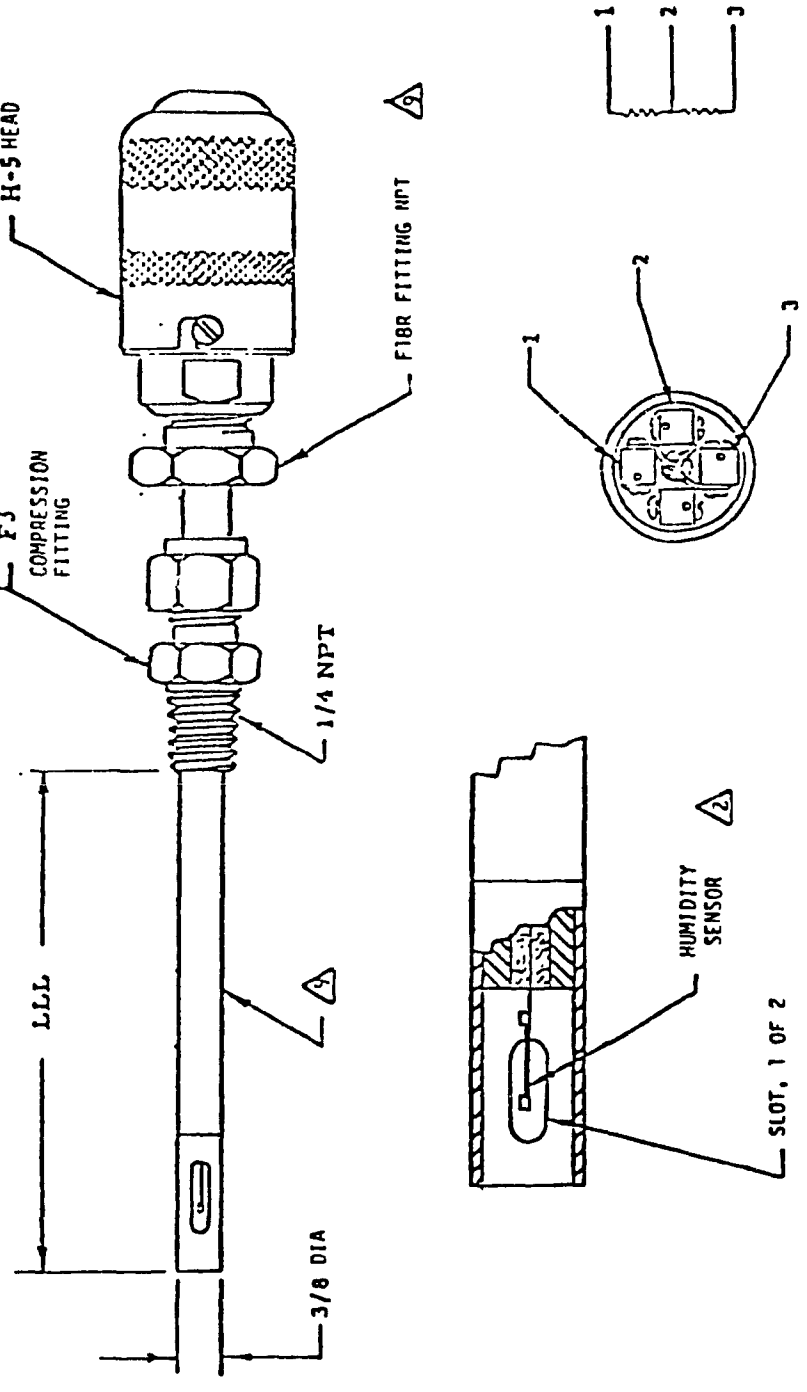

FIG. 3.7 RELATIVE HUMIDITY SENSOR [FROM DRAWING A-11180, HY-CAL ENGINEERING LTD., SANTA FE, CALIFORNIA]

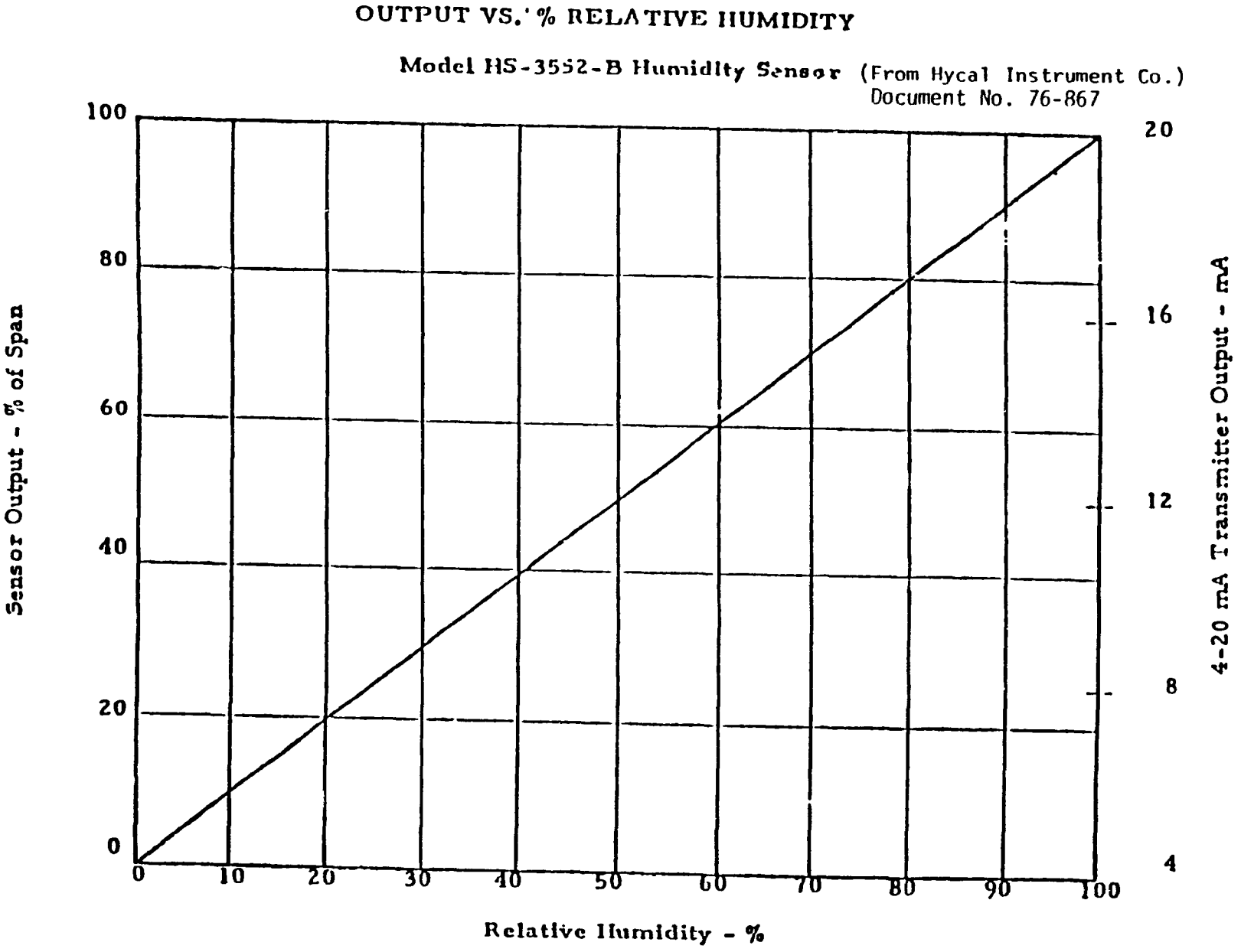

FIG. 3.8 HUMIDITY SENSOR CALIBRATION DATA.

3.5 Air-Static Pressure: (Fig. 3.9)

Strain-gauge type, automatic gas pressure transducers are used for the air-static pressure measurement. As shown in Fig. 3.9, these transducers are located at the center of each of the four duct faces, at the section wnere the static pressure measurement was required, in accordance with ASHRAE Standard 33-78, section 5.1.9.

4 REFRIGERANT-SIDE MEASUREMENTS

Tne concentration of the transported oil in the evaporator is measured by sampling tests, in accordance with the procedures outlined in tne ASHRAE Standard - 69 [33].

4.1 Temperature: (Fig. 3.10)

Tne refrigerant temperature is measured by pre-calibrated, automatic, plantinum resistance thermometers. The location of the temperature measurements are shown in Fig. 3.1. The temperature sensors are equiped with a linearized bridge-amplifier and a scanner for selection of the range of operation, and for calibration.

4.2 Pressure: (Fig. 3.11)

Refrigerant (liquid and vapour) pressure is measured by strain gauge type (liquid/gas) pressure transducers, pre-calibrated for use in the pressure ranges encountered in the present experimental study.

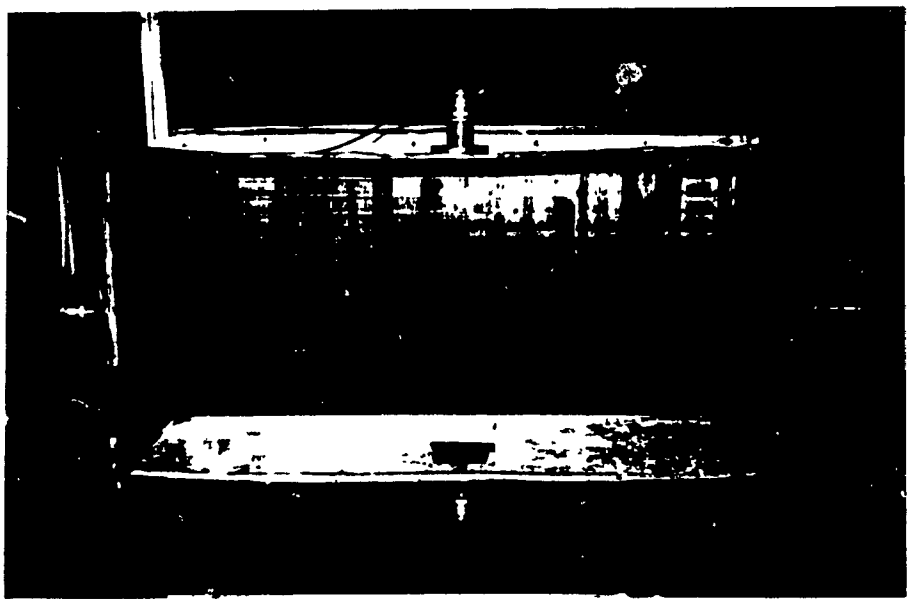

FIG. 3.9 LOCATION OF THE AIR STATIC PRESSURE TRANSDUCERS

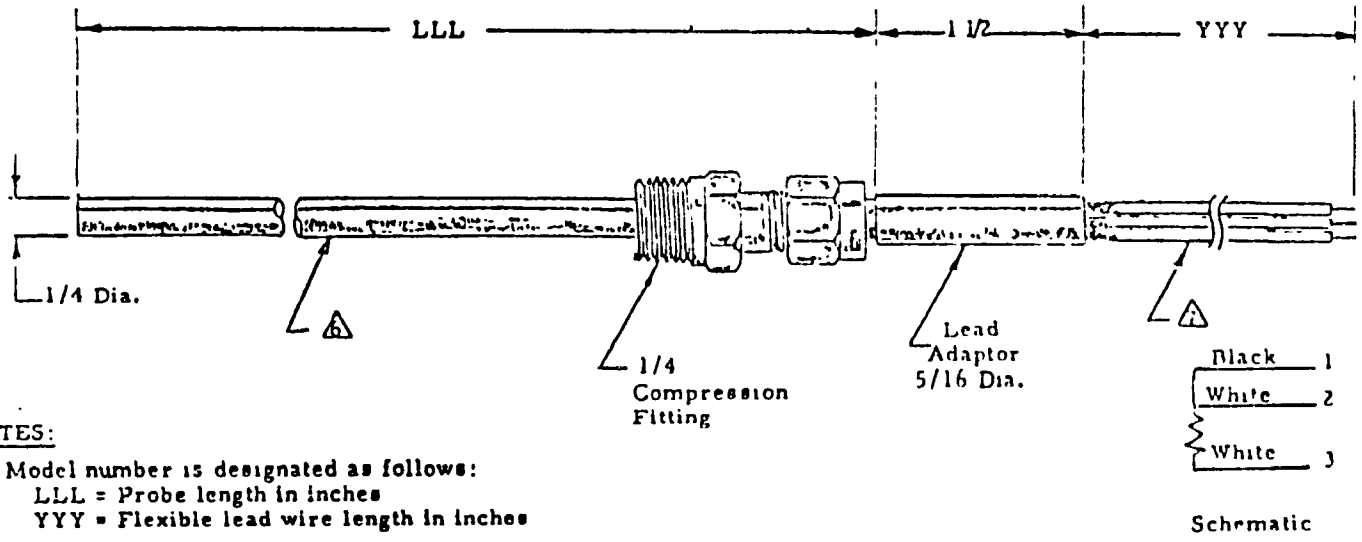

NOTES:

1. Model number is designated as follows:
   LLL = Probe length in inches
   YYY = Flexible lead wire length in inches
2. Sensing Element: Platinum
3. Sensor Type: Continuous platinum resistance element over full length LLL with no intermediate connections or thermoelectric junctions, fully enclosed
4. Ice Point Resistance: 100 ± 0.5 ohms
5. Temperature Range: -30 to 150°C

⚠ Sheath Material: 304 stainless steel

⚠ Flexible Lead Wire: 3 wires, 22 AWG nickel coated stranded copper, FEP teflon over each, equal internal lengths

FIG. 3.10 REFRIGERANT TEMPERATURE SENSOR [FROM DRAWING A-11180, HY-CAL ENGINEERING LTD., SANTA FE, CALIFORNIA]

FIG. 3.11 REFRIGERANT PRESSURE TRANSDUCER

[FROM DRAWING A-13180, HY-CAL ENGINEERING LTD., SANTA FE, CALIFORNIA]

SPECIFICATIONS

Pressure Ranges:	0-500 lbf/in^2
Pressure Limits:	150% rated pressure or 10,000 psi whichever is less will not damage the transducer
Excitation Voltage:	10 VDC or AC rms rated 15 VDC or AC rms maximum
Sensitivity:	2 mV/V ± 5%
Zero Balance:	Within ± 5% of full range output
Non-linearity:	± 0.25% of full range
Hysteresis:	± 0.1% of full range
Repeatability:	Better than ± 0.1% of full range
Resolution:	Infinite
Input Impedance:	350 ohms ± 5%
Output Impedance:	350 ohms ± 10%
Thermal Zero Shift:	±2% F.S./100°F
Thermal Sensitivity Shift:	±2% F.S./100°F
Temperature Range:	0°F to +200°F, or -18°C to +130°C
Pressure Connection:	7/16-20 UNF-3A male x 0.6" long
Electrical Connector:	Bendix PT02H-10-6P (mating half PT06A-10-6S(SR))
Weight:	13.5 ounces
Wetted Surfaces:	17-4PH Stainless Steel, Buna N "O" ring

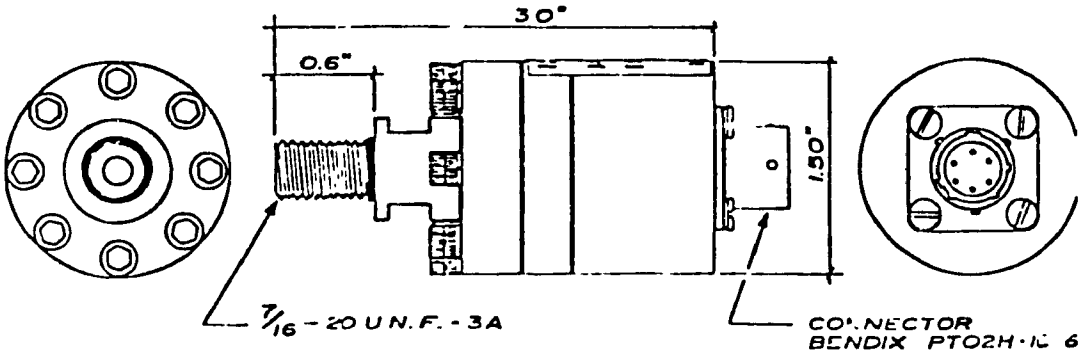

4.3 Flow-Rates:

Liquid refrigerant flow is measured by a variable-area flowmeter (rotameter) with two calibrated tubes to cover the flow range utilized in the tests. A liquid sub-cooler is installed ahead of the flow meter to prevent vaporizaton of the refrigerant, and sight-glasses are located before and after the flow meter to observe the existance of vapour bubbles, in accordance with the ASHRAE Standard 410-72.

5 TUBE SURFACE TEMPERATURE MEASUREMENT

Tube surface temperature is measured by copper constantan thermocouples soldered to the top and bottom portions of the tube cross-section (see Fig. 3.12); the average of the two reacings is used as the tube surface temperature. Tube surface temperature is measured at the entering and leaving sections of 4 different refrigerant circuits, and the average value is used in the data reduction calculations to minimize error.

6 CONDENSER WATER-SIDE MEASUREMENTS

6.1 Temperature:

Water temperature is measured by well-type temperature sensors located at the inlet and outlet of the water circuit of the condenser (see Fig. 3.1).

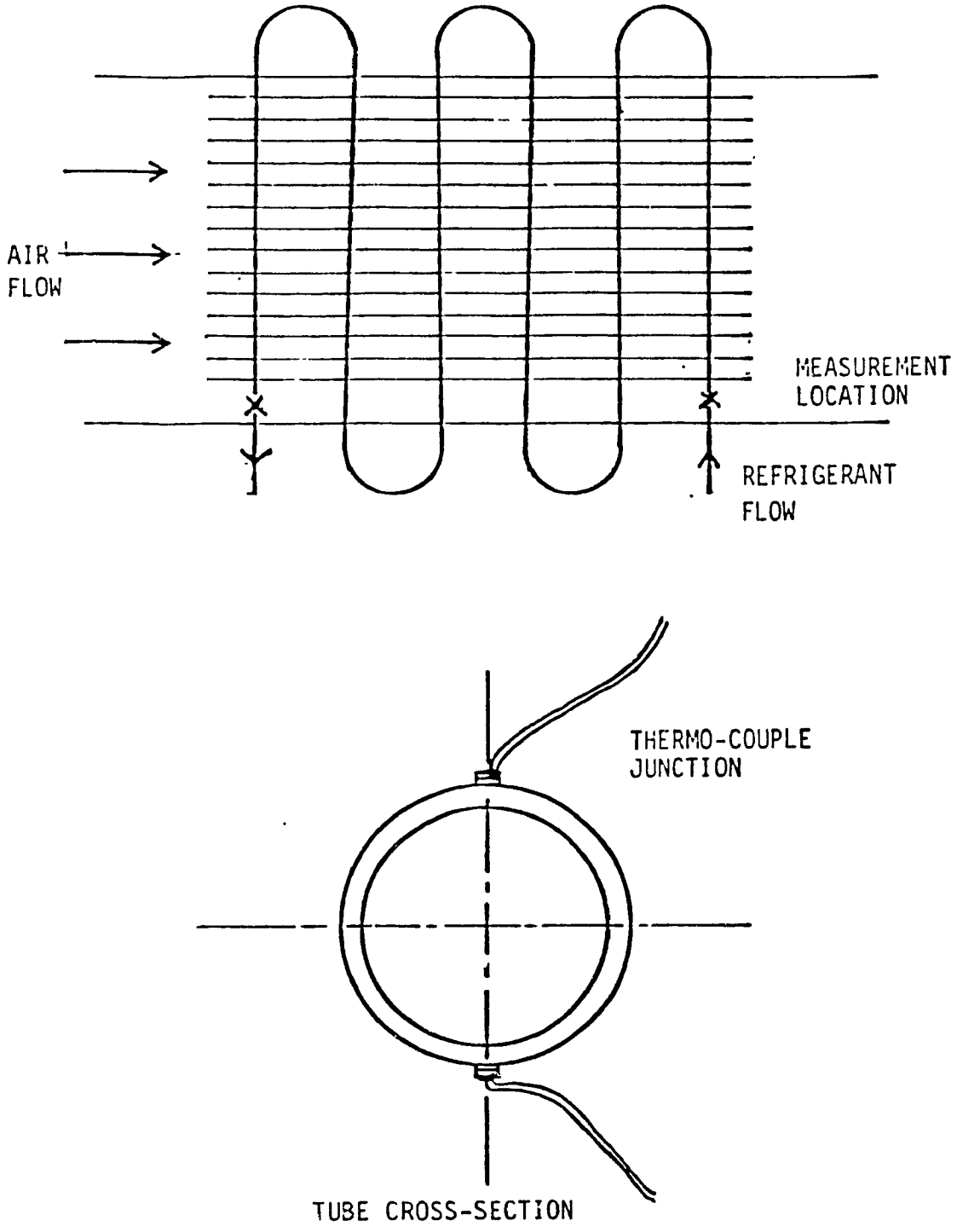

FIG. 3.12 TUBE SURFACE TEMPERATURE MEASUREMENT

7 DATA ACQUISTION SYSTEM

To monitor and record large number of data during the tests, an automatic data acquisition system was used. The system has the following major features:

A. A special reference junction for a range of thermocouples with linearizing circuit (see section 3.1).
B. Reference junctions for accepting signals through the linearizing transmitters from the platinum resistance thermometers.
C. Reference junctions for air static pressure transducers and refrigerant pressure transducers.
D. Reference junctions for relative humidity sensors.
E. Continuous and fixed time interval scanning of connected data points.
F. Printer connected to the scanning options listed in item 'E'.
G. Digital display of data connected to the scanning options listed under item 'E', or for display of one or more selected data points.

The uncertainty analysis for the experimental measurements are presented in Appendix-7.

CHAPTER 4

DESCRIPTION OF THE TEST PROCEDURE AND THE EXPERIMENTAL DATA REDUCTION METHOD

CHAPTER 4

In this chapter, description of the test coils, experimental procedure, and the data reduction method are presented.

4.1. DESCRIPTION OF THE TEST COILS

A photograph of a typical test coil is shown in Fig. 4.1, and details of the test coil specifications are presented in Appendix-1.

The test coils are constructed by a local manufacturer using standard construction practices recommended by ASHRAE [31]. The coil heat transfer surface is steam-jet cleaned, and the tube surface temperature measurement thermocouples are soldered (see Chapter 3, Section 3.4) prior to installation in the test facility.

The face area for all test coils is kept the same to facilitate the use of a single transition duct (item 2, Fig. 3.2).

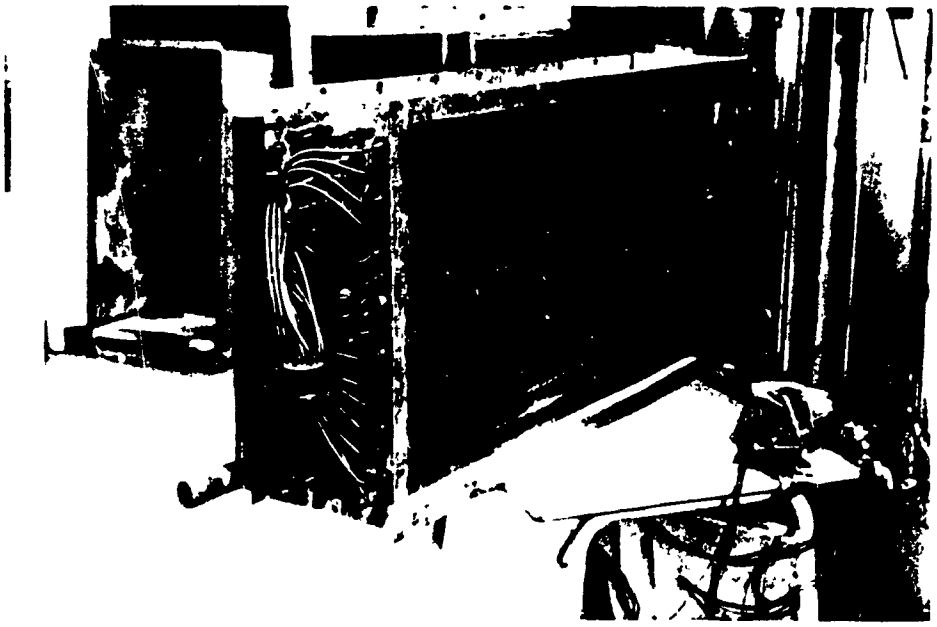

FIG. 4.1 TYPICAL TEST COIL

4.2. GENERAL TEST CONDITIONS

Tests are conducted for entering air conditions, generally in the range 26 to 28 °C dry bulb (D.B.) temperature and 18 to 20 °C wet bulb (W.B.) temperature which represent typical summer mixed air conditions in commercial buildings. For each of the coils (10 coils), tests are conducted for the air side fully dry and fully wet conditions; for each of the surface conditions, tests are conducted for three (3) different air flow velocities, in the range 1 to 4 m/s. For each velocity, four (4) sets of data are recorded at 20 minutes intervals, and the average values of the measurements are used in the data reduction calculations. On the refrigerant side, R-22 is used as the coolant in all tests. The leaving refrigerant vapour super heat is kept in the range of 5 to 6 °C.

4.3. TEST PROCEDURE

After installation of the test coil in the experimental apparatus (see Fig. 3.2), the variable air volume fan (item, 1, Fig. 3.2) is adjusted to provide the required volume flow rate. The air velocity at the coil face is then measured by pilot-tube traverse method. The tests are performed in accordance with the methods recommended by the A.R.I. Standard [32].

4.3.1 Air-Side Wet Surface Tests:

The refrigeration, heating and humidification systems are re-adjusted to provide fully wet surface conditions for the air-side of the coil heat transfer surface. The existance of the fully wet surface condition is ensured when the measured tube surface temperatures at the entering and leaving section of the coil (ts_1 and ts_2) in the direction of air flow, are lower than the corresponding air dew-point temperatures ($t_{a,1,sat}$) and ($t_{a,2,sat}$) calculated from the air dry bulb ($t_{a,1}$ and $t_{a,2}$) and wet bulb ($t'_{a,1}$) and ($t'_{a,2}$) temperature measurements (see Fig. 4.2).

Over a 20 minute test period, four (4) sets of measurements are made for each air flow velocity, and the average value of the measurements are recorded (see Appendix-5 - sample test data summary).

4.3.2 Air-Side Dry Surface Tests:

The heating, humidification and refrigeration systems are re-adjusted to provide fully dry surface conditions for the air-side which are ensured when the measured tube surface temperatures at the air-side entering and leaving sections are higher than the corresponding air dew-point temperatures. The rest of the experimental procedure is similar to that for the wet surface case (section 4.3.1).

4.4. TEST DATA REDUCTION METHOD

In this section, the calculation method for the average heat transfer and pressure drop factors for the air-side (for dry and wet surface conditions), and for the corresponding refrigerant side, is presented.

A schematic representation of the thermodynamic conditions for the working fluids entering and leaving the heat exchanger, is shown in Fig. 4.2. The variations of the air, tube surface and refrigerant temperatures along the tube surface, are shown in Fig. 4.3. A schematic representation of typical resistances to heat flow in finned-tube heat exchangers under wet surface conditions, is shown in Fig. 4.4. Equations for the heat transfer and flow surface area calculations are shown in Table 4.2.

The test data reduction method is based on the procedures recommended in Ref. [32].

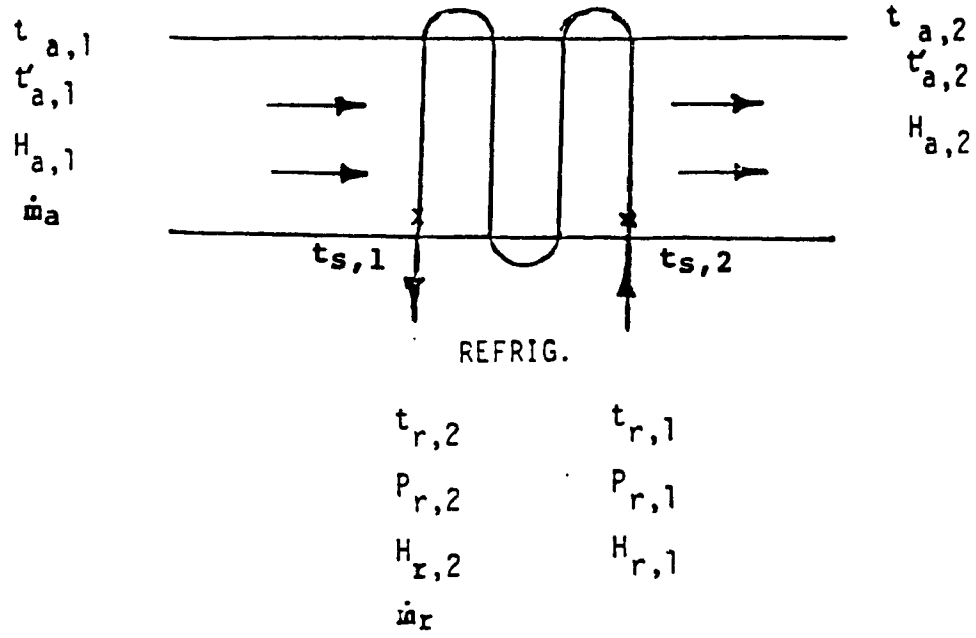

FIG. 4.2 WORKING FLUID PROPERTIES IN THE TEST COIL

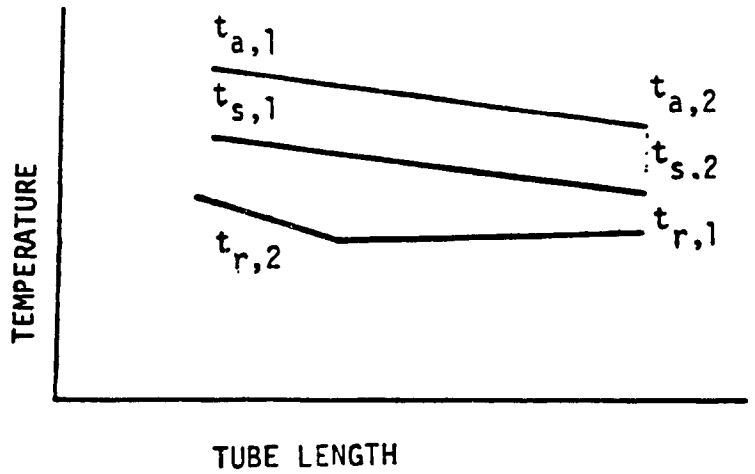

FIG. 4.3 AIR, TUBE SURFACE AND REFRIGERANT TEMPERATURE VARIATIONS ALONG THE TUBE CIRCUIT

NOTE: DIRECTION OF AIR FLOW PERPENDICULAR TO THE PLANE OF THE PAPER

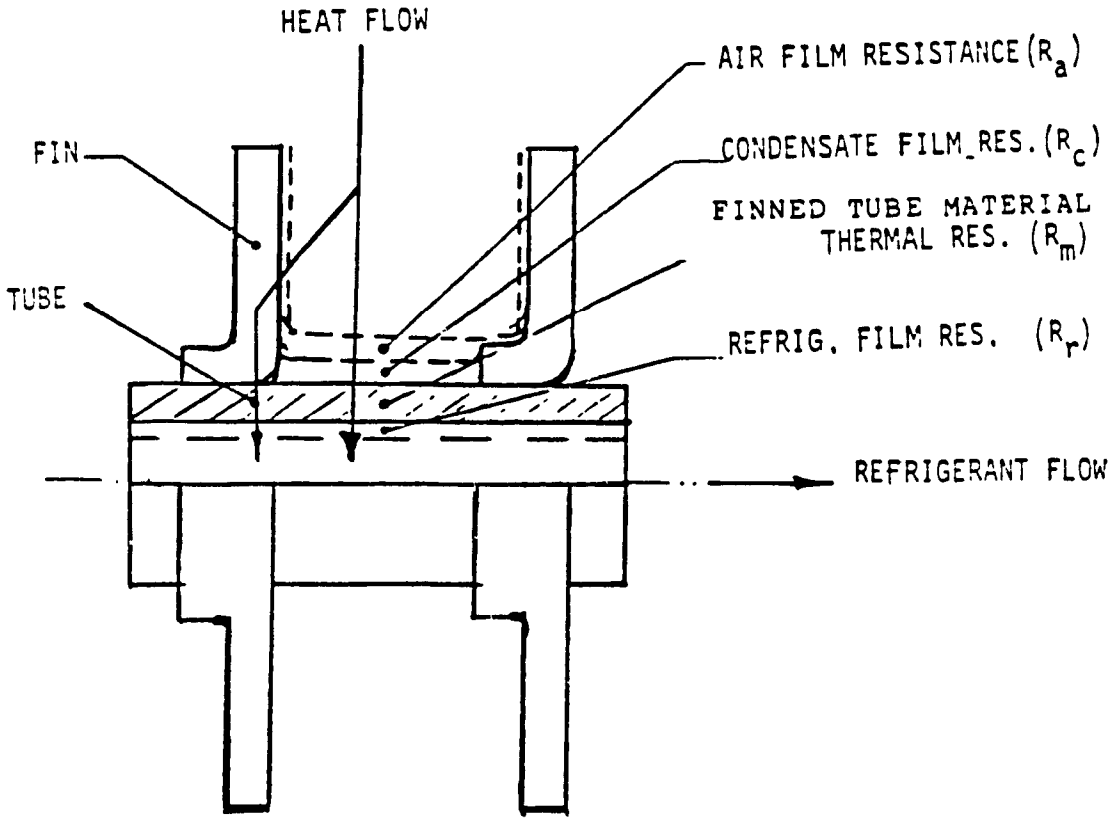

FIG. 4.4 RESISTANCES TO HEAT FLOW IN TYPICAL FINNED TUBE COILS

TABLE 4.1 EQUATIONS FOR THE HEAT TRANSFER SURFACE AND FLOW AREA CALCULATIONS [32] (See Fig. 2.2)

1. Primary Surface Area (A_p)

$$A_p = \pi D_o L_T (1 - N_f Y_f) N_{TR} N_R \tag{4.1}$$

2. Secondary Surface Area (A_s):

$$A_s = 2L_d L_F N_f - 0.5 \pi D_o^2 N_{TR} N_R \tag{4.2}$$

3. Total Air Side Surface Area (A_o):

$$A_o = A_s + A_p \tag{4.3}$$

4. Tube Inside Surface Area (A_I):

$$A_I = \pi D_I L_T N_T \tag{4.4}$$

5. Coil Face Area (A_f):

$$A_f = C_H C_W \tag{4.5}$$

6. Minimum Air Flow Area ($A_{m,f}$):

$$A_{m,f} = (C_W - N_f Y_f) [C_H - (N_{TR} D_o)] \tag{4.6}$$

The following assumptions are used in the calculation of the average heat transfer and pressure drop factors from the experimental data:

1) Uniform conditions for moist air exist at the entrance of the coil.

2) The condensate film thickness is assumed to be uniform (about 0.1 mm, see Chapter-2, Section-4 Item B). The moist air is assumed to completely mixed between the rows due to the cross-counter flow arrangement.

3) All the heat transfered from the air is assumed to be absorbed by the refrigerant.

4) The refrigerant is completely evaporated in the coil circuits.

5) The transported lubricating oil (about 2% by weight) is completely soluble in the refrigerant (R-22) at the evaporator temperature (about 4.4°C) [27].

6) The refrigerant liquid-vapour mixture (under the test conditions) is assumed to be homogeneous (see Chapter-2, Section 4.6).

Other assumptions used in the data reduction calculations are indicated at the appropriate sections.

A. DRY SURFACE TEST DATA REDUCTION METHOD:

The air-side dry surface capacity ($Q_{a,D}$) is given by:

$$Q_{a,D} = m_a C_p (t_{a,1} - t_{a,2}) \quad (4.7)$$

where

m_a - air mass flow rate (from the experimental data)

C_p - specific heat of air at the average air temperature

$t_{a,1}$ and $t_{a,2}$ - air temperature, entering and leaving the coil, respectively

The corresponding refrigerant-side capacity (Q_R) is given by:

$$Q_r = m_r (H_{r,2} - H_{r,1})$$

where

m_r - Refrigerant liquid mass flow rate (from the experimental data)

$H_{r,1}$ and $H_{r,2}$ - Entering and leaving refrigerant enthalpy, respectively (calculated from the refrigerant-side entering and leaving conditions, from the experimental data)

In order to minimize the experimental error, the average coil capacity (Q_D) is expressed as follows:

$$Q_D = (Q_{a,D} + Q_r)/2 \quad (4.9)$$

The heat balance (HBT) between the air-side and refrigerant side heat transfer capacities is given by:

$$(HBT) = 100\ (Q_{a,D} - Q_r)/Q_D \qquad (4.10)$$

In accordance with the standards [31 and 32], the performance test is considered invalid if the heat balance (HBT) exceeds the following range:

$$-5 < (HBT) < +5$$

The overall heat transfer coefficient ($h_{o,D}$) for the air-side dry surface conditions may be expressed as follows [32]:

$$h_{o,D} = q_D\ (c_{pa}) \ /\ A_o\ (LMHD)_{a,r} \qquad (4.11)$$

where,

$$(LMHD)_{a,r} = [(\Delta H)_{D,1} - (\Delta H)_{D,2}\ /\ \ln\ (\Delta H_{D,1}) / (\Delta H)_{D,2}] \qquad (4.12)$$

$$(\Delta H)_{D,1} = (H_{a,1} - H_{r,2})$$

$$(\Delta H)_{D,2} = (H_{a,2} - H_{r,1})$$

For the cross-counter flow arrangement, the correction factor for $(LMHD)_{a,r}$ is approximately equal to one [7] and

$(LMHD)_{a,r}$ - Logarithmic mean enthalpy difference between the air and the refrigerant streams (from the experimental data)

A_o - Defined at Eqn. 4.3

$H_{a,1}$ and $H_{a,2}$ - Air enthalpy at the entering and leaving conditions respectively (from the experimental data).

$H_{r,1}$ and $H_{r,2}$ - Refrigerant enthalpy at the entering and leaving conditions, respectively (from the experimental data).

The heat transfer from the air to the refrigerant side occurs through two parallel paths (see Fig. 4.4), one through the bare tube surface, and the other through the fin surface. The overall resistance to heat flow ($R_{O,D}$) may then be expressed as follows [7]:

$$R_{O,D} = 1/h_{O,D} = (A_o t_t/A_p K_t) + A_o/(h_t A_p + h_f A_s n_{f,D}) + (Ao/A_I h_r) \quad (4.13)$$

where

$$\eta_{f,D} = (\phi A_s + A_p)/A_o \quad (4.14)$$

and

A_p, A_s, A_i and A_o - Heat transfer surface areas - defined in Table 4.1.

h_t and h_f - Air side convective heat transfer coefficient for the bare tube portion and for the finned portion, respectively, for the air-side dry surface conditions.

h_r - Refrigerant-side average two-phase heat transfer coefficient, assumed to be uniform along the tube circuit, for low refrigerant mass velocities considered ($G_{r,l} < 120$ kg/m^{2}s) [4]

t_t and k_t - Thickness and thermal conductivity of the tube material respectively.

$\eta_{f,D}$ - Fin efficiency for dry surface conditions.

ϕ - Fin efficiency parameter determined from the procedure outlined in Ref. [32].

Since the primary surface area (A_p) is about 5% of the total surface area (A_o) for the coil configuration considered in the present study, it is assumed that the air-side dry surface heat transfer coefficient (h_{aD}) = h_f = h_t; hence, the Eqn. 4.13 may be modified as follows [32]:

$$R_{o,D} = 1/h_{o,D} = (R_m + R_{a,D} + R_r) \tag{4.15}$$

where

$$R_m = (A_o/A_p)(t_t/K_t) \tag{4.16}$$

$$R_{a,D} = [A_o/(A_p + c_{f,D}\ A_s)]/h_{a,D} \tag{4.17}$$

$$R_r = (A_o/A_I)/h_r \tag{4.18}$$

R_m and $R_{a,D}$ are the resistances to heat flow from the tube portion and the finned portion (respectively), and R_r is the thermal resistance due to the refrigerant film. Since the fin surface area is 95% of the total surface, the air-side heat transer coefficient ($h_{a,D}$) may be expressed as follows [32]:

$$1/R_{a,D} = h_{a,D} = Q_D/A_o\ (LMTD)_{a,s} \tag{4.19}$$

where

$$(LMTD)_{a,s} = [(\Delta t)_1 - (\Delta t)_2] \ / \ \ln [(\Delta t)_1/(\Delta t)_2] \tag{4.20}$$

$$(\Delta t)_1 = (t_{a,1} - t_{s,1}) \tag{4.21}$$

$$(\Delta t)_2 = (t_{a,2} - t_{s,2}) \tag{4.22}$$

and

Q_D - Defined at Eqn. (4.9)

$t_{a,1}$ and $t_{a,2}$ - Air dry bulb temperature, entering and leaving the coil, respectively (from the experimental data).

$t_{s,1}$ and $t_{s,2}$ - Tube surface temperature, entering and leaving the coil, respectively (from the experimental data).

Thus, $R_{o,D}$ and $R_{a,D}$ may be computed from the experimental data, (Eqns. 4.11 and 4.19) and R_m is computed from Eqn. 4.16. The refrigerant-side average (two-phase) thermal resistance (R_r) may then be computed [(from Eqn. (4.15)] as follows: [32]:

$$R_r = R_{o,D} - (R_{a,D} + R_m) \tag{4.23}$$

The corresponding average two-phase heat transfer coefficient (h_r) may be expressed as follows:

$$h_r = (A_o/A_I)/R_r \tag{4.24}$$

Air-side non-dimensional dry surface heat transfer factor ($j_{a,D}$) is given (from Eqn. 2.1):

$$J_{a,D} = h_{a,D}\, Pr^{2/3} /G_{m,f}\, C_{Pa} \tag{4.25}$$

where

$h_{a,D}$ - defined at 4.19

Pr - air Prandtl number, at the average air D.B. temp.

$G_{m,f}$ - air mass flux, based on the minimum flow area

$C_{p,a}$ - air specific heat, at the average air D.B. temp.

The refrigerant-side average Nusselt number (Nu_r) may be expressed in terms of the corresponding average two-phase heat transfer coefficient (h_r) and the refrigerant liquid thermal conductivity ($k_{r,l}$) as follows (see Chapter-2, Section 4.6) [15]:

$$Nu_r = h_r D_I / K_{r,l} \qquad (4.26)$$

Eqn. 4.26 is valid in the range $10^9 < Re^2_{r,l} K_f < 0.7 \times 10^{12}$, which is the case for the present study,

where,

h_r - defined at Eqn. 4.24

$K_{r,l}$ - refrigerant liquid thermal conductivity, at the average refrigerant temp. [The change in the refrigerant thermal conductivity due to the oil (2% by weight) is neglected]

D_I - tube inside diameter.

$Re_{r,l}$ and K_f - defined at Eqn. 2.31 and 2.32, respectively.

The air side pressure drop factor ($f_{a,D}$) is computed from Eqn. 2.4, and the non-dimensional refrigerant-side pressure drop factor (f_r) is computed from Eqn. 2.33 (from the experimental data).

The dry surface experimental data are shown in Appendix-3, and a discussion of the results is presented in Chapter-5.

B. AIR-SIDE WET SURFACE TEST DATA REDUCTION METHOD:

Air-side wet surface total heat transfer (latent and sensible) capacity ($Q_{a,w}$) is given by [32]:

$$Q_{a,w} = m_a (H_{a,2} - H_{a,1}) \qquad (4.27)$$

where

m_a - air mass flow rate (from experimental data).

$H_{a,2}$, $H_{a,1}$ - leaving and entering air enthalpy, respectively.

The refrigerant-side heat transfer capacity (Q_r) is given by eqn. 4.8. The average coil capacity (Q_w) for the air-side wet surface conditions is given by:

$$Q_w = (Q_{a,w} + Q_r)/2 \qquad (4.28)$$

The heat balance between the air-side and the refrigerant-side (HBT) is given by:

$$(HBT) = 100 (Q_{a,w} - Q_r)/Q_w \qquad (4.29)$$

The overall heat transfer coefficient ($h_{o,w}$) for the air-side wet surface conditions (neglecting the heat content in the condensate) may be expressed as follows [32]:

$$h_{o,w} = Q_w C_p / A_o (LMHD)_{a,r} \quad (4.30)$$

where

$$(LMHD)_{a,r} = [(\Delta H)_{w,1} - (\Delta H)_{w,2}] / \ln [(\Delta H)_{w,1}/(\Delta H)_{w,2}] \quad (4.31)$$

$$(\Delta H)_{w,1} = (H_{a,1} - H_{r,2}) \quad (4.32)$$

$$(\Delta H)_{w,2} = (H_{a,2} - H_{r,1})$$

$H_{a,1}$ and $H_{a,2}$ - Air enthalpy entering and leaving the coil, respectively, from the wet surface tests.

$H_{r,1}$ and $H_{r,2}$ - Refrigerant enthalpy, entering and leaving coil, for the air-side wet surface tests.

The enthalpy potential method described in detail in Ref. [7], is used for computing the air-side wet surface heat transfer coefficient ($h_{a,w}$) with the assumption that the saturation curve in the psychrometric chart is a straight line over a small interval of temperature. The slope of the saturation curve (b) between two temperatures (t_1 and t_2) and the corresponding saturated enthalpies ($H_{1,sat}$ and $H_{2,sat}$), may be expressed as follows:

$$b = [(H_{1,sat}) - (H_{2,sat})]/(t_1 - t_2) \quad (4.33)$$

The overall thermal resistance ($R_{o,w}$) for the air-side wet surface conditions, may be expressed as follows [7]:

$$R_{o,w} = 1/h_{o,w} = b_{a,w}/(h_{a,w}\eta_{f,w}) + b_t(A_o/A_p)\, t_t/k_f + b_r(A_o/A_I)/h_r \quad (4.34)$$

where,

$$h_{a,w} = 1/[(C_{p,a}/b_c h_c) + (t_c/k_c)] \qquad (4.35)$$

and $b_{a,w}$, b_t, b_r, b_c - slope of the saturation curve at the temperature of the fins, bare tube-surface, refrigerant and the condensate film, respectively.

$h_{a,w}$ - air-side wet surface heat transfer coefficient

t_t, k_t, h_r - defined at Eqn. 4.13

$\eta_{f,w}$ - fin efficiency, computed in accordance with the procedure defined in Ref. [32].

h_c, t_c, k_c - the heat transfer coefficient, thickness, and - the thermal conductivity of the condensate film, respectively. It is assumed that t_c = 0.1 mm and is uniform on the air-side surface.

From Eqns. 4.30 and 4.35 the air-side and the refrigerant-side average heat transfer coefficient ($h_{a,w}$ and h_r) are calculated (similar to the method used for the dry surface condition). The air-side total heattransfer factor ($j_{a,w}$) is given by [13]:

$$J_{a,w} = [h_{a,w}/G_{m,f}\, C_{p,a}]\, Sc^{2/3} \qquad (4.36)$$

where

$h_{a,w}$ - given by Eqn. 4.35

$G_{m,f}$ - air mass velocity based on the minimum flow area ($A_{m,f}$)

Sc - Schmidt number (about 0.6 in the normal air conditioning range) [13].

The air-side wet surface pressure drop factor ($f_{a,w}$) is computed from Eqn. 2.4 The methods for calculation of the refrigerant side Nusselt number (Nu_r) and the pressure drop factor (f_r) are similar to those for the corresponding air-side dry surface case.

The experimental data for the wet surface conditions are shown in Appendix 3. Sample data reduction calculations are shown in Appendix-5.

A discussion of the experimental results from the present study, and comparisons with relevant data from the existing studies, are presented in Chapter-5.

CHAPTER 5

ANALYSIS OF THE EXPERIMENTAL RESULTS

CHAPTER - 5

ANALYSIS OF THE EXPERIMENTAL RESULTS

Analysis of the test results, and a discussion of the effects of coil geometric parameters and the fluid flow parameters on the average heat transfer and pressure drop factors, are presented in this chapter. Comparison is made with relevant experimental data from the existing studies.

The experimental data from the present study are shown in Appendix-3, and the corresponding coil geometric data are shown in Appendix-1. The experimental data from the existing studies used for comparison are presented in Chapter-2. A comparison of the air-side dry and wet surface test results is presented in Section-6 of this chapter.

1. AIR-SIDE DRY SURFACE AVERAGE HEAT TRANSFER FACTOR ($j_{a,D}$):

The experimental data for the air-side dry surface heat transfer factor ($j_{a,D}$) from the present study and the relevant data from the existing studies [7 and 13] are shown in Fig. 5.1. The test data and results may be summarized as follows:

i) For a given coil configuration (P_s, D_o, S_L and S_T), the air side surface average heat transfer factor ($j_{a,D}$) is a decreasing linear function of the air flow Reynolds number (Re_a).

ii) For a given tube diameter (D_o), tube spacing (S_L and S_T) and air flow Reynolds number, when the fin density (P_s) is increased (in the range $3.1 \leq P_s \leq 5.5$ fins/cm), the corresponding $j_{a,D}$ decreases (see Table 5.1) due to increase in the air mass flux ($G_{m,f}$) caused by the reduction in the flow area. ($j_{a,D} = h_{a,D} P_r^{2/3}/G_{m,f} Cp_a$)

iii) For a given coil configuration, the effect of the number of tube rows (N_r) on $j_{a,D}$ is insignificant (2 to 8%) in the test range considered.

For a given fin density (P_s), the effects of D_o, S_L and S_T on ($j_{a,D}$) are insignificant in the test range considered; for example, for 4.7 fins/cm, the reduction in $j_{a,D}$ is almost the same (from 14% to 11%, See Table 5.1a) for the three coils considered (curves 3, 6 and 8 - See Fig 5.1) inspite the variation in these parameters. Similarly, for a given Reynolds number when P_s is increased, the corresponding reduction in $J_{a,d}$ from the present and McQuiston studies is also observed to be independent of the variations in D_o, S_L and S_T (See Table 5.1 B).

Therefore when fin density is increased, an increase in mass flux ($G_{m,f}$) caused by the decrease in free flow area ($A_{m,f}$) is the primary reason for reduction in $J_{a,D}$ and the changes in the other geometric parameters (D_o, S_L and S_T) do not have a siginificant effect on $J_{a,D}$ in the test range considered.

For a given air flow Reynolds number, when the fin density is increased (for a given D_o, S_L and S_T) while the average $j_{a,D}$ may decrease, the corresponding heat transfer rate may increase due to increase in the heat transfer surface area (A_o). Hence, for energy effective design of DX-coils, the effect of the fin density on both the heat transfer factor ($J_{a,D}$) and the heat transfer rate (Q_D) should be investigated.

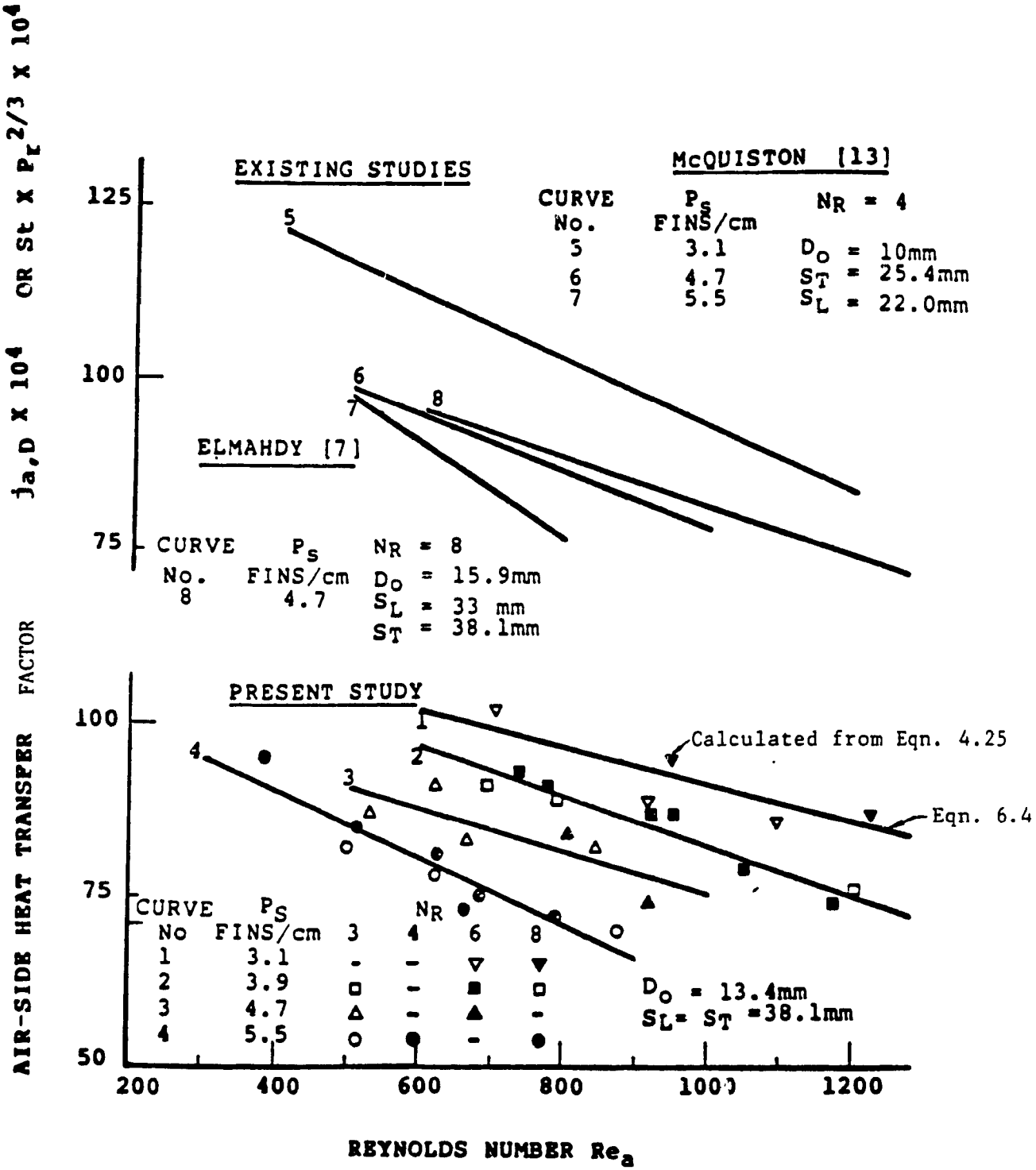

FIG. 5.1 AIR-SIDE DRY SURFACE HEAT TRANSFER FACTOR ($j_{A,D}$)
EXPERIMENTAL DATA, PRESENT AND EXISTING STUDIES

TABLE 5.1 **COMPARISON OF THE EXPERIMENTAL DATA FROM THE PRESENT AND EXISTING STUDIES [13 and 7].**

AIR-SIDE DRY SURFACE AVERAGE HEAT TRANSFER FACTOR (see Fig. 5.1)

A. EFFECTS OF THE REYNOLDS NUMBER (Re_a) on $j_{a,D}$

Fin Density (P_s) (fins/cm)	Increase in the Reynolds number (Re_a) from - to	Percent change in $j_{a,D}$		
		Present study	McQuiston study [13]	Elmahdy study [7]
3.1	700 - 1100	-13%	-11%	--
4.7	600 - 900	-14%	-11%	-12%
5.5	500 - 900	-18%	-18%	--

B. EFFECT OF THE FIN DENSITY (P_s) on $j_{a,D}$

Re_a	increase in P_s (fins/cm) from - to	present change in $j_{a,D}$	
		Present study	McQuiston Study [13]
600	3.1 to 5.5	-20%	-20%
800	3.1 to 5.5	-24%	-24%

2. AIR-SIDE DRY SURFACE AVERAGE PRESSURE DROP FACTOR ($f_{a,D}$):

The experimental data for the air-side dry surface average pressure drop factor ($f_{a,D}$) for the present and the existing studies, are shown in Fig. 5.2. The test results may be summarized as follows:

i) For a given coil configuration (P_s, D_o, S_L and S_T), the average pressure drop factor ($f_{a,D}$) is a decreasing linear function of the square of the Reynolds number (Re^2).

ii) For a given D_o, S_L, S_T and Re_a, when the fin density is increased (in the range $3.1 \leq P_s \leq 5.5$), the corresponding $f_{a,D}$ decreases (see Table 5.2-B) due to the increasing effect of the laminar boundary layer on the fin surface over the turbulence caused by the tubes [18].

iii) For a given coil configuration, the effect of the tube rows (in the range $3 \leq N_R \leq 8$) on $f_{a,D}$ is insignificant (about 5%).

For a given fin density (P_s) in a given range on Re_a, (See table 5.2A) the percentage decrease in $f_{a,D}$ for coils with smaller D_o, S_L and S_T (curves 5, 6 and 7, Fig. 5.2) is twice as high as that for the coils from the present study (See Fig. 5.1 for coil physical data). When the S_L and S_T are smaller, the space available for full development of vortices due to tubes is smaller, which results in reduced turbulence level and reduced pressure drop and hence smaller $f_{a,D}$.

This is due to increasing effect of the laminar boundary layer combined with decreasing influence of the turbulence, as explained in the previous paragragh.

That is, increase in fin density P_s and reduction in D_o, S_L and S_T result in a smaller $f_{a,D}$ and hence reduced air pressure drop across the coil, which is an advantage.

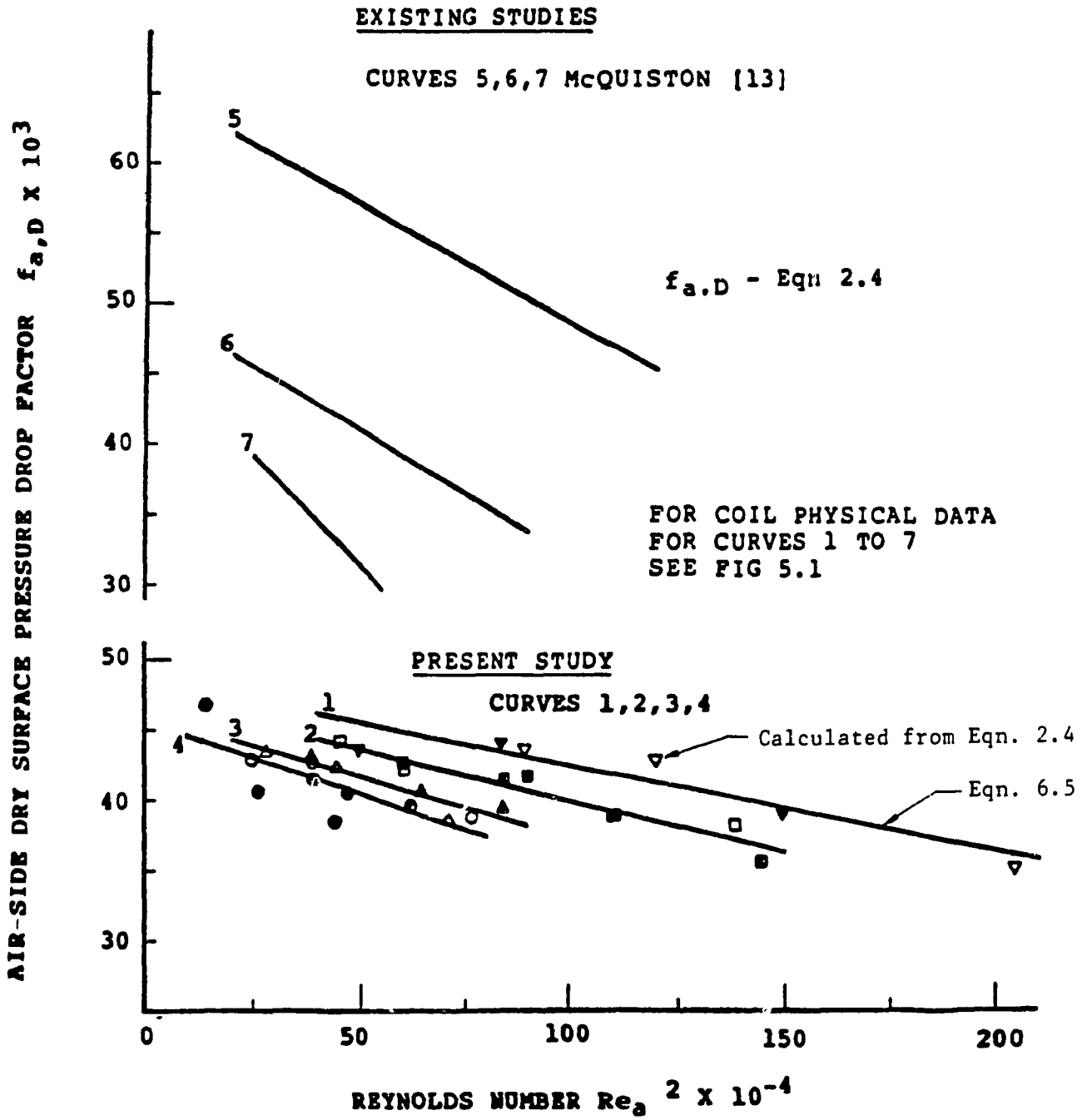

FIG 5.2 AIR-SIDE DRY SURFACE PRESSURE DROP FACTOR ($f_{a,D}$) EXPERIMENTAL DATA, PRESENT AND EXISTING STUDIES

TABLE 5.2 COMPARISON OF THE EXPERIMENTAL DATA FROM THE PRESENT AND THE EXISTING STUDIES [13]

AIR-SIDE DRY SURFACE AVERAGE PRESSURE DROP FACTOR ($f_{a,D}$)

A. EFFECT OF AIR FLOW REYNOLDS NUMBER ON $f_{a,D}$

Fin Density	Increase in the Reynolds Number ($Re^2_a \times 10^{-4}$) from - to	Percent Change in $f_{a,D}$	
		present study	McQuiston Study [13]
3.1	50 - 100	-7%	-15%
4.7	30 - 70	-8%	-16%
5.5	30 - 50	-9%	-18%

B. EFFECT OF THE FIN DENSITY (P_s) on $f_{a,D}$

$Re^2_a \times 10^{-4}$	Increase in P_s (fins/cm) from - to	Percent change in $f_{a,D}$	
		present study	McQuiston study [13]
40	3.1 - 5.5	- 10%	- 40%
55	3.1 - 5.5	- 15%	- 45%

3. AIR-SIDE WET SURFACE AVERAGE HEAT TRANSFER FACTOR ($j_{a,w}$)

The experimental data for the air-side wet surface average heat transfer factor ($j_{a,w}$), for the present and the existing studies [7, and 13], are shown in Fig. 5.3. The test results may be summarized as follows:

i) For a given coil configuration (P_s, D_o, S_L and S_T), the air-side wet surface heat transfer factor ($j_{a,w}$) is a decreasing linear function of the Reynolds number (Re_a).

ii) For a given D_o, S_L, S_T and Re_a, when the fin density (P_s) is increased, the corresponding $j_{a,w}$ decreases (similar to the dry surface case).

iii) For a given coil configuration and Re_a, the $j_{a,w}$ is 20 to 40% higher than the corresponding, $j_{a,D}$ due to the simultaneous latent and sensible heat transfer.

iv) The effect of tube rows on $j_{a,w}$ is found to be insignificant (2 to 8%) in the test range considered ($3 < N_R < 8$) this is similar to the effect found for the corresponding dry surface case.

From Table 5.3, at low fin densities (3.1 fins/cm or less), the reduction in $j_{a,w}$ corresponding to a given increase in Re_a is approximately the same for the coils tested, inspite of smaller D_o, S_L and S_T for the coils tested by McQuiston. As the fin density is increased, the reduction in $j_{a,w}$ increases for all coils tested.

This increase can be attributed to the additional turbulence caused by the condensate film. However, the percentage reduction in $j_{a,w}$ for the coils tested in the present study (higher D_o, S_L and S_T) is much higher compared to that for coils tested by McQuiston. This can be attributed to lower levels of turbulence caused by the tubes in coils with smaller D_o, S_L and S_T which offer smaller resistence, resulting in smaller reduction in $j_{a,w}$.

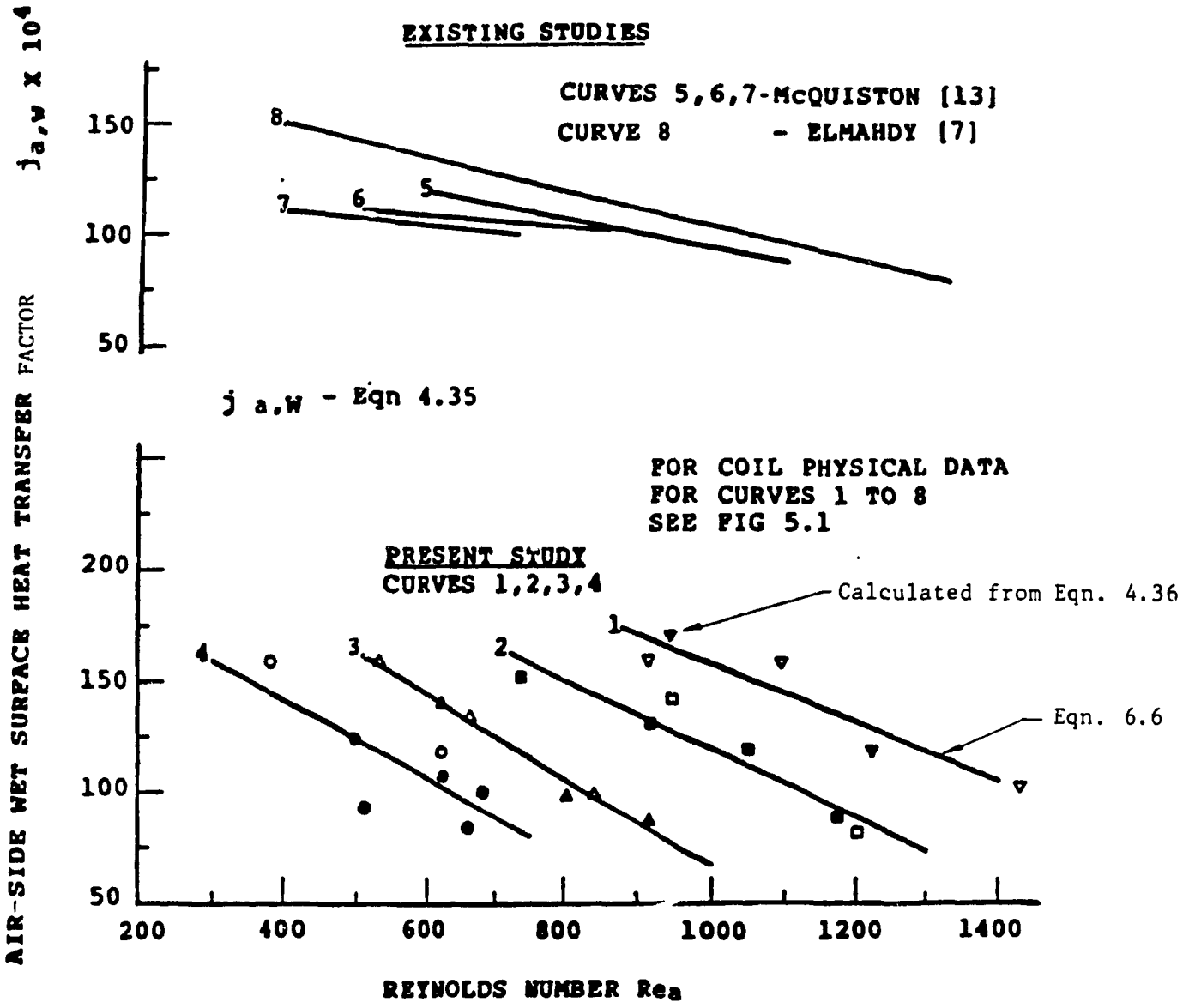

FIG 5.3 AIR-SIDE WET SURFACE HEAT TRANSFER FACTOR ($j_{a,W}$)
EXPERIMENTAL DATA, PRESENT AND EXISTING STUDIES

TABLE 5.3 **COMPARISON OF THE EXPERIMENTAL DATA FROM THE PRESENT AND THE EXISTING STUDIES**

AIR-SIDE WET SURFACE HEAT TRANSFER FACTOR ($j_{a,w}$)

EFFECT OF REYNOLDS NUMBER (Re_a) on $j_{a,w}$

Fin density (P_s) fins/cm	Increase in the Reynolds number (Re_a) from - to	Present change in $j_{a,w}$		
		Present study	McQuiston study [13]	Elmahdy study [7]
3.1	900 - 1100	-14%	-11%	—
4.7	500 - 800	-25%	-13%	11%
5.5	400 - 700	-40%	-15%	—
	D_o (mm)	13.4	10.0	15.9
	S_L	38.1	22.0	33.0
	S_T	38.1	25.4	38.1

4. AIR-SIDE WET SURFACE AVERAGE PRESSURE DROP FACTOR ($f_{a,w}$):

The experimental data for the average pressure drop factor ($f_{a,w}$) for the present and the existing studies are shown in Fig. 5.4. The test results may be summarized as follows:

i) For a given coil configuration, the $f_{a,w}$ is a decreasing linear function of Re_a^2

ii) For a given Re_a, D_o, S_L and S_T, when the fin density is increased, the corresponding $f_{a,w}$ decreases (similar to the dry surface case).

iii) The effect of the tube rows on $f_{a,w}$ is also found to be negligible (2 to 6%).

iv) For a given coil configuration and Reynolds number (Re_a), the average $f_{a,w}$ is generally higher (20 to 30%) than that for the corresponding dry surface case due to the increased surface roughness caused by the condensate film.

Comparing Tables 5.2 and 5.4 (for the corresponding dry surface tests) the effects of increase in fin density and smaller D_o, S_L and S_T are similar for both dry and wet surface conditions. However at high fin density (5.5 fin/cm) the percent reduction in $f_{a,w}$ for the coil with smaller D_o, S_L and S_T (coils used by McQuiston) is only 5% than that for the present study.

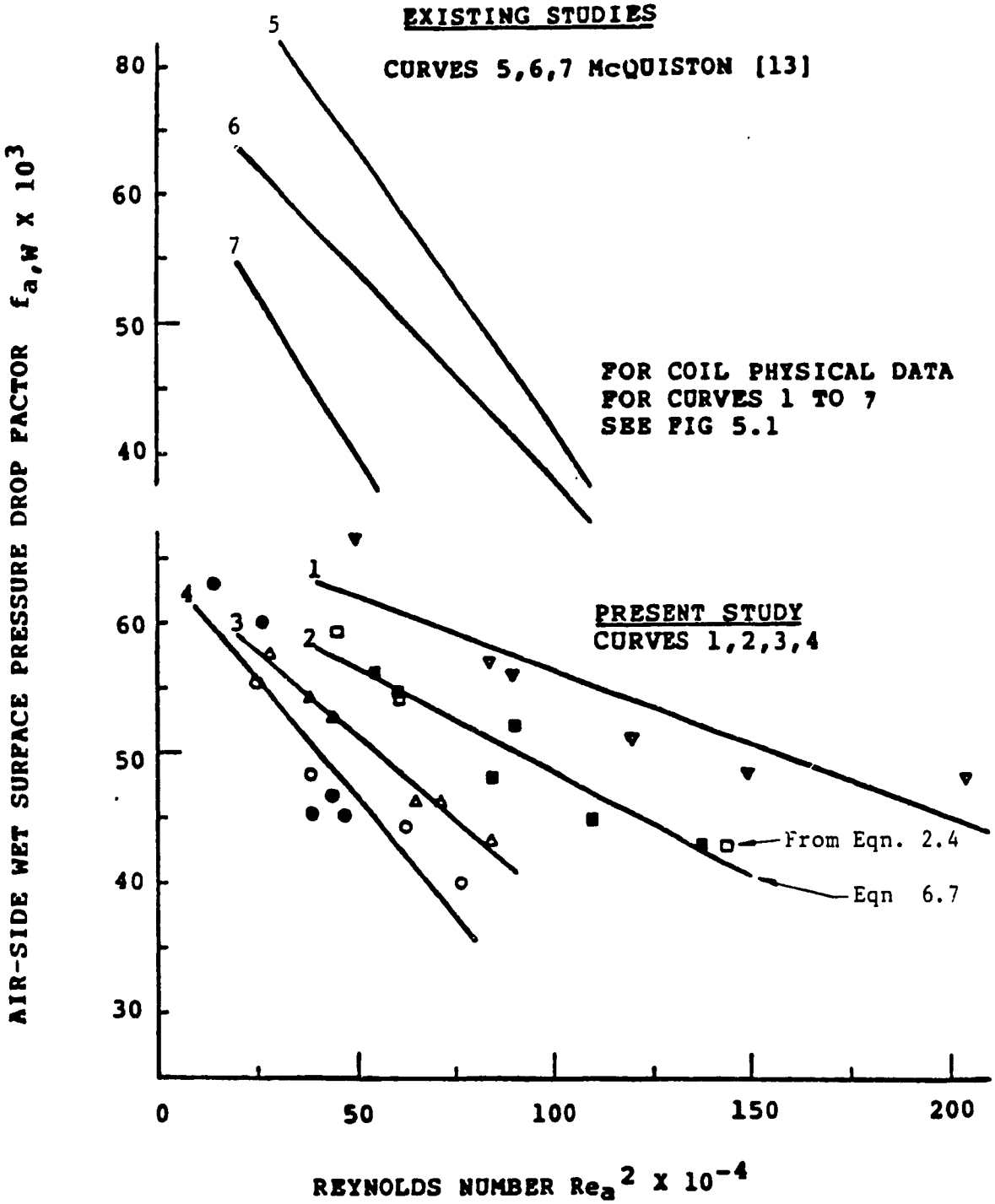

FIG 5.4 AIR-SIDE WET SURFACE PRESSURE DROP FACTOR ($f_{a,w}$)
EXPERIMENTAL DATA, PRESENT AND EXISTING STUDIES

TABLE 5.4 COMPARISON OF THE EXPERIMENTAL DATA FROM THE PRESENT AND THE EXSITING STUDIES -

AIR-SIDE WET SURFACE PRESSURE DROP FACTOR ($f_{a,w}$)

Fin density (P_s) fins/cm	Increase in Reynolds number ($Re_a^2 \times 10^{-4}$)	Percent change in $f_{a,w}$	
		Present study	McQuiston study [13]
3.1	50 - 100	- 15%	- 35%
4.7	25 - 75	- 20%	- 30%
5.5	25 - 50	- 20%	- 25%

5. REFRIGERANT-SIDE TEST RESULTS:

In this section, a discussion of the refrigerant-side test results for the air-side dry and wet surface tests, are presented and comparisons are made with the experimental data from the existing studies.

The experimental data for the refrigerant liquid flow Reynolds number ($Re_{r,l}$ - Eqn. 2.31) and the corresponding boiling number (k_f - Eqn. 2.32) for the air-side dry and wet surface tests are shown in Figs. 5.5 and 5.6 respectively. For a given circuit length (L_e), the average boiling number (K_f) is higher for the wet surface tests (compared to the corresponding dry surface tests) due to higher air-side heat flux (q).

For both the air-side dry and wet surface tests (Fig. 5.5 or 5.6), the average boiling number is dependent on the circuit length. The boiling number decreases when the circuit length is increased, due to reduction in the corresponding heat flux (q).

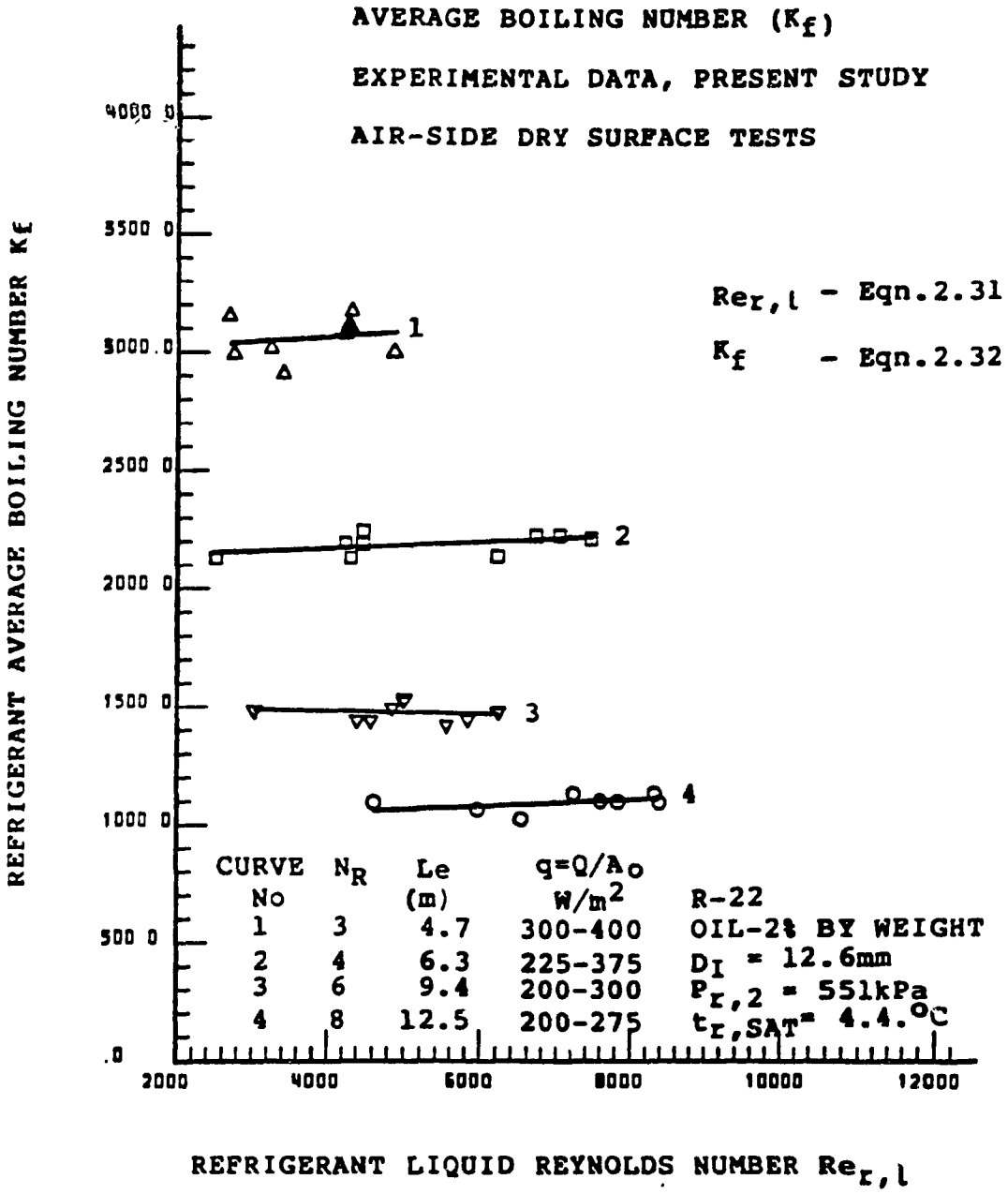

FIG. 5.5 REFRIGERANT AVERAGE BOILING NUMBER (K_f)
AIR-SIDE DRY SURFACE TESTS, PRESENT STUDY

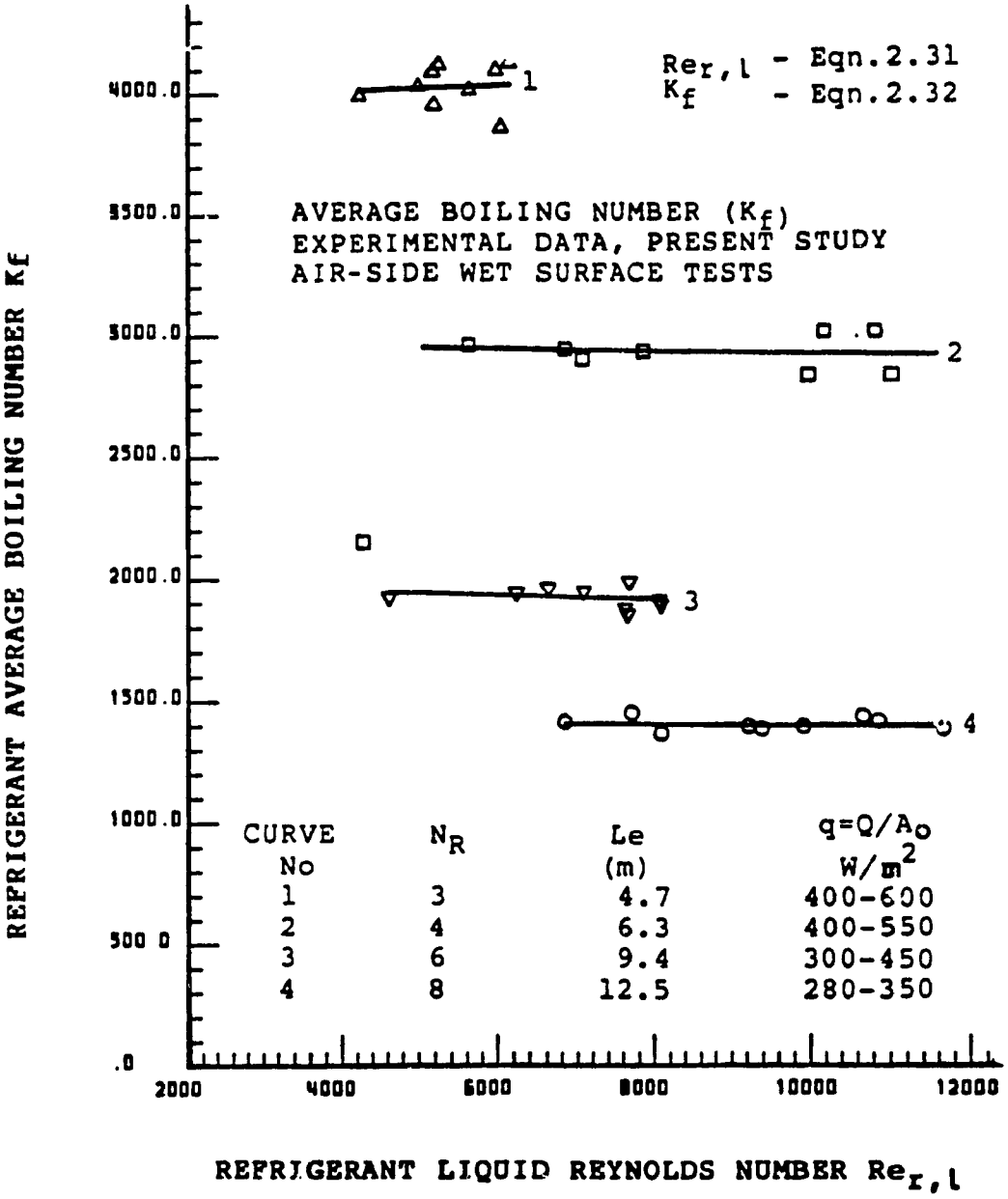

FIG. 5.6 REFRIGERANT AVERAGE BOILING NUMBER (K_f)
AIR-SIDE WET SURFACE TESTS, PRESENT STUDY

The heat transfer parameter ($Re^2_{r,l}K_f$) and the pressure drop parameter ($Re_{r,l}/K_f$) proposed by Pierre [15 and 16] are empirical non-dimensional correlations developed from comparison of the experimental data for average heat transfer and pressure drop coefficients for boiling refrigerants in tubes. No explanation of the physical significance of these parameters was offered either by Pierre or by others [4, 12, B45, B50, B52, B53] who used these parameters in the analysis of their experimental data. However, these parameters provided a good means for comparison of the refrigerant-side heat transfer and pressure drop factors. In addition, Anderson et al [4] compared their experimental data with the results obtained from a number of existing correlations for prediction of the refrigerant-side heat transfer and pressure drop, and stated that "among the correlations considered, those proposed by Pierre show the best agreement" for the range of refrigerant mass flux typically found in air conditioning applications. Hence, these heat transfer and pressure drop parameters proposed by Pierre were used in the analysis of the refrigerant-side experimental data.

The experimental data for the average Nusselt number (Nu_r) for the air-side dry and wet surface tests are shown in Figs. 5.7 and 5.8 respectively. The test results may be summarized as follows:

i) For boiling refrigerants inside horizontal tube circuits of DX-coils, the average Nusselt number (Nu_r) is an increasing function of the heat transfer parameter ($Re_{r,l}/K_f$) [in the

range $25 \times 10^9 < Re^2_{r,l}/K_f < 350 \times 10^{11}$] for complete evaporation of R-22 with about 2% by weight of oil (see Chapter-2, Section 3.6).

ii) The experimental data from the existing studies [15] [based on boiling refrigerants (oil-free) in straight unfinned tubes] are 20% to 40% lower than those from the present study. The increase in the average Nusselt number (with the presence of about 2% oil) is due to the effect of oil which inhibits wall dryout thereby increasing the average heat transfer coefficient [30]. The difference in the Nu_r (with and without oil) increases when the heat transfer parameter ($Re^2_{r,l}\ K_f$) is increased.

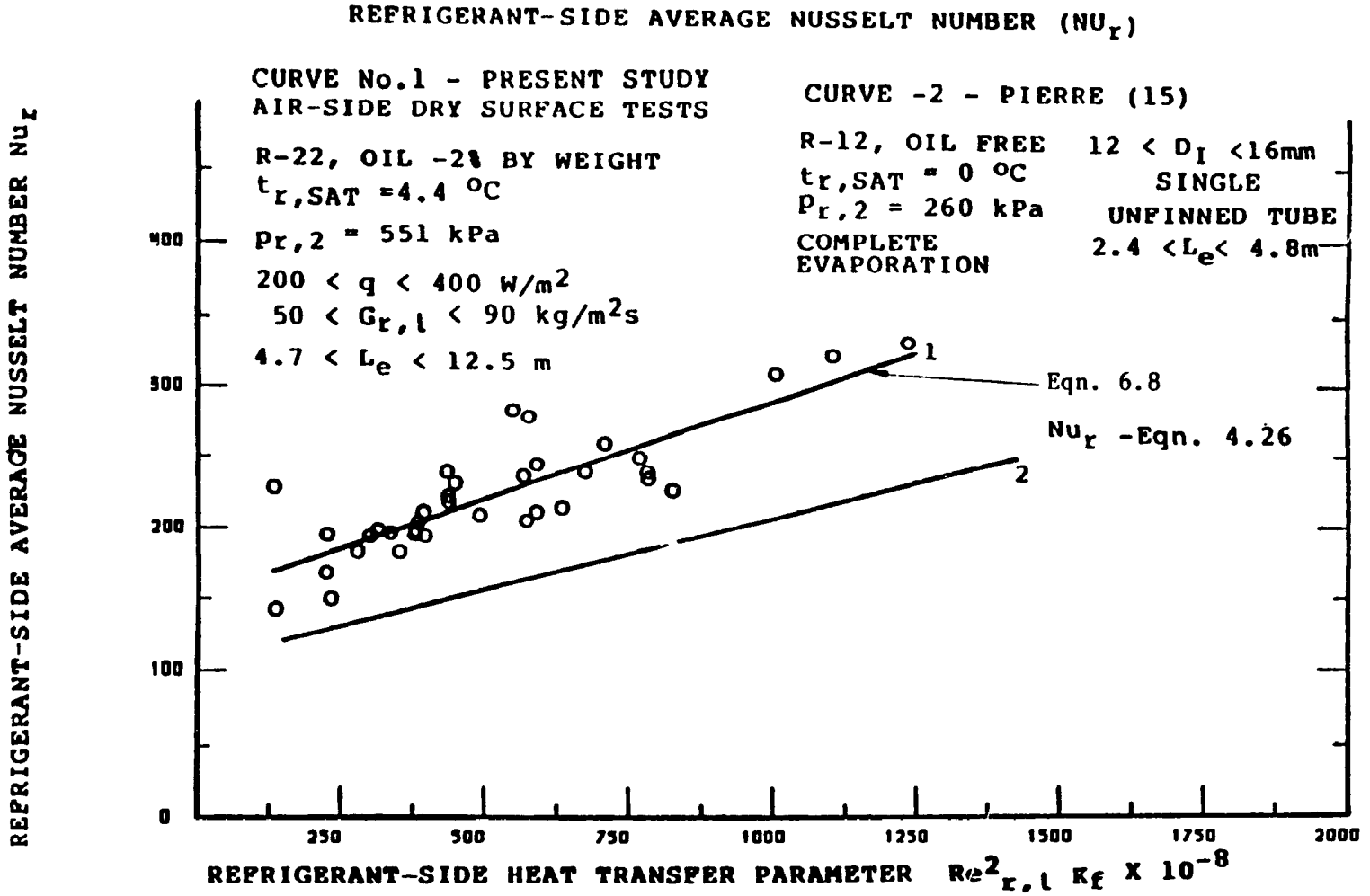

FIG. 5.7 REFRIGERANT-SIDE AVERAGE NUSSELT NUMBER (Nu_r) EXPERIMENTAL DATA, AIR-SIDE DRY SURFACE TESTS

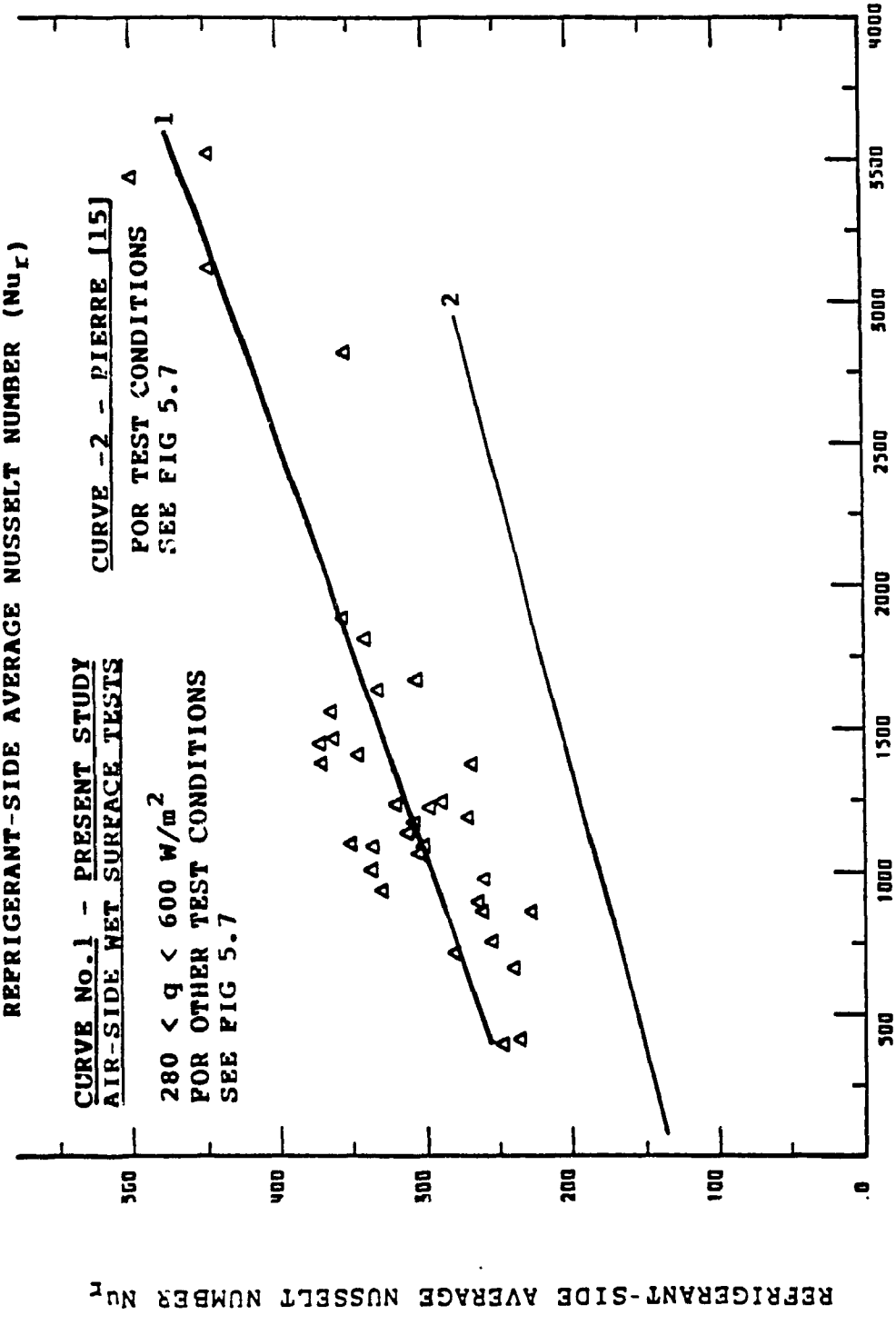

FIG. 5.8 REFRIGERANT-SIDE AVERAGE NUSSELT NUMBER (Nu_r)
AIR-SIDE WET SURFACE TESTS

The experimental data for the refrigerant-side average two-phase pressure drop factor (f_r) for the air-side dry and wet surface conditions are shown in Figs. 5.9 and 5.10, respectively. From this data the following conclusions may be reached:

i) For boiling refrigerants in horizontal tubes in the turbulant region ($Re_{r,l}/K_f > 1$), the refrigerant-side average pressure drop factor (f_f) is a marginally decreasing function of the pressure drop parameter [see Section 3.6].

ii) The pressure drop factor for the present study (with about 2% by weight of oil) is about 25% higher than that for the existing studies [16] [based on boiling oil-free R-22, in unfinned straight tubes]. The increase in the pressure drop factor with the presence of oil may be attributed to the additonal shear force due to the dissolved oil [30].

iii) The air-side heat flux intensity has no significant effect on the refrigerant-side pressure drop factors.

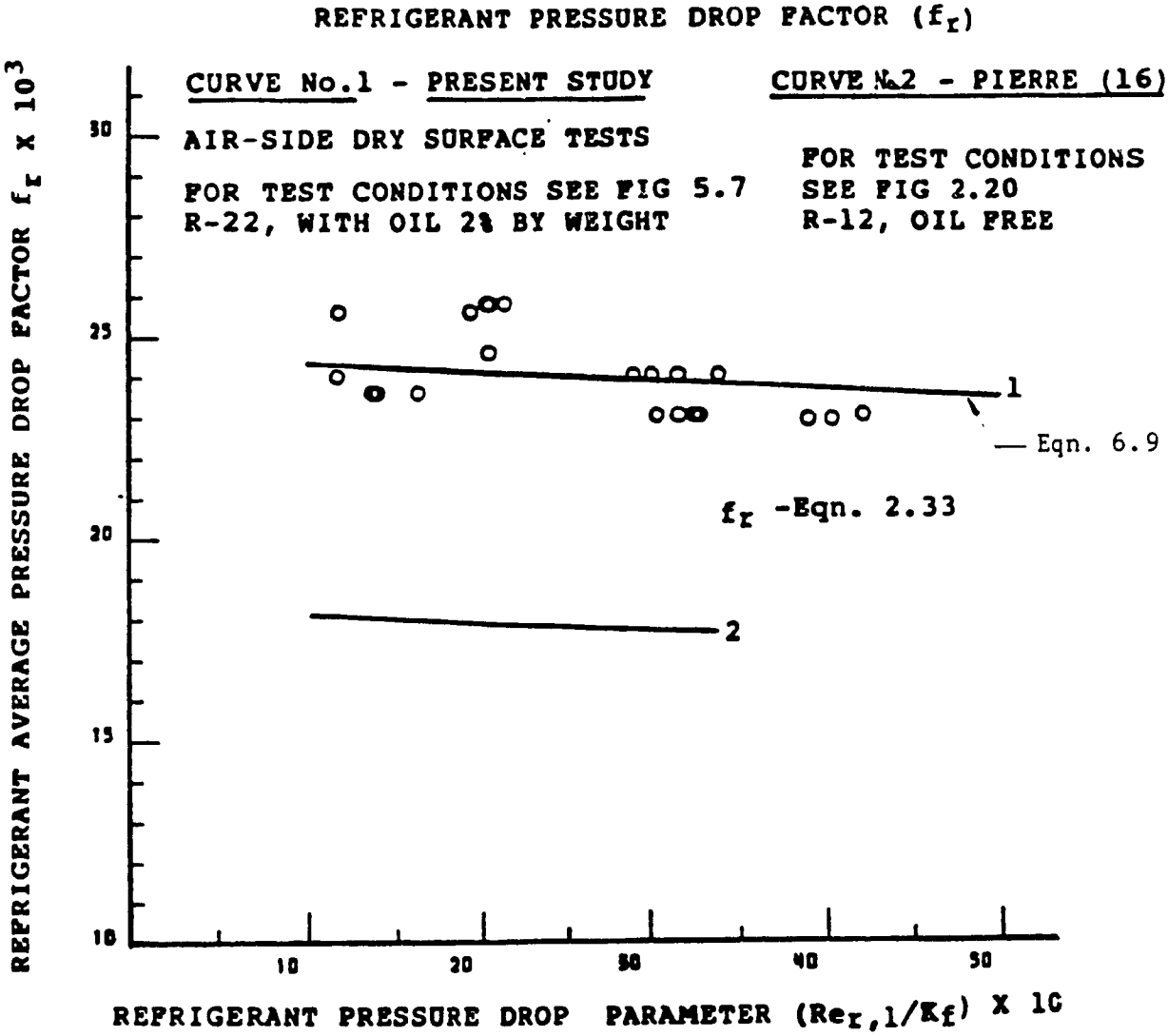

FIG. 5.9. REFRIGERANT AVERAGE PRESSURE DROP FACTOR (f_r)
EXPERIMENTAL DATA, AIR-SIDE DRY SURFACE TESTS

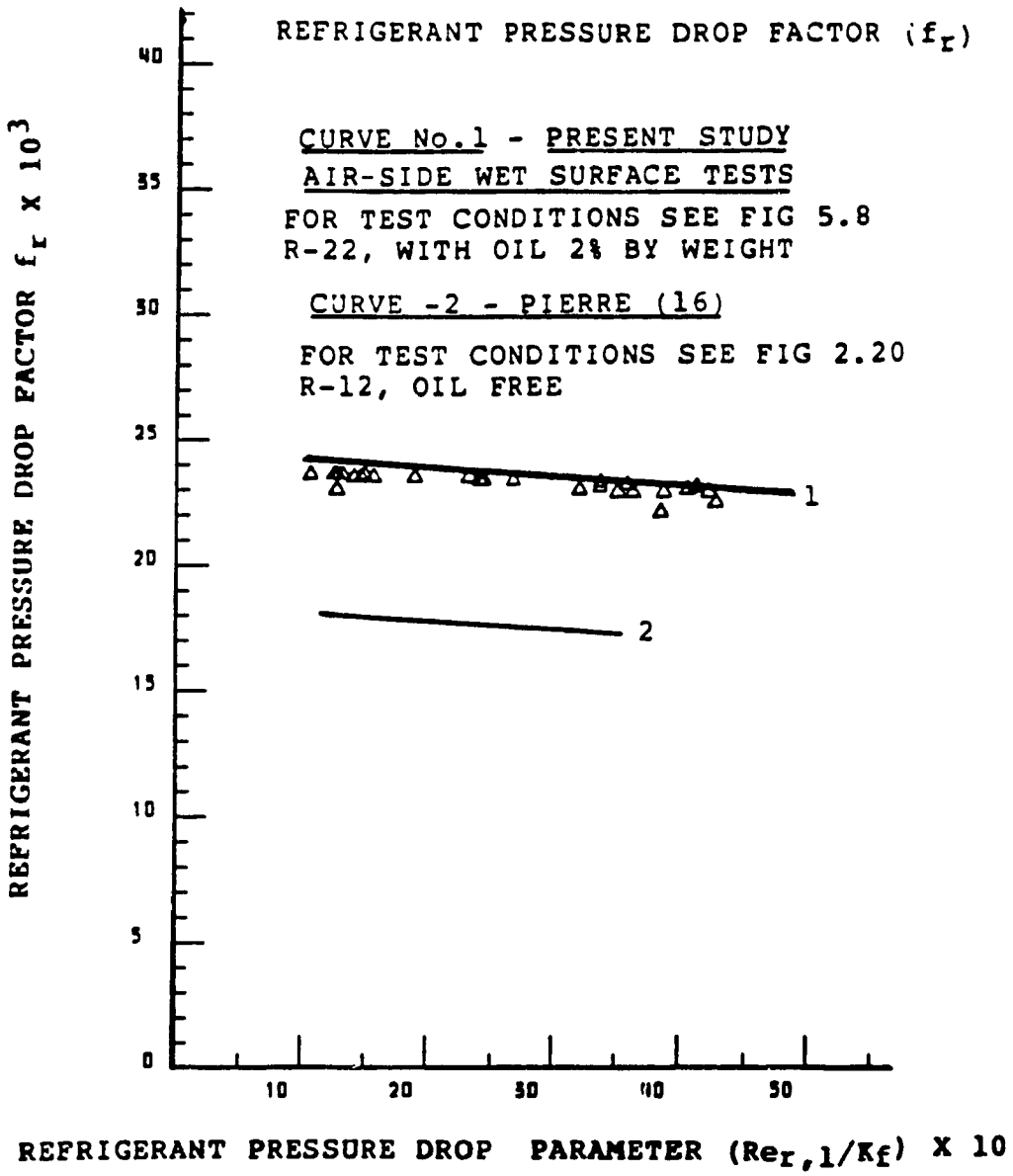

FIG. 5.10. REFRIGERANT PRESSURE DROP FACTOR (f_r)
EXPERIMENTAL DATA, AIR-SIDE WET SURFACE TESTS

6. COMPARISON OF THE AIR-SIDE DRY AND WET SURFACE TEST RESULTS:

A comparison of the heat transfer and pressure drop factors (for the air and the refrigerant sides) for the air-side dry and wet surface conditions is presented in this Section.

i) Air-Side Heat Transfer Factor:

A comparison of the percentage difference between the air-side dry and wet surface heat transfer factors (for a given fin spacing) is shown in Table 5.5. The test results may be summarized as follows:

A) For a given Reynolds number (Re_a), the air-side average heat transfer factors for both dry and wet surface conditions is influenced by the coil geometric parameters D_o, S_L, S_T, and P_S.

B) The effect of tube rows on the average heat transfer factor for both the dry and wet surface conditions is insignificant

C) For a given coil configuration (P_s, D_o, S_L and S_T), the wet surface heat transfer factor ($j_{a,w}$) is higher than that for the corresponding dry surface ($j_{a,D}$) [for a given Re_a]. This results from the higher heat flux intensity (q) due to simultaneous sensible and latent heat transfer.

D) The percentage change in $j_{a,w}$ compared to the corresponding $j_{a,D}$ decreases when the Reynolds number is increased (for a given coil configuration), similar to that found by Elmahdy [7] [see Fig. 2.11].

E) For a given Reynolds number, the percentage change in $j_{a,w}$ (compared to the corresponding $j_{a,D}$) decreases when the fin density is increased.

TABLE 5.5 COMPARISON OF THE DRY AND WET SURFACE HEAT TRANSFER FACTORS [FROM FIGS. 5.1 and 5.3]

P_s fins/cm	Re_a	$(j_{a,w} - j_{a.D})/j_{a,w} \times 100$		
			Existing Studies (1)	
		Present study	McQuistion [15]	Elmahdy [7]
3.1	900	43%	18%	—
	1000	40%	12%	—
4.7	600	37%	18%	35%
	800	22%	15%	20%
5.5	500	33%	13%	—
	700	20%	13%	—

ii) **Air-Side Pressure Drop Factor:**

A comparison of the percentage difference between the air-side dry and wet surface pressure drop factors for the experimental data from the present and the existing studies [13] is shown in Table 5.6. The results may be summarized as follows:

A) For a given coil configuration, the wet surface average pressure drop factor ($f_{a,w}$) is higher than that for the corresponding dry surface ($f_{a,D}$) due to additional friction resulting from the condensate film.

B) The effect of tube rows on the pressure drop factor for both the dry and wet surface conditions is insignificant.

C) For a given fin spacing and Reynolds number, the change in $f_{a,w}$ with respect to the corresponding $f_{a,D}$ depends on the tube spacing (S_L and S_T) and the tube diameter (D_o).

TABLE 5.6 COMPARISON OF THE AIR-SIDE DRY AND WET SURFACE PRESSURE DROP FACTORS [FROM FIGS. 5.2 AND 5.4]

P_s fins/cm	$Re_a^2 \times 10^{-4}$	$[(f_{a,w} - f_{a,D})/f_{a,w}] \times 100$	
		present study	McQuiston study [13]
3.1	50	26%	11%
	100	25%	10%
5.5	30	21%	42%
	50	20%	40%

CHAPTER - 6

CORRELATIONS FOR THE HEAT TRANSFER AND PRESSURE DROP FACTORS FOR DX-COILS

CHAPTER - 6

CORRELATIONS FOR THE HEAT TRANSFER AND PRESSURE DROP FACTORS FOR DX-COILS

In this chapter, the correlations for heat transfer and pressure drop factors are presented for the air and the refrigerant-sides of DX-Coils (developed from the experimental data). A comparison of the results with the relevant existing correlations is also made.

1. CORRELATIONS FOR THE HEAT TRANSFER AND PRESSURE FACTORS

Based on the existing literature, the average heat transfer and pressure drop factors for the air-side of finned-tube coils, may be expressed in terms of non-dimensional coil geometric groups and the corresponding air flow Reynolds number (see Chapter-2, Section 4.1). Regression analysis technique [34] may be used to develop correlations for prediction of the average heat transfer and pressure drop factors from the experimental data. To facilitate such analysis, the air-side dry surface average heat transfer factor ($j_{a,D}$) may be expressed as follows:

$$j_{a,D} = C_1 (S_f/Y_f)^{C_2} (S_f/D_h)^{C_3} (D_o/S_T)^{C_4} (D_o/S_L)^{C_5} (A_{m,f}/A_F)^{C_6} (A_o/A_p)^{C_7} (Re_a)^{C_8} \quad (6.1)$$

where,

S_f, Y_f, D_o, S_L, and S_T - coil geometric parameters - defined in Fig. 2.2

D_h - defined at Eqn. 2.3

Re_a - Defined at Eqn. 2.12

$A_o, A_p, A_{m,f}$ - defined in Table 4.1

C_1 to C_8 - constants, determined from experimental data (from regression analysis.

The dry surface pressure drop factor may also be expressed in a form similar to Eqn. 6.1. For a given air flow Reynolds number. The air side wet surface heat transfer and pressure drop factors ($j_{a,W}$ and $f_{a,w}$) may be expressed as functions of those for the corresponding dry surface case ($J_{a,D}$ and $f_{a,D}$) [13].

The refrigerant-side average Nusselt number (Nu_r) may be expressed as a function of the ratio of the total air-side surface area (A_o) to the tube inside surface area (A_I), and the two-phase heat transfer parameter ($Re^2_{r,l}\ K_f$) as follows [4] (see Chapter-2, Section 4.6):

$$Nu_r = C_9\ (A_o/A_I)^{C_{10}}\ (Re^2_{r,l}\ K_f)^{C_{11}} \qquad (6.2)$$

where:

$Re_{r,l}$ - refrigerant liquid flow Reynolds number

K_f - refrigerant boiling number - defined at Eqn. - 2.32

A_o/A_I - defined in Table - 4.1

The corresponding refrigerant-side average pressure drop factor (f_r) may be expressed as a function of the two-phase pressure drop parameter ($Re_{r,l}/K_f$) as follows [16]:

$$f_r = C_{12} \, (Re_{r,l}/K_f)^{C_{13}} \qquad (6.3)$$

The constants (C_9 to C_{13}) in the equations 6.2 and 6.3 may be determined from the experimental data (from regression analysis).

From the following experimental data for fourteen (14) coil configurations from the present and the existing studies (see Chapter-5), using regression analysis routine (available at the computer center of Concordia University) to eliminate insignificant groups in the above equations (6.1 to 6.5), the following correlations are developed:

$$j_{a,D} = 0.053 \, (A_o/A_p)^{-0.24} \, (Re_a)^{-0.18} \qquad (6.4)$$

$$f_{a,D} = 0.589 \, (A_o/A_p)^{-0.28} \, (Re_a)^{-0.27} \qquad (6.5)$$

$$j_{a,W} = 0.0025 \, (j_{a,D})^{-0.94} \, (S_f/Y_f)^{+1.15} \, (Re_a)^{-0.92} \qquad (6.6)$$

$$f_{a,W} = 0.318 \, (f_{a,D})^{-0.04} \, (S_f/Y_f)^{0.4} \, (Re_a)^{-0.42} \qquad (6.7)$$

$$Nu_r = 0.049 \, (Re^2_{r,l} \, K_f)^{0.32} \, (A_o/A_I)^{0.18} \qquad (6.8)$$

$$f_r = 2.7 \, (Re_{r,l}/K_f)^{-0.16} \qquad (6.9)$$

The Equations 6.4 to 6.9 determined for complete evaporation of R-22, with the presence of 2% by weight of transported lubricating oil (viscosity of about 200 SSU at 20°C) are valid in the following range:

$$11.2 < A_o/A_p < 50$$

$$12 < S_f/Y_f < 22$$

$$20 < A_o/A_I < 50$$

$$300 < Re_a < 1500$$

$$2.5 \times 10^{10} < (Re^2_{r,l}\ K_f) < 30 \times 10^{12}$$

$$1 < (Re_{r,l}/K_f) < 4$$

$$60 < G_{r,l} < 120\ kg/m^2s$$

The range of the dimensionless groups considered in the regression analysis are shown in Table 6.1. The physical data for the coils considered are shown in Appendix-1. The experimental data from the present and the existing studies [7, 13, 15 and 16] are presented in Chapter-5. (Figs. 5.1, to 5.4 and 5.7 to 5.10).

By substituting Eqn. 6.4 into Eqn. 6.6 and Eqn. 6.5 into Eqn. 6.7, the air-side wet surface average heat transfer and pressure drop factor may also be expressed as follows:

$$J_{a,W} = 0.04\ (A_o/A_p)^{0.23}\ (S_f/Y_f)^{+1.15}\ Re_a^{-0.75} \qquad (6.10)$$

$$f_{a,w} = 0.325\ (A_o/A_p)^{+0.01}\ (S_f/Y_f)^{0.4}\ Re_a^{-0.41} \qquad (6.11)$$

A discussion of the results from the correlations developed is presented in the following sections.

TABLE 1 RANGE OF THE DIMENSIONLESS GROUPS USED IN THE REGRESSION ANALYSIS

[from the present and the existing studies [7 and 13]

	(S_f/y_f)	(S_f/D_h)	(D_o/S_T)	(D_o/S_L)	$(A_{m,f}/A_F)$	(A_o/A_p)	(A_o/A_I)	Re_a	$(Re_{r,1}^2 K_f) \times 10^{-10}$	$(Re_{r,1}/K_f)$
MIN	11.9	9.6	0.18	0.18	0.54	11.2	21.8	300	2.5	1
MAX	21.6	9.8	0.38	0.45	0.60	49.0	49.0	1500	30	4

2. DISCUSSION OF THE RESULTS FROM THE CORRELATIONS DEVELOPED:

In this section, a comparison of the computed data from the correlations from the present and the existing studies, with the corresponding experimental data, is presented. A summary of the mean, maximum, and minimum relative deviations for the results from the correlations (from the present and the existing studies) is shown in Table 6.2. A discussion of the correlations developed in the present study is presented in the following sections.

TABLE 6.2 COMPARISON OF THE RELATIVE DEVIATIONS OF THE COMPUTED DATA FOR CORRELATIONS FROM THE PRESENT AND THE EXISTING STUDIES [FIGS. 6.1 TO 6.6]

	Mean (absolute) Relative Deviation (%)			Maximum Relative Deviation (%)			Minimum Relative Deviation (%)		
	Present study	McQuiston [13]	Elmahdy [7]	Present Study	McQuiston	Elmahdy	Present Study	McQuiston	Elmahdy
				A. AIR SIDE CORRELATIONS					
1) $j_{a,D}$	(Eqn. 6.4) 4.8	(Eqn. 2.15) 10.5	(Eqn. 2.5) 10.0	9.6	17.2	2.1	-18.7	-21.3	-23.7
2) $f_{a,D}$	(Eqn. 6.5) 6.9	(Eqn. 2.19) 20.3	-----	12.4	33.6	----	-34.1	-51.6	----
3) $j_{a,w}$	(Eqn. 6.6) 14.4	(Eqn. 2.27) 19.9	(Eqn. 2.9) 14.0	30.4	35.6	33.8	-40.7	-42.5	-30.2
4) $f_{a,w}$	(Eqn. 6.7) 7.0	(Eqn. 2.28) 12.3	----	10.2	41.4	----	-33.5	-50.8	----

B. REFRIGERANT-SIDE CORRELATIONS

	Present study	Existing studies	Present study	Existing study	Present study	Existing study
5) Nu_r	(Eqn. 6.8) 8.6	(Eqn. - 3.29) [15] 31.7	27.8	-18	-31.6	-40.1
6) f_r	(Eqn. 6.9) 12	(Eqn. 2.37) [16] -41%	25.3	-20	-67	-766

A) AIR-SIDE DRY SURFACE PRESSURE DROP FACTOR CORRELATION:

A comparison of the experimental data with the corresponding computed data (from the present and existing correlations) for the air-side dry surface average heat transfer factor ($j_{a,D}$) is shown in Fig. 6.1. The average dry surface heat transfer factor may be predicted within about ± 10% uncertainty from Eqn. 6.4. From Table 6.2, the mean relative deviation for Eqn. 6.4 is 4 to 5% lower than that for the existing correlations (Eqn. 2.5 and 2.15). Hence, it is concluded that Eqn. 6.4 provides better prediction for $j_{a,D}$ compared to the existing correlations in the range of validity defined [at Eqn. 6.9].

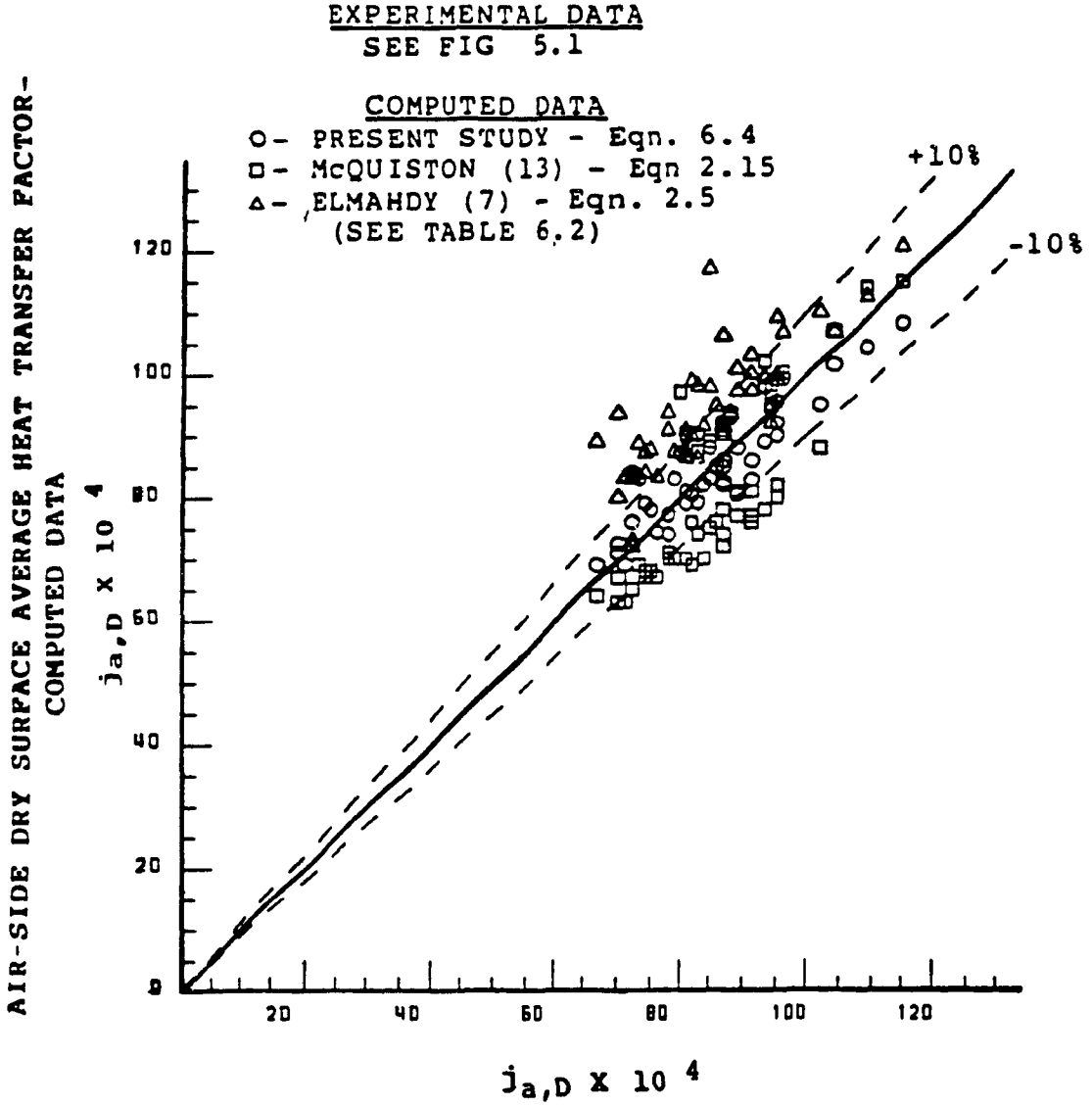

FIG.6.1 COMPARISON OF THE EXPERIMENTAL AND COMPUTED DATA-

AIR-SIDE DRY SURFACE AVERAGE HEAT TRANSFER FACTOR ($j_{a,D}$)

B) AIR-SIDE DRY SURFACE PRESSURE DROP FACTOR CORRELATION:

For the air-side dry surface pressure drop factor ($f_{a,D}$), comparisons of the experimental data from the present and the existing studies (see Fig. 5.2) with the computed data, are shown in Fig. 6.2. The average pressure drop factor may be predicted within about $\pm$ 15% uncertainty from Eqn. 6.5. From Table 6.2, the mean deviation for Eqn. 6.5 is considerably smaller than that for the McQuiston correlation (Eqn. 6.3). Therefore, it is concluded that Eqn. 6.5 provides better predictions for $f_{a,D}$ compared to the existing correlation, in the range of validity defined (at Eqn. 6.9).

The dry surface pressure drop factor ($f_{a,D}$) is also most sensitive to A_o/A_p in the test range considered (Eqn. 6.4). The effects of surface area ratio (A_o/A_p) on $f_{a,D}$ are similar to those on the corresponding $j_{a,D}$.

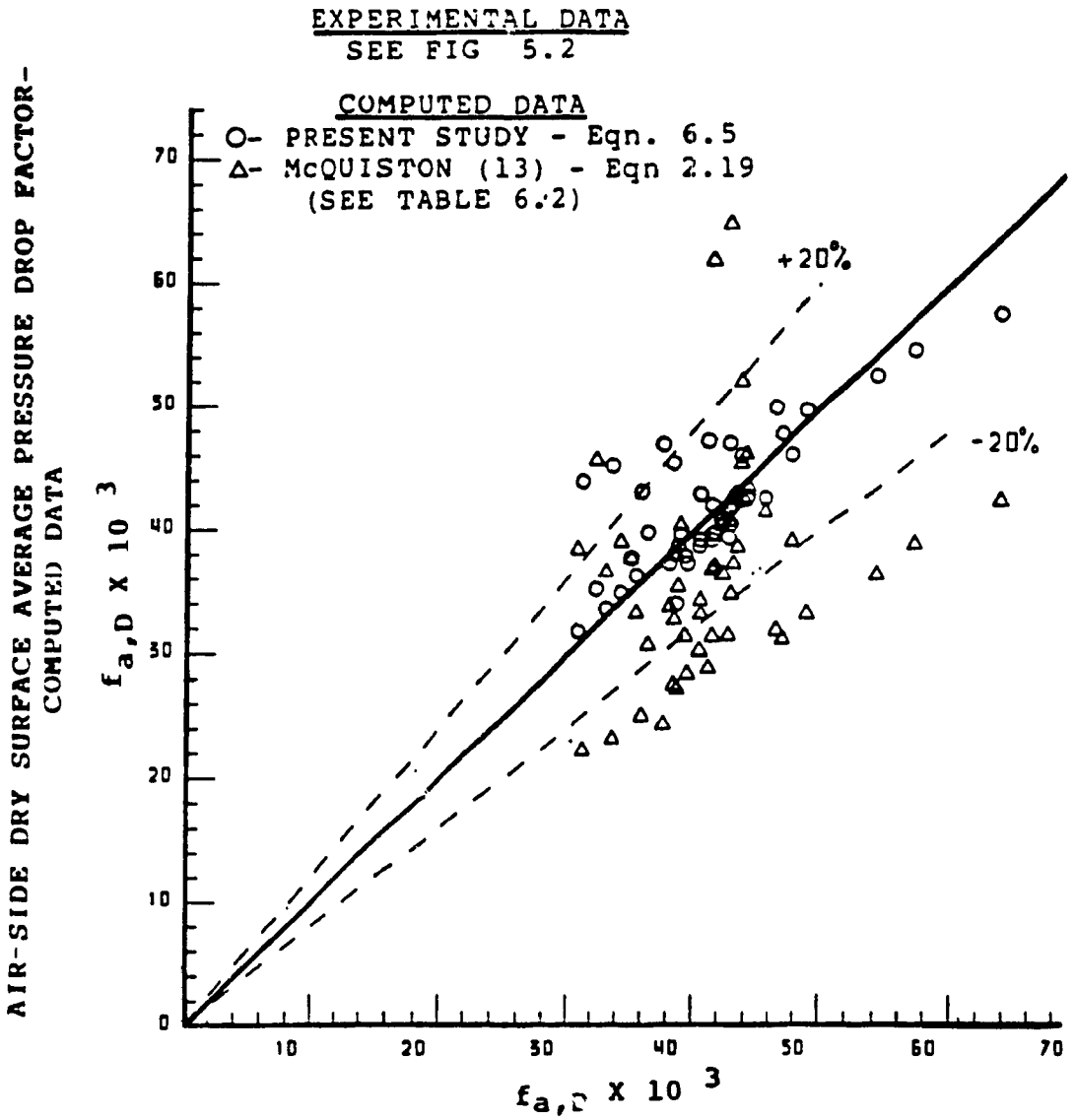

AIR-SIDE DRY SURFACE AVERAGE PRESSURE DROP FACTOR-($f_{a,D}$)
EXPERIMENTAL DATA (PRESENT AND EXISTING STUDIES)

FIG.6.2 COMPARISON OF THE EXPERIMENTAL AND COMPUTED DATA-
AIR-SIDE DRY SURFACE AVERAGE PRESSURE DROP FACTOR ($f_{a,D}$)

C. AIR-SIDE WET SURFACE HEAT TRANSFER FACTOR CORRELATION:

For the air-side wet surface heat transfer factor ($j_{a,w}$), comparison of the experimental data (Fig. 5.3) with the computed data are shown in Fig. 6.3. The experimental and the computed data for $j_{a,w}$ (Eqn. 6.6) agreed within about ± 20%, for 80% of the data considered. The larger error (compared to $j_{a,D}$) may be due to the higher turbulence for fin densities greater than 4.7 fins/cm with the presence of condensate film. This phenomenon was also reported by McQuiston [13]. From Table-6.2, the mean deviation for Eqn. 6.6 is smaller than that for the (Eqn. 2.27 and is about the same as that for Eqn. 2.9. Hence, it is concluded that Eqn. 6.6 provides satisfactory estimates of $j_{a,w}$ in the range of validity defined (at Eqn. 6.9).

The air-side wet surface average heat transfer factor (Eqn. 6.10) is most sensitive to the parameter S_f/Y_f, and then to A_o/A_p which indicates that the fin spacing (for a given fin thickness) has a significant effect on the $J_{a,W}$. For a given D_o, S_L, S_T and Y_f, when the fin density (P_s) is increased, the surface area ratio (A_o/A_p) increases and the and the corresponding ratio of fin spacing to fin thickness (S_f/Y_f) decreases. In the test range considered, when P_s is increased (for a given Re_a), the corresponding $j_{a,w}$ decreases due to larger reduction in the term $(S_f/Y_f)1.15$ [in Eqn. 6.10]. That is, the effect of the fin spacing (for a given fin thickness) on $j_{a,w}$ may be more significant compared to that on the corresponding $j_{a,D}$.

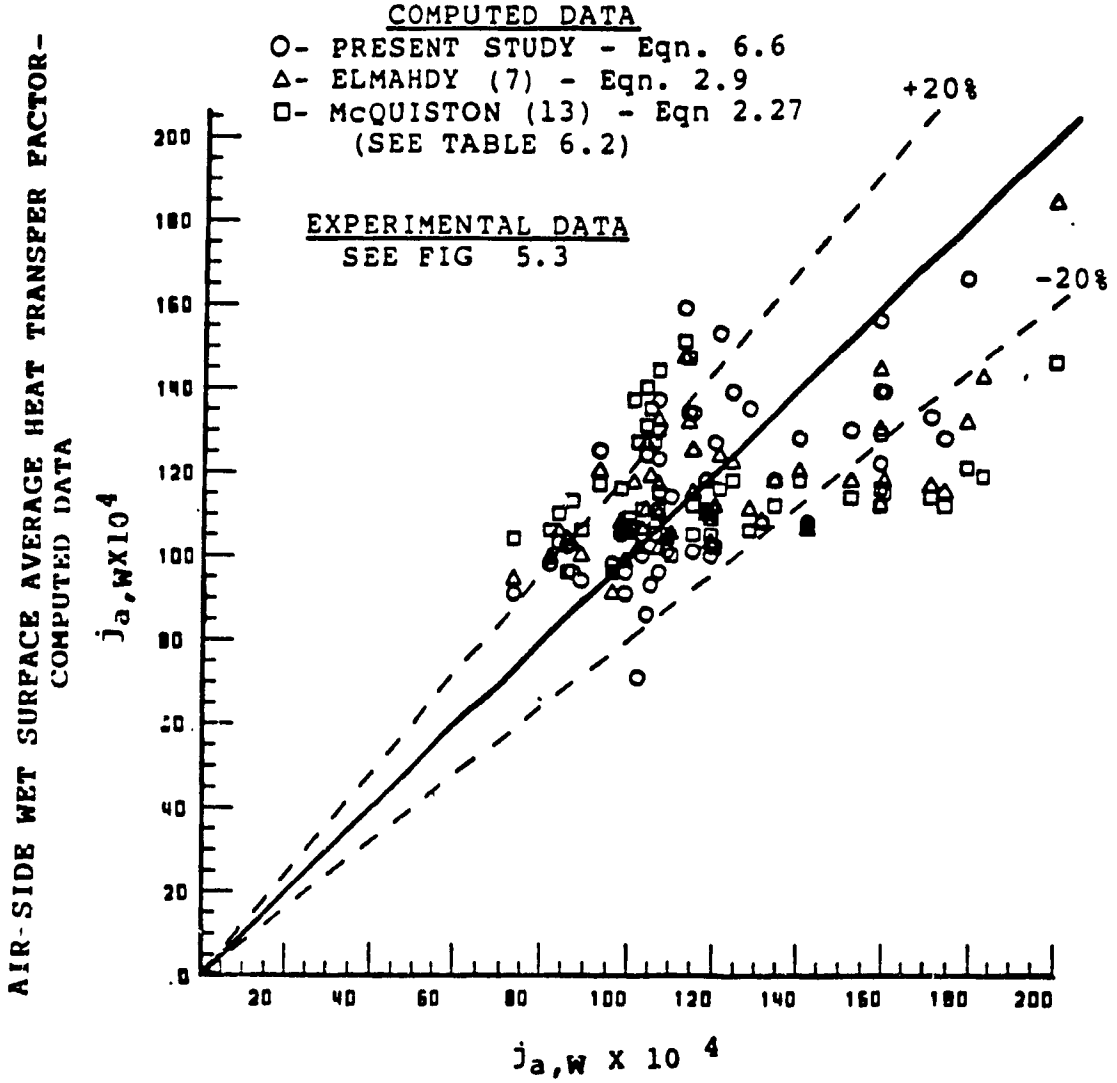

AIR-SIDE WET SURFACE AVERAGE HEAT TRANSFER FACTOR-
EXPERIMENTAL DATA (PRESENT AND EXISTING STUDIES)

FIG.6.3 COMPARISON OF THE EXPERIMENTAL AND COMPUTED DATA-
AIR-SIDE WET SURFACE AVERAGE HEAT TRANSFER FACTOR ($j_{a,w}$)

D. AIR-SIDE WET SURFACE PRESSURE DROP FACTOR CORRELATION:

For the air-side wet surface pressure drop factor ($f_{a,w}$), a comparison of the experimental data (Fig. 5.4) with the computed data is shown in Fig. 6.4. The average $f_{a,w}$ may be predicted within about $\pm$ 10% error for 90% of the data. From Table 6.2, the mean deviation for Eqn. 6.7 is lower than that for Eqn. 6.28. Hence, it is concluded that the correlation developed (Eqn. 6.7 or 6.11) provides better prediction for $f_{a,w}$ compared to the existing correlation.

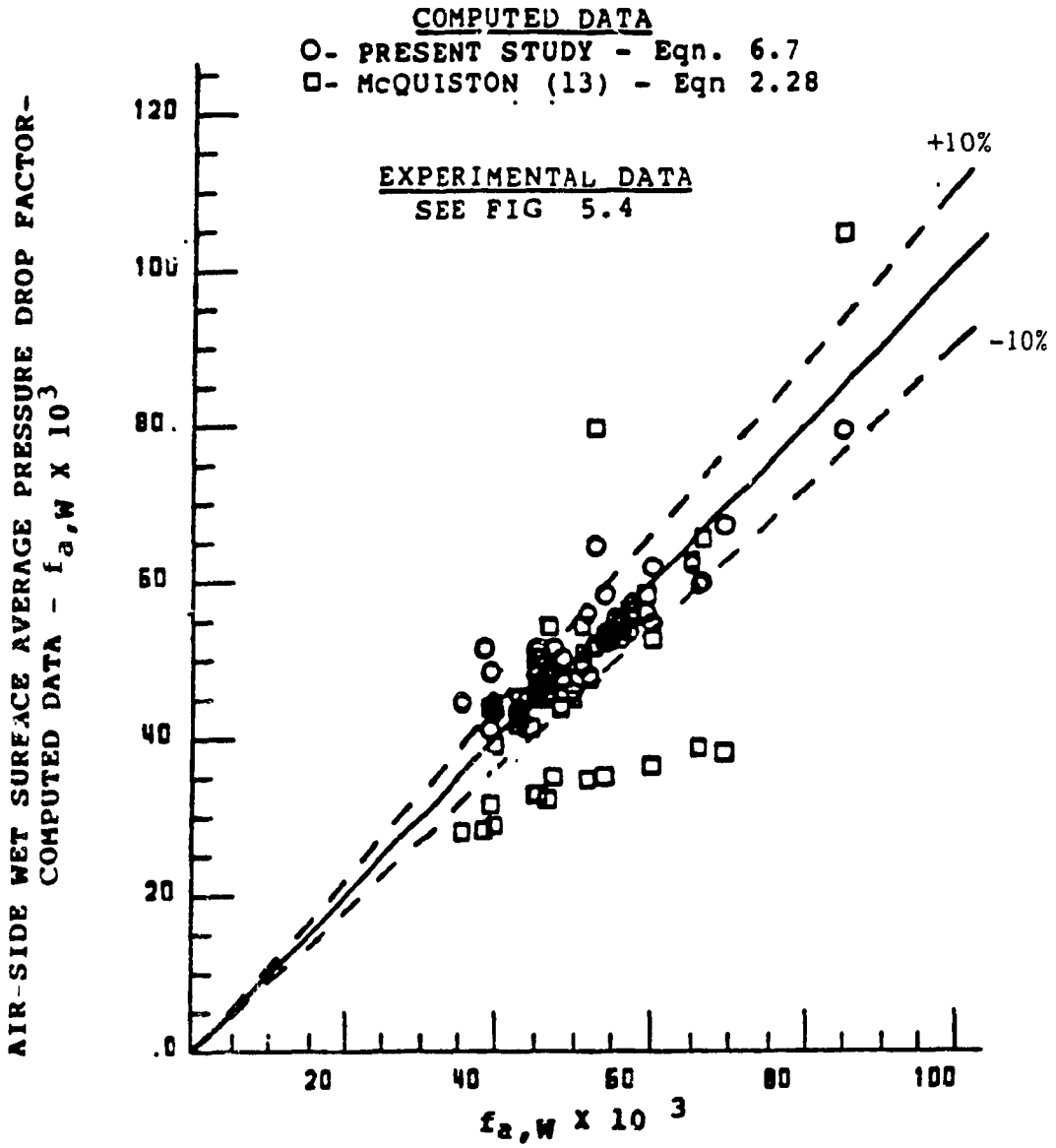

AIR-SIDE WET SURFACE AVERAGE PRESSURE DROP FACTOR-
EXPERIMENTAL DATA (PRESENT AND EXISTING STUDIES)

FIG.6.4 COMPARISON OF THE EXPERIMENTAL AND COMPUTED DATA-
AIR-SIDE WET SURFACE PRESSURE DROP FACTOR ($f_{a,W}$)

E) REFRIGERANT SIDE AVERAGE NUSSELT NUMBER (Nu_r) CORRELATION:

A comparison of the experimental data (from the present study) for the refrigerant side average Nusselt number (for the air side dry and wet surface tests) with the corresponding computed data (from Eqn. 6.8) is shown in Fig. 6.5. The average Nusselt number may be predicted within about $\pm$ 20% uncertainty (for both the air side dry and wet surface conditions) from Eqn. 6.8. The results from the existing correlation (Eqn. 2.29 - for oil-free boiling refrigerants) are 20% to 40% lower than those from Eqn. 6.8 (with about 2% oil, for the air side wet surface tests - see Fig. 6.6) and the difference may be attributed to the presence of oil which is known to enhance the average heat transfer coefficient [30]. The air side wet surface tests are used for comparison due to the limitations in the range of validity of the existing correlation (Eqn. 2.29).

Eqn. 6.8 is most sensitive to the heat transfer parameter ($Re^2_{r,l}$ K_f) and then to the surface area ratio (A_o/A_l) in the range of validity considered.

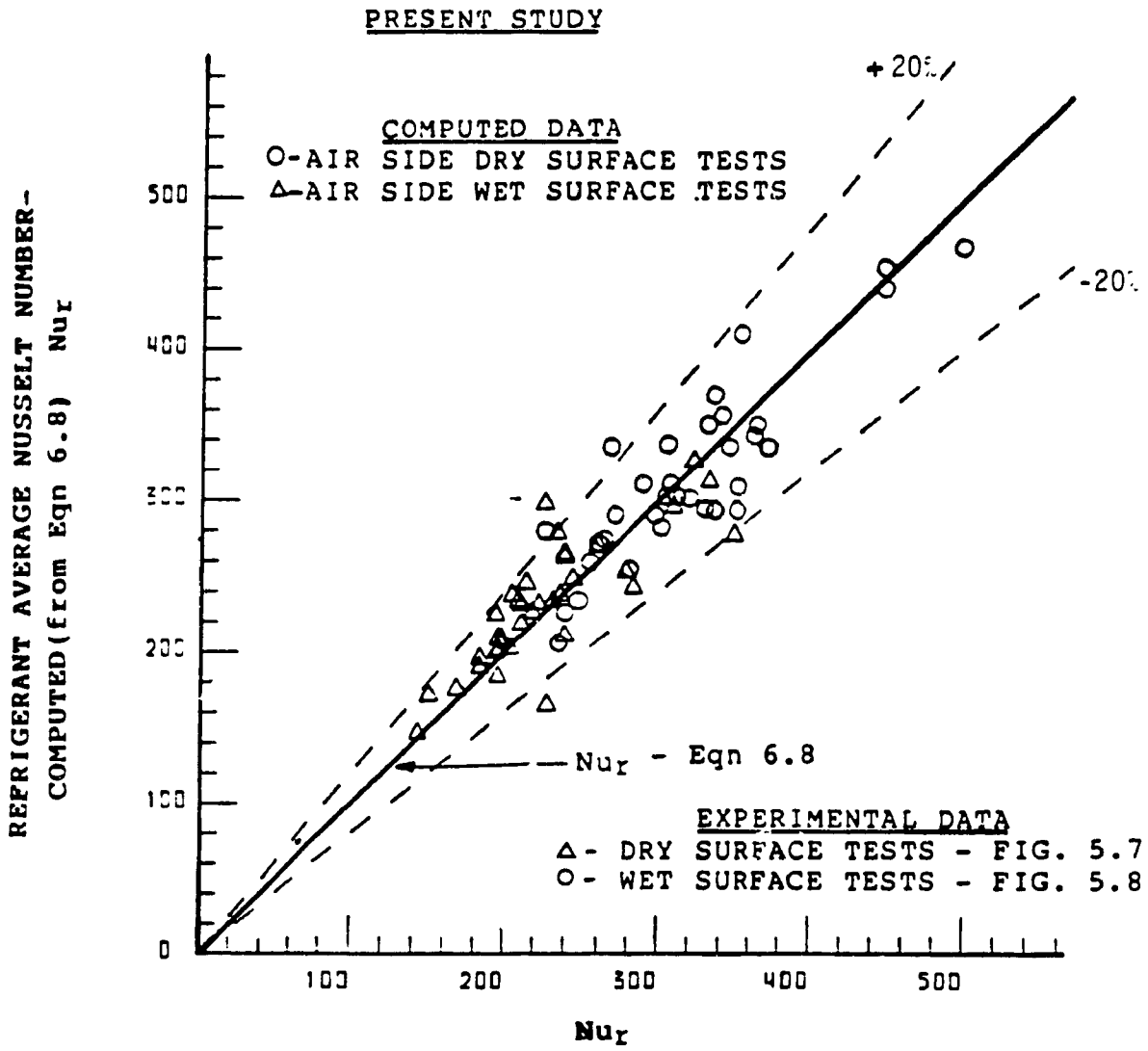

FIG. 6.5 COMPARISON OF THE EXPERIMENTAL AND COMPUTED DATA- REFRIGERANT SIDE AVERAGE NUSSELT NUMBER (Nu_r) PRESENT STUDY

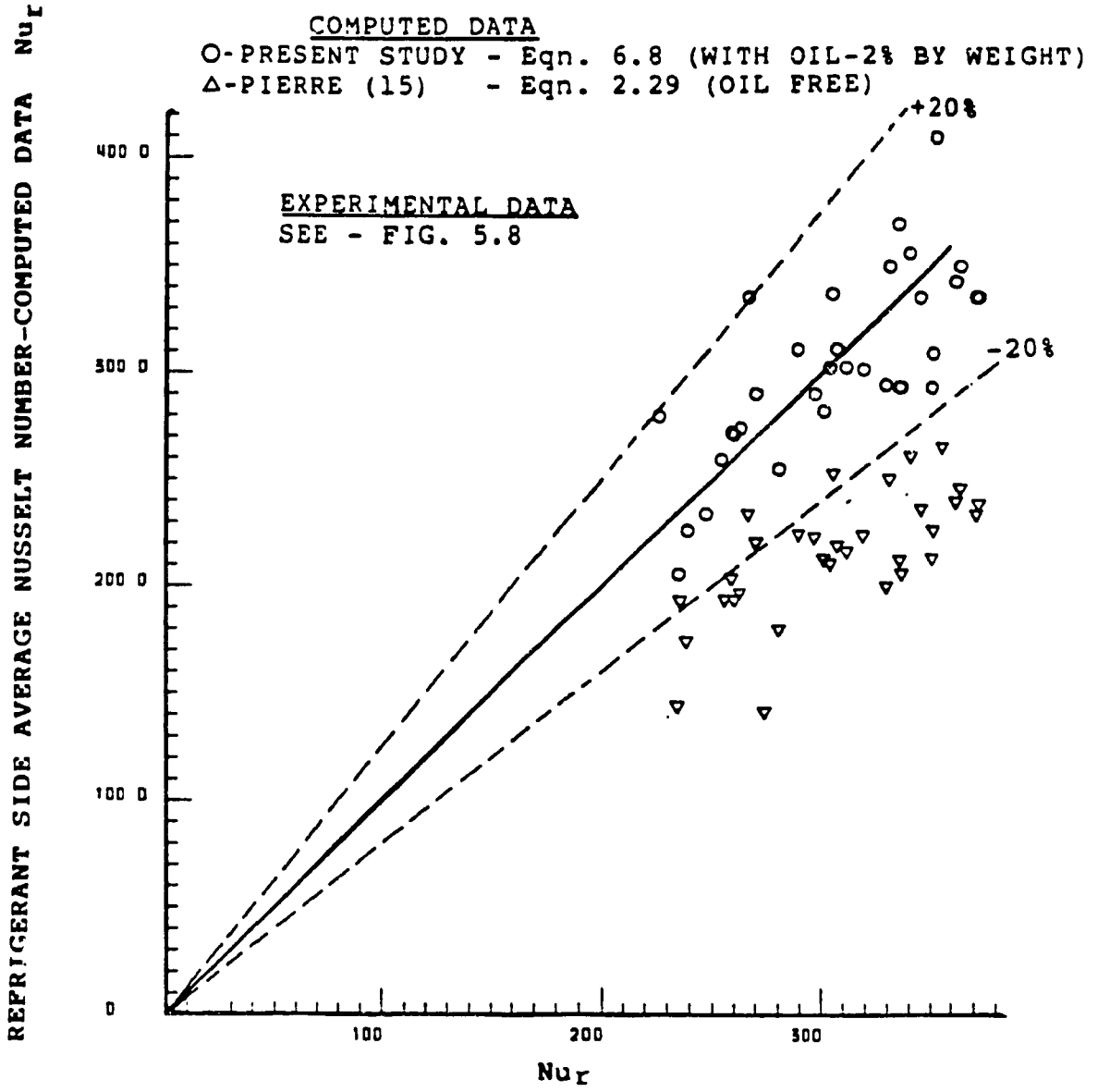

REFRIGERANT SIDE AVERAGE NUSSELT NUMBER-
EXPERIMENTAL DATA - PRESENT STUDY (AIR SIDE WET SURFACE TESTS)

FIG. 6.6 COMPARISON OF THE EXPERIMENTAL AND COMPUTED DATA-REFRIGERANT SIDE AVERAGE NUSSELT NUMBER (Nu_r) PRESENT AND THE EXISTING STUDIES

F) REFRIGERANT-SIDE PRESSURE DROP FACTOR (f_r) CORRELATION:

A comparison of the experimental data from the present study (for both the air-side dry and wet surface tests) with the computed data for f_r is shown in Fig. 6.7. The agreement between the experimental and computed data for f_r is within $\pm$ 20% for 90% of the data. The results from the existing correlation (Eqns. 2.37 - for oil-free flow) are 30% to 40% lower than those from Eqn. 6.9 which indicates that the presence of oil (about 2% by weight) tends to increase the average pressure drop factor.

The pressure drop factor (Eqn. 6.9) is a decreasing function of the pressure drop parameter ($Re_{r,l}/K_f$). When the pressure drop parameter is increased from 1 to 4, the corresponding change in f_r is relatively small (about 6%) in the test range considered (see Fig. 5.9 and 5.10).

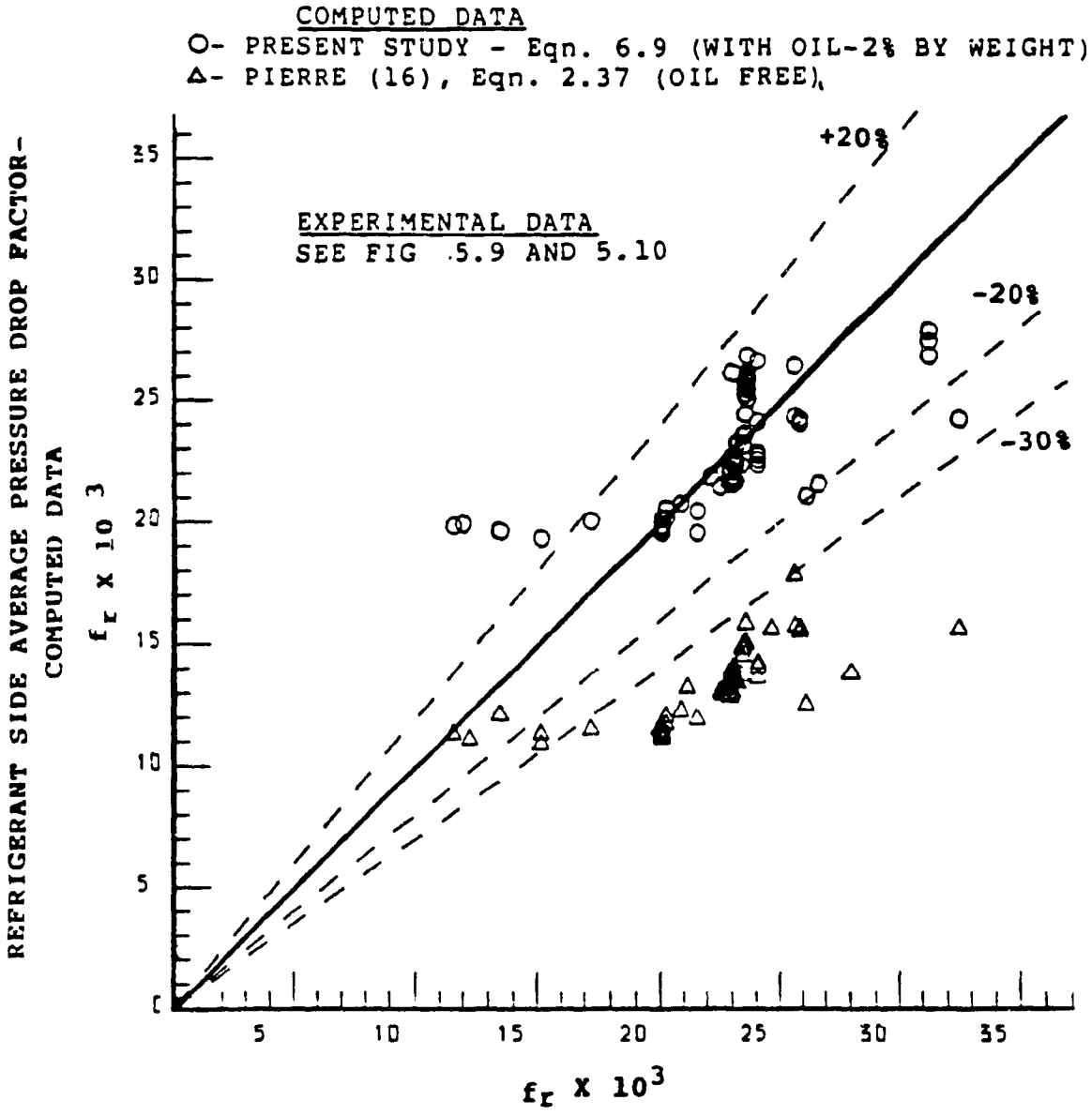

REFRIGERANT-SIDE AVERAGE PRESSURE DROP FACTOR (f_r) EXPERIMENTAL DATA, AIR-SIDE DRY AND, WET SURFACE TESTS, PRESENT STUDY

FIG.6.7 COMPARISON OF THE EXPERIMENTAL AND COMPUTED DATA-REFRIGERANT-SIDE PRESSURE DROP FACTOR (f_r)

CHAPTER 7

DX-COIL SELECTION METHOD

CHAPTER 7

DX-COIL SELECTION METHOD

In typical comfort air conditioning applications, air-cooling coils operate generally under partially wet surface conditions [32]. The selection methods for chilled water coils are well documented [35]. However, methods for selection of DX-coils are almost non-existant in the present literature mainly due to lack of correlations for prediction of the heat transfer and pressure drop factors for boiling refrigerants in the tube circuits [35]. The DX-coil selection method described in Ref. [12] utilizes a computer program (proprietary) which is not available for public review. Therefore, a method for selection of DX-coils based on the correlations for the heat transfer and pressure drop prediction developed is presented in this Chapter. To validate the selection method, additional tests were conducted (at partially wet surface conditions - (see Appendix-3).

A comparison of the results from the selection method with the corresponding experimental results is also presented.

1. GENERAL DESCRIPTION OF THE SELECTION METHOD:

The dimensional parameters for DX-coils (see Fig. 2.2) are generally determined by the coil manufacturers, based on the anticipated range of the coil performance requirements (Q, Δp_a, Δp_r), space limitations (for packaged systems), manufacturing limitations (methods and

available equipment), and cost (capital and operating) considerations [35]. The selection method presented is limited to the considerations related to the energy requirements due to the coil.

Selection of a DX-coil for a given comfort air conditioning application involves three major steps as follows:

A. Determination of the coil operating conditions.

B. Calculation of the performance (Q, Δp_a and Δp_r) for alternative coil configurations (among the available pre-designed configurations) for the operating conditions determined (in step A).

C. Determination of the optimum configuration and the corresponding performance (for the available alternatives).

A. COIL OPERATING CONDITIONS

For a given comfort air conditioning application, the required coil heat transfer capacity (Q_{REQ}), air mass flow rate (m_a) across the coil, and the entering air conditions ($t_{a,1}$ and W_1) may be determined from the building thermal load calculations [36]. The refrigerant vapour pressure leaving the coil ($p_{r,2}$) [suction pressure] may be determined from the compressor inlet requirements. The refrigerant (super heated vapour) temperature leaving the coil ($t_{r,2}$) may be determined from the suction pressure ($p_{r,2}$) and the characteristics of the thermostatic

expansion valve. Thus, the coil operating conditions (Q_{REQ}, $t_{a,1}$, W_1, m_a, $p_{r,2}$ and $t_{r,2}$) may be established.

B. CALCULATION OF THE COIL PERFORMANCE

Typical temperature (and enthalpy) variations for the working fluids in DX-coils are shown in Fig. 7.1. In compact platefinned-tube coils for cross-counter flow arrangement of working fluids (fully mixed conditions), the dry/wet surface boundary may be assumed to occur along of one of the tubes depending on the entering air dew-point temperature ($t_{a,1,sat}$) and the tube surface temperature (t_s). The boundary conditions are defined in Fig. 7.1

As discussed earlier (Chapter-5), for a given coil configuration (P_s, D_o, S_L and S_T) and the surface condition (fully dry or wet), the air-side heat transfer and pressure drop factors ($j_{a,D}$, $j_{a,w}$, $f_{a,D}$ and $f_{a,w}$) may be assumed to be uniform across the coil (in the range $300 < Re_a < 1500$). The corresponding refrigerant – side factors (Nu_r and f_r) may also be assumed to be uniform (in the range $25 \times 10^9 < Re^2_{r,i} K_f < 350 \times 10^9$, and $G_{r,1} < 120$ kg/m^{2}s). For partially wet surface conditions where both the boundary conditions and the coil leaving conditions are unkown, the coil performance data (Q, Δp_a and Δp_r) may be computed from row-by-row heat balance calculations described in Section-3 of this Chapter.

C. DETERMINATION OF THE OPTIMUM COIL CONFIGURATION

In order to minimize the energy consumption (due to the DX-coil), the coil which may provide the required heat transfer rate (Q_{REQ}) and minimum air and refrigerant-side pressure drop (Δp_a and Δp_r) may then be selected from the available configuration alternatives.

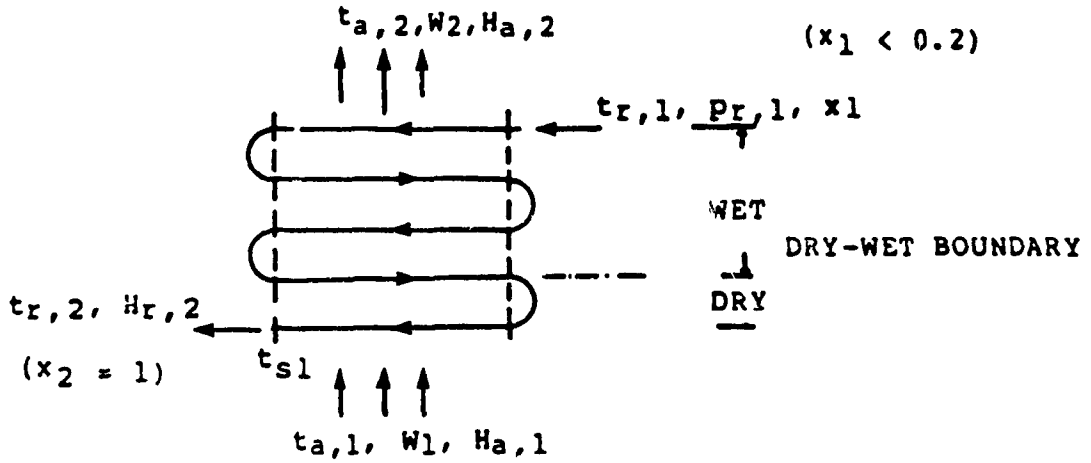

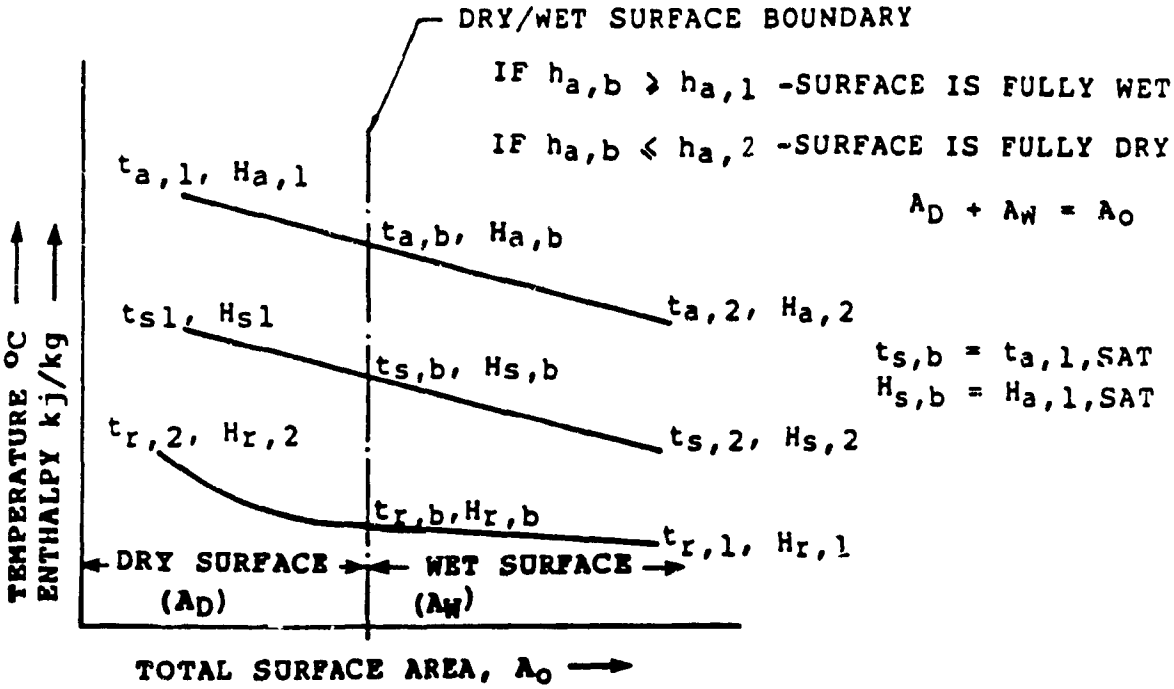

FIG. 7.1 TYPICAL TEMPERATURE AND ENTHALPHY VARIATIONS ALONG A FINNED TUBE CIRCUIT FOR PARTIALLY WET SURFACE CONDITIONS (CROSS-COUNTER FLOW) [35]

2. ASSUMPTION USED IN THE DX-COIL SELECTION METHOD:

The following assumptions are used in the DX-coil selection method:

A. Fully mixed conditions for the moist air exist at the entrarce of the coil.

B. Homogeneous liquid vapour mixture conditions exist for the refrigerant along the tube circuits.

C. The refrigerant is fully evaporated in the tube circuits.

D. About 2% by weight of oil, completely soluble in the refrigerant is present in the evaporator.

E. All the heat transferred from the air is absorbed by the refrigerant.

F. The condensate mass flow and the corresponding heat content are neglected.

G. The heat loss from the return-bends to the ambient is neglected.

Other assumptions used in the selection method are stated at the appropriate sections in the Chapter.

Tne selection method is valid in the following range:

$$11 < A_o/A_p < 50$$

$$12 < S_f/Y_f < 22$$

$$20 < A_o/A_I < 50$$

$$3 < N_R < 9$$

$$30 < L_T < 120 \text{ cm}$$

$$300 < Re_a < 1500$$

$$60 < G_{r,l} < 120 \qquad (kg/m^2s)$$

$$1 < Re_{r,l}/K_f < 4$$

$$2.5 \times 10^{10} < Re^2_{r,l}\ K_f < 30 \times 10^{12}$$

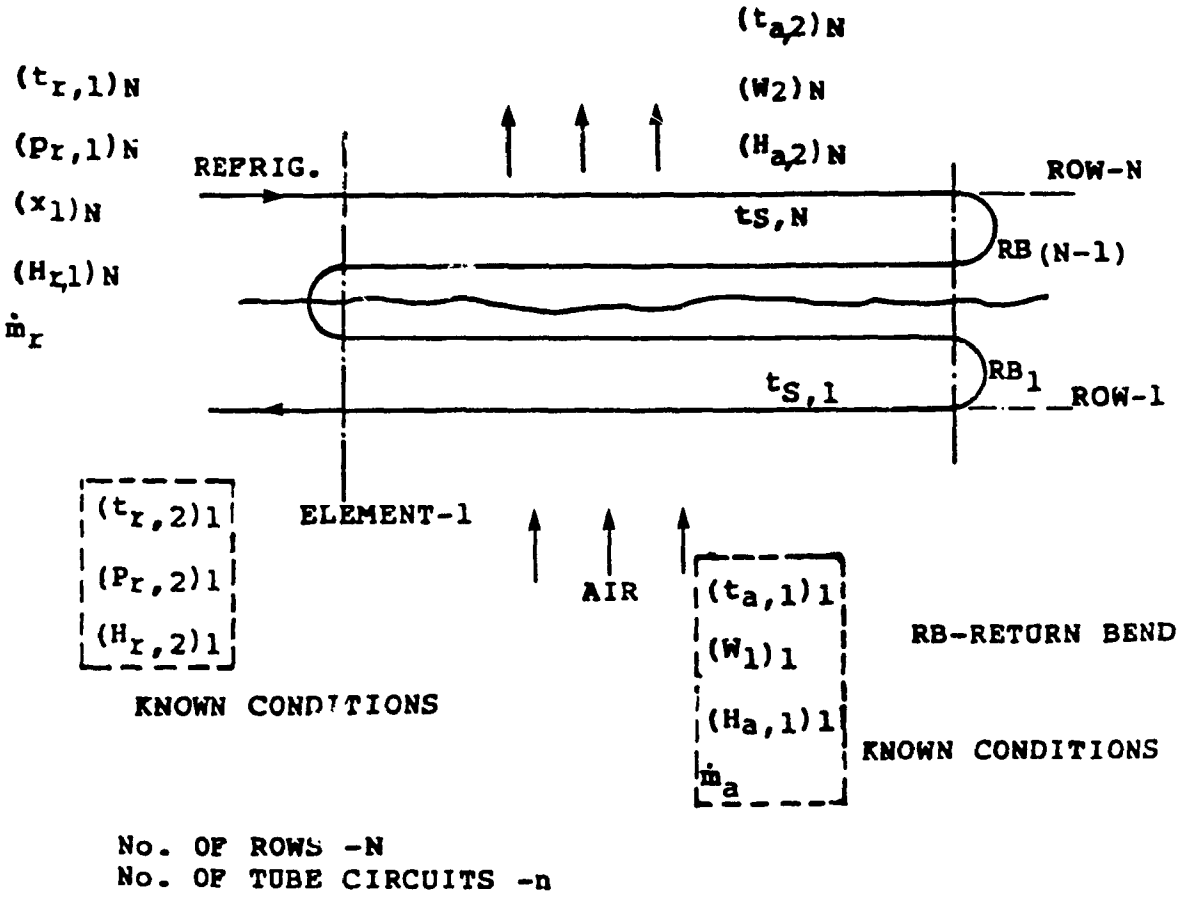

FIG. 7.2 THERMODYNAMIC CONDITION OF THE WORKING FLUIDS IN THE HEAT EXCHANGER (PLAN VIEW)

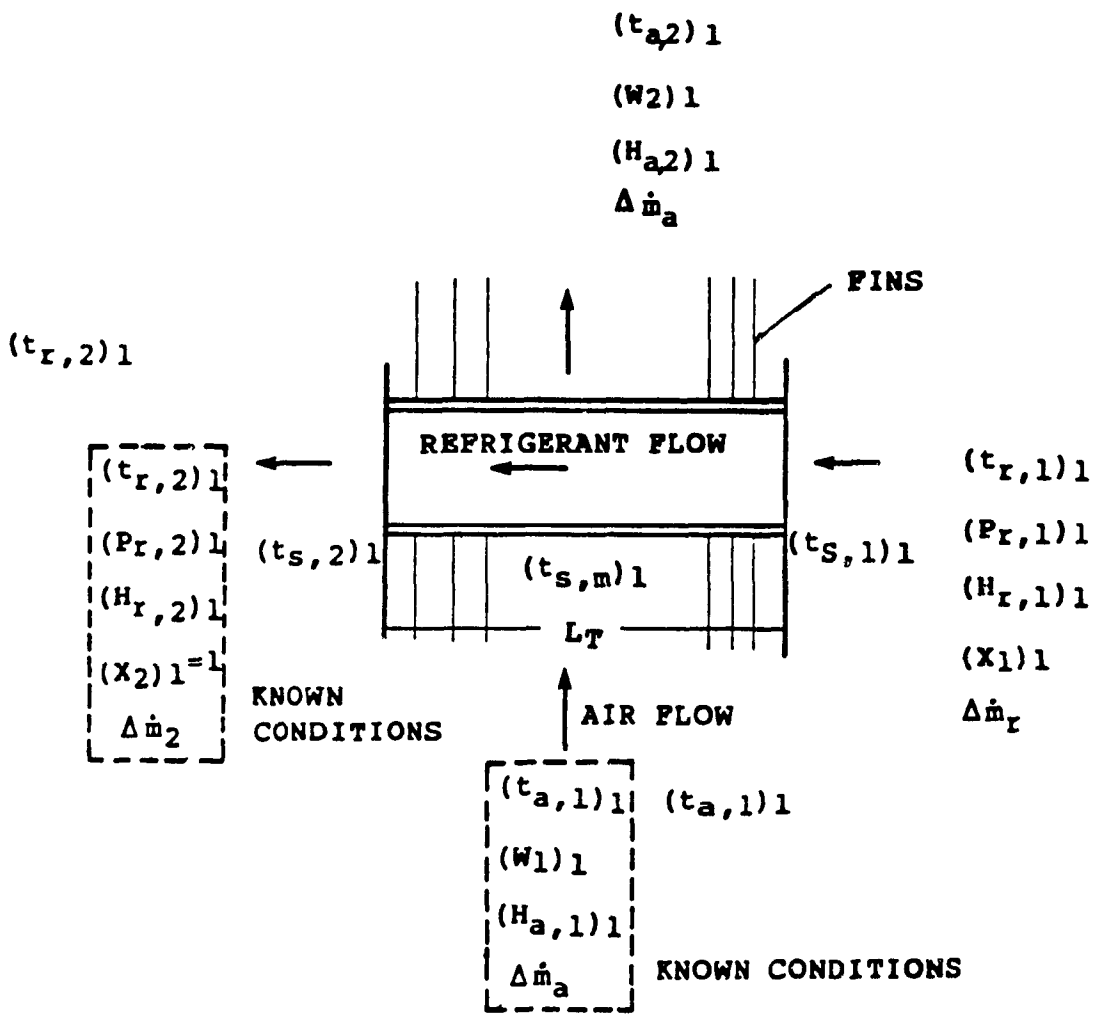

FIG. 7.3 THERMODYNAMIC CONDITIONS OF THE WORKING FLUIDS FOR THE FIRST ROW

3. ROW-BY-ROW HEAT BALANCE CALCULATION METHOD:

The thermodynamic conditions of the working fluids in a typical tube circuit are shown in Fig. 7.2 and the corresponding local conditions are shown in Fig. 7.3.

3.1 Heat Balance Calculations for the First Row (Row-1)

For a cross-counter flow arrangement of the working fluids in typical air cooling and dehumidifying coils, sensible heat transfer occurs primarily in Row-1 [9], and the refrigerant is generally in the super heated vapour phase in the tube (in Row-1) [13]. For small tube length ($30 < L_T < 120$ cm), the sensible heat transfer rate (from the air) for a given row ($\Delta Q_{D,i}$) may be expressed as follows [from Eqn. 4.15]:

$$\Delta Q_{D,i} = [(t_{a,1})_i - (t_{r,2})_i] \,/\, [(1/\Delta A_o h_{a,D}) + (1/\Delta A_I h_r) + (R_m/\Delta A_o)] \quad 7.1$$

where, for row-1,

$$(t_{a,1})_1 = t_{a,1} \qquad \text{(given condition)} \qquad (7.2)$$

$$(t_{r,2})_1 = t_{r,2} \qquad \text{(given condition)} \qquad (7.3)$$

$$h_{a,D} = j_{a,D}\, G_{m,f}\, C_p\, Pr^{-2/3} \qquad (7.4)$$

$$h_r = Nu_r\, K_{r,1}/D_I \qquad (7.5)$$

$J_{a,D}$ - given by Eqn. 6.4

Nu_r - given by Eqn. 6.5

R_m - given by Eqn. 4.16

ΔA_o, ΔA_I - total air-side surface and tube internal surface areas per row, given by Eqns. 4.3, and 4.4, respectively.

In order to determine the refrigerant-side average heat transfer coefficient (h_r), the corresponding average Nusselt number (Nu_r) and the average boiling number (K_f) may be computed as follows:

1. The refrigerant liquid mass flow rate (m_r) is given by:

$$m_r = Q_{REQ} / (H_{r,1}) - (H_{r,2}) \qquad (7.6)$$

where

Q_{REQ} - Required coil heat transfer rate (given)

$(H_{r,1})$ - Enthalpy of the refrigerant liquid entering coils (which is assumed to be equal to the enthalpy of refrigerant leaving condenser - see Fig. 2.6)

$(H_{r,2})$ - Enthalpy of the refrigerant vapour (superheated) leaving the coil (at $p_{r,2}$ and $t_{r,2}$ - given)

2. The refrigerant liquid flow Reynolds number $Re_{r,l}$ may than be computed from Eqn. 2.31.

3. The vapour fraction of the refrigerant entering the coil (x_1) may be computed as follows:

$$x_1 = (H_{r,1} - H_f)/H_{fg} \qquad (7.7)$$

where

H_f - Enthalpy of liquid at the evaporator pressure (at $P_{r,2}$)

H_{fg} - Latent heat of refrigeration (at $P_{r,2}$)

The error in x_1 (due to the pressure drop in the coil) is negligible (< 5%) in the range of refrigerant mass flux and the tube circuit length considered ($60 < G_{r,1} < 120$ kg/m^{2}s, $30 < L_T < 120$ cm).

4. The average boiling number (K_f) may be computed from Eqn. 2.34, and the corresponding Nusselt number may then be computed from Eqn. 6.8.

5. The air-side conditions leaving the row-1 may be computed as follows:

A. The change in the enthalpy of the air leaving row-1 ($\Delta H_{a,1}$) is given by:

$$\Delta H_{a,1} = (\Delta Q_{1,D}/\Delta m_a) \qquad (7.8)$$

where

Δm_a - Air mass flow rate across tube circuit

$\Delta Q_{D,1}$ - Defined at Eqn. 7.1

B. The average air dry bulb temperature $[(t_{a,2})_1]$ and humidity ratio $[(w_2)_1]$ leaving row-1 are given by:

$$(t_{a,2})_1 = (t_{a,1})_1 - [\Delta H_{a,1}/C_p] \quad (7.9)$$

$$(W_2)_1 = W_1 \quad \text{(since the surface is dry)} \quad (7.10)$$

6. The air pressure drop across row-1 ($\Delta P_{a,1}$) may be computed from Eqn. 2.4, where $f_{a,D}$ is given by Eqn. 6.6

7. The refrigerant enthalpy entering row-1 $[(H_{r,1})_1]$ may be computed as follows:

The change in the refrigerant enthalpy in row-1 ($\Delta H_{r,1}$) is given by:

$$\Delta H_{r,1} = \Delta Q_{1,D}/\Delta m_r \quad (7.11)$$

Hence,

$$(H_{r,1})_1 = (H_{r,2})_1 - \Delta H_{r,1} \quad (7.12)$$

where

Δm_r - Refrigerant mass flow rate per circuit

8. The refrigerant pressure drop in row-1 ($\Delta p_{r,1}$) may be computed from Eqn. 3.33 as follows:

$$\Delta p_{r,1} = f_r(DP) \qquad (7.13)$$

where

f_r - given by Eqn. 6.9

(DP) - given by Eqn. 2.36

Since the ratio of the tube diameter to the tube length (D_I/L_T) and the change in the vapour fraction per row are small (< 1%) for typical comfort air conditioning applications, [compared to $f_r(DP)$] the term (DX) [Eqn. 2.34] may be neglected.

9. The refrigerant pressure entering row-1 may then be computed as follows:

$$(p_{r,1}) = (p_{r,2}) - \Delta p_{r,1} \qquad (7.14)$$

10. The vapour fraction of the refrigerant entering row-1 is computed as follows:

$$x_1 = [(H_{r,1})_1 - (H_f)_1] / (H_{fg})_1 \qquad (7.15)$$

where

$(H_{r,1})_1$ - given by Eqn. 7.11

$(H_f)_1$ - refrigerant liquid entnalpy at $(p_{r,1})_1$

$(H_{fg})_1$ - latent heat of vaporization at $(p_{r,1})_1$

From the refrigerant thermodynamic properties, the refrigerant temperature entering row-1 $[(t_{r,1})_1]$ may be computed, from $(H_{r,1})_1$ and $(p_{r,1})_1$.

3.2 Heat Balance Calculations for Row-2:

1) The entering air-side average conditions for row-2 may be expressed as follows:

$$(t_{a,1})_2 = (t_{a,2})_1 \qquad (7.16)$$

$$(W_1)_2 = (W_2)_1$$

where

$(t_{a,2})_1$ - given by Eqn. 7.9

$(W_2)_1$ - given by Eqn. 7.10

2) The refrigerant pressure leaving row-2 $(p_{r,2})_2$ may be expressed as follows:

$$(p_{r,2})_2 = (p_{r,1})_1 - (\Delta p_r)_{RB,1} \qquad (7.17)$$

where

$(p_{r,2})_2$ - given by Eqn. 7.14

$(\Delta p_r)_{RB,1}$ - given by Eqn. 2.44

3) The refrigerant enthalpy leaving row-2 $[(H_{r,2})_1]$ is equal to the corresponding enthalpy entering row-1 $[(H_{r,1})_1]$ since the heat loss from the unheated return-bend is neglected.

4) The refrigerant temperature leaving row-2 $[(t_{r,2})_2]$ may then be computed from the refrigerant properties at $[(p_{r,2})_2$ and $(H_{r,2})_2]$.

5) Assuming air-side dry surface conditions for row-2, the corresponding estimated heat transfer rate $(\Delta Q'_{D,2})$ may be computed from Eqn. 7.1. Since fully mixed conditions are assumed for the working fluids, and the corresponding temperature drop for a given tube row is generally small, the estimated mean tube surface temperature for row-2 may be expressed as follows (from Eqn. 4.19):

$$(t_s)_2 = [(t_{a,1})_2 - \Delta Q'_{D,2}] / [h_{a,D}(\Delta A_o)] \qquad (7.18)$$

6) The tube air-side surface condition (dry or wet) for row-2 may be determined as follows:

if $(t'_s)_2 \quad (t_{a,1})_{2,sat}$ - the tube surface is dry (7.19)

if $(t_{s_2}) < (t_{a,1})_{2,sat}$ - the tube surface is wet (7.20)

7) If the tube surface is dry, then the actual heat transfer rate $Q_{D,2} = Q'_{D,2}$ (from Eqn. 7.1), and the corresponding air-side conditions leaving the row $[(t_{a,2})_2, (w_2)_2$, and $\Delta p_{a,2}]$ and the refrigerant side conditions entering the row $[(p_{r,1})_2, (t_{r,1})_2, (x_1)_2$, and $\Delta p_{r,2}]$ may be computed similarly to those for row-1.

8) If the tube surface is wet, the corrected mean tube surface temperature $(t_s)_2$ may be computed from the coil characteristic (C) as follows [32]:

$$C = \frac{R_r + R_m}{C_p R_{a,w}} = [(t_s)_2 - (t_{r2})_2] / [(H_{a,1})_2 - (H_s)_2] \quad (7.21)$$

where

C - coil characteristic, which is constant for a given coil configuration, in the range of comfortair conditioning applications [32].

R_r - Refrigerant-side average thermal resistance $[=A_o/(A_I h_r)]$

R_m - Finned tube material thermal resistance (Eqn. 4.16)

$R_{a,w}$ - Air-side wet surface average thermal resistance, computed from Eqn. 4.36, where $j_{a,w}$ is given by Eqn. 6.6

$(t_{r,2})_2$ - Refrigerant temperature leaving the row

$(H_{a,1})_2$ - Air enthalpy entering the row

$(H_s)_2$ - Saturated enthalpy at $(t_s)_2$

Therefore, for known values of C, $(t_{r,2_2})$ and $(H_{a,1_2})$, the corresponding $(t_s)_2$ and $(H_s)_2$ may be computed from the moist air physical properties.

9) The heat transferred (sensible and latent) from the moist air to the heat transfer surface $(\Delta Q_w)_2$ of row-2 may be expressed as follows:

$$(\Delta Q_w)_2 = [(H_{a,1})_2 - (H_s)_2] \Delta A_o / (C_p R_{a,w}) \qquad (7.22)$$

10) The corresponding air enthalpy change across the row $(\Delta H_{a,w})_2$ and the leaving air enthalpy $(H_{a,2})_2$ may be expressed as follows:

$$(\Delta H_{a,w})_2 = (\Delta Q_w)_2 / (\Delta m_a) \qquad (7.23)$$

$$(H_{a,2})_2 = (H_{a,1})_2 - (\Delta H_{a,w})_2 \qquad (7.24)$$

11) The air dry bulb temperature and the corresponding humidity ratio leaving row-2 $[(t_{a,2})_2$ and $(W_s)_2]$ are computed from $(H_{a,2})_2$ from the moist air properties by trial and error.

12) The air pressure drop across the row $(\Delta p_{a,w})_2$ may be computed from Eqn. 2.4, where $f_{a,w}$ is given by Eqn. 6.11.

13) The corresponding refrigerant conditions entering the row $[(t_{r,1})_2$, $(p_{r,1})_2$, $(x_1)_2]$ and the corresponding refrigerant pressure drop $(\Delta p_{r,2})$ may be computed similarly to those for row-1.

3.3 Heat Balance Calculations: for the Subsequent Rows:

For each of the subsequent row (row-3 to row-n), the air conditions leaving the row $[(t_{a,1})_i$ - $(w_2)_i]$, the refrigerant-side conditions entering the row $[(t_{r,1})_i$, $(p_{r,1})_i$, $(x_1)_i]$, the corresponding pressure drops $[(\Delta p_a)_i$ and $(\Delta p_r)_i]$ and the heat transfer rate $[(\Delta Q_D)_i$ or $(\Delta Q_w)_i]$ are computed similarly to those for row-2.

3.4 Summation Calculations:

In order to determine the coil performance [Q, Δp_a and Δp_r], the following summation calculations are performed.

1) The total coil capacity (Q) may be expressed as follows:

$$Q = \sum_{i=1}^{N} (\Delta Q_{D,i} + \Delta Q_{w,i}) \qquad (7.26)$$

2) The total air pressure drop across the coil may be determined as follows:

$$\Delta p_a = \sum_{i=1}^{N} (\Delta p_{a,D,i} + \Delta p_{a,w,i}) \qquad (7.27)$$

3) The total refrigerant pressure drop may be computed as follows:

$$\Delta p_r = (p_{r,2})_1 - (p_{r,1})_N \qquad (7.28)$$

4. COMPUTER ASSISTED SELECTION METHOD:

A computer assisted method for the selection of DX-coils has been developed from the row-by-row heat balance calculations described in the previous section. A flow chart of the method is shown in Fig. 7.4. This method may be used for prediction of the performance data for a given coil configuration for given operating conditions defined in Section 1.A of this Chapter. In addition, the method may also be used for selection of the coil configuration (among the available alternatives) for minimum air and refrigerant side pressure drop, in order to minimize the energy consumption. Applications of the method for energy effective operation of DX-coils are presented in Appendix 6.

In order to validate this method, additional tests for the air side partially wet surface conditions are conducted, and the results are shown in Appendix-3. The partially wet surface conditions (for the air-side) are ensured when the measured average tube surface temperature for the first row (in the direction of the air flow) is greater than the entering air saturation temperature and the measured average tube surface temperature for the last row is less than the coil leaving air saturated tempature ($t_{a,2,sat}$). The corresponding heat transfer capacities (Q_a and Q_r) are computed from Eqns. 4.27 and 4.28 respectively, and the air and the refrigerant pressure drop across the coil are measured similarly to those described for the fully dry or wet surface tests.

A comparison of the experimental data (for the partially wet surface tests) with the corresponding computed data (from the selection method) is shown in Table 7.1. From this method, the average coil capapcity (Q) and the air pressure drop across the coil (Δp_a) may be predicted within + 10% error, and the corresponding refrigerant side pressure drop may be predicted within + 20% error.

TABLE 7.1 COMPARISON OF THE EXPERIMENTAL AND COMPUTED COIL PERFORMANCE DATA (PARTIALLY WET SURFAE TESTS)

(1) COIL REF NO.	(2) TEST REF. NO.	N_R	P_s fins/cm	Δt_a (°C)			ΔH_a (kJ/kg)			Q (kW)			Δp_a (Pa)			Δp_r (kPa)		
				EXP	COMP.	Δ%	EXP	COMP.	Δ%	EXP	COMP.	Δ%	EXP	COMP.	Δ%	EXP	COMP	Δ%
01	07	3	3.9	8.3	6.3	-24.0	12.6	11.3	-10.3	22.9	20.6	-10	67.2	62.2	-7.4	1.9	2.0	5.3
02	14	3	4.7	8.1	5.8	-28.4	12.6	12.1	4.0	23.4	22.5	-3.8	74.7	67.2	-10.0	1.7	1.9	11.8
03	21	3	5.5	10.1	7.3	-27.0	12.6	12.4	-1.6	25.3	24.9	-1.6	110.1	119.6	8.7	2.7	2.7	0
04	28	4	5.5	8.1	6.8	-16.0	16.8	16.3	-3.0	37.2	36.1	-3	170.1	180.1	5.9	4.1	2.7	-34
05	35	6	3.1	9.3	8.2	-11.8	17.4	18.1	4.0	35.9	37.2	3.6	120.5	129.5	7.5	6.1	4.3	-29.5
06	42	6	3.9	10.8	10.9	0.9	17.0	17.2	1.2	38.5	39.4	2.3	149.5	162.0	8.4	8.4	9.6	14.3
07	79	6	4.7	8.1	8.6	6.2	18.3	19.3	5.5	41.1	43.2	5.1	200.5	206.8	3.1	7.0	7.9	12.9
08	56	8	3.1	12.8	12.0	-6.2	22.7	21.2	-6.6	40.3	37.7	-6.5	128.1	119.6	-6.6	11.2	11.0	-1.8
09	63	8	3.9	12.8	10.9	-14.8	23.4	23.7	1.3	52.0	52.7	1.4	250.1	274.0	9.6	11.0	13.8	25.5
10	70	8	5.9	15.8	12.0	-24	31.2	31.4	0.6	52.0	52.6	1.2	254.2	274.0	7.8	13.0	14.7	13.1
*ABSOLUTE MEAN DIFFERENCE						15.9%			3.8%			3.85%			7.5%			14.8%

(1) - see Appendix-1
(2) - see Appendix-3

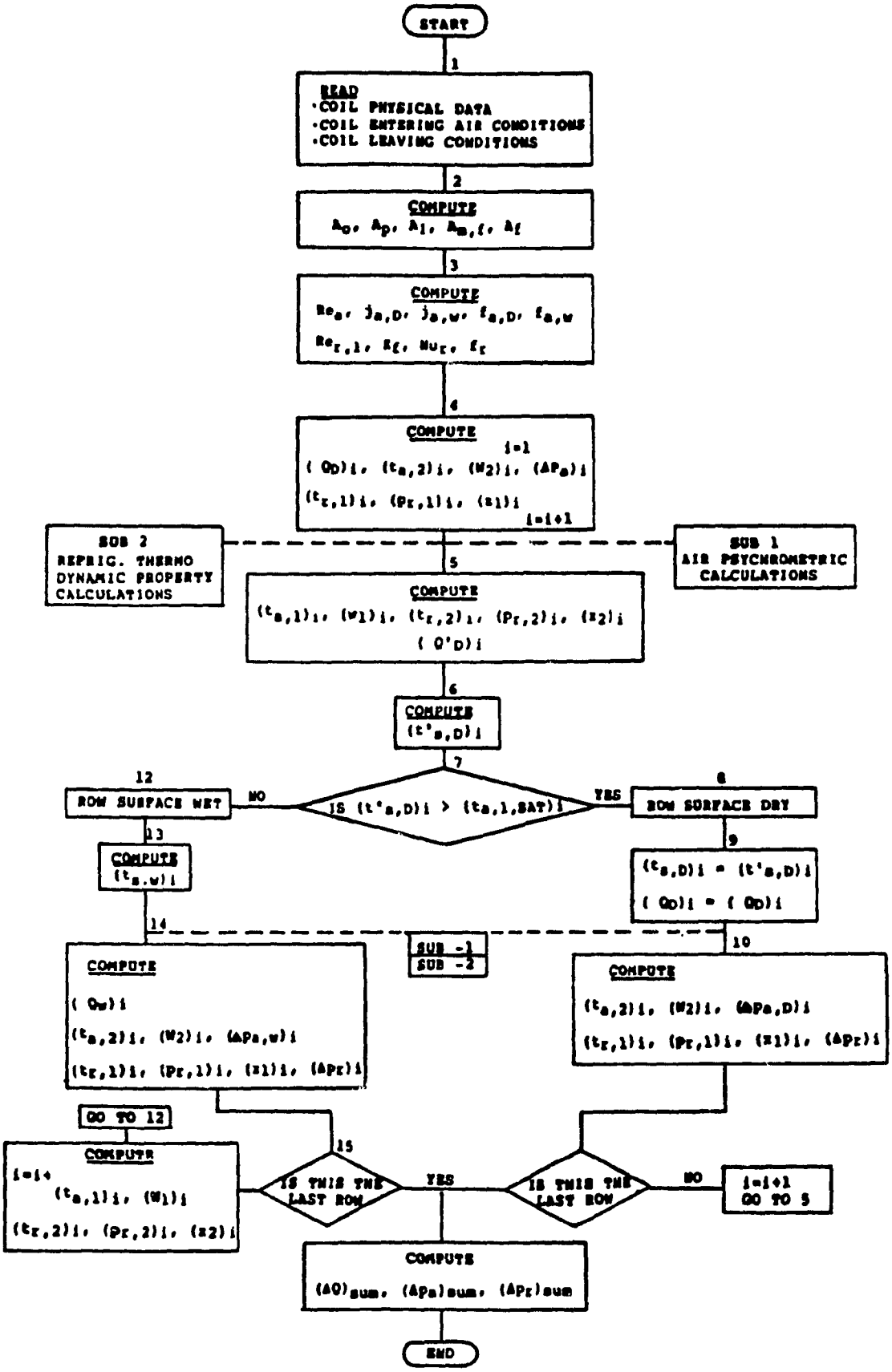

FIG. 7.4 FLOW CHART FOR THE COMPUTER ASSISTED COIL SELECTION METHOD

CHAPTER - 8

CONCLUSIONS AND RECOMMENDATIONS

1. CONCLUSIONS

Performance of multi-row, plate finned-tube, direct-expansion coils is presented through experimental studies; ten coils, with varied fin density and tube rows are tested under dry and wet surface conditions for the air side. Such studies on the performance of DX-coils for comfort air conditioning applications are not available in the present literature.

Correlations for prediction of the average heat transfer and pressure drop factors for the working fluids in DX-coils (air and refrigerant) are developed from the experimental data by regression analysis; such correlations for the refrigerant side of DX-coils are not available in the existing literature.

A method for the selection of DX-coils is also developed (based on the correlations developed) in order to determine the coil configuration for minimizing the air-side and refrigerant-side pressure drop across the coil.

The Major findings from this study may be summarized as follows:

i) For a given air flow Reynolds number (Re_a), the air side average heat transfer and pressure drop factors for platefinned tube multi-row DX-coils are dependent on the tube diameter (D_o), tube spacing (S_L and S_T), fin density (P_S), and the fin thickness (Y_f).

ii) The effect of the tube rows on the air-side average heat transfer and pressure drop factors is found to be insignificant for typical air flow conditions encountered in comfort air conditioning applications ($300 < Re_a < 1500$).

iii) For a given air flow Reynolds number, tube diameter (D_o), and the tube spacing (S_L and S_T), the air side average heat transfer and pressure drop factors decrease when the fin density is increased. However, the corresponding heat transfer rate and the air pressure drop across the coil may increase (due to increase in the heat transfer surface area). Consequently, for energy effective selection of DX-coils, the effects of the coil geometric parameters on both the heat transfer rate and the corresponding air pressure drop should be considered.

iv) The air-side average heat transfer and pressure drop factors for DX-coils for the dry surface condition ($j_{a,D}$ and $f_{a,D}$) are most sensitive to the ratio of the air-side total surface area to the tube surface area (A_o/A_p); the corresponding factors for the wet surface condition ($j_{a,w}$ and $f_{a,w}$) are most sensitive to the ratio of the fin spacing to the fin thickness (S_f/Y_f) due to the presence of the condensate film.

v) The refrigerant-side average Nusselt number in DX-coils [for refrigerant mass flux ($G_{r,l}$) < 120 kg/m^{2}s] is most sensitive to the heat transfer parameter ($Re^2_{r,l}\ k_f$). The average Nusselt

number is also dependent on the ratio of the air side total surface area to the tube internal surface area (A_o/A_I). The corresponding average pressure drop factor (f_r) is a decreasing function of the pressure drop parameter ($Re_{r,l}/k_f$).

vi) The presence of oil in the refrigerant (about 2% by weight) may increase the average Nusselt number by 20 to 40% compared to the corresponding oil-free flow. The corresponding increase in the average pressure drop factor (with oil) is about 25%.

2. RECOMMENDATIONS:

In the present study, the coil tests are conducted for the refrigerant mass flux less than 120 kg/m^{2}s. Additional studies are required to determine the refrigerant side heat transfer and pressure drop factors at higher mass flux ($G_{r,l}$ > 120 kg/m^{2}s).

Additional studies are also required to evaluate the effects of oil concentration on the refrigerant heat transfer and pressure drop factors in DX-coils.

The effects of the coil geometrical parameters (such as the tube diameter and tube spacing) on the air-side heat transfer and pressure drop factors should be investigated.

REFERENCES

1. "Quarterly Reports on the Energy Supply and Demand in Canada", Published by Statics Canada, Ottawa, Ontario, 1984.

2. Brooks, D.B., and Doe, J., "Energy Conservation, How Big a Target", ASHRAE Journal, Vol. 18, No. 8, August, 1984.

3. Elmahdy, A.H., and Mitalas, G.P., "Fortran IV Program to Simulate Cooling and Dehumidifying Finned-Tube Multi-Row Heat Exchangers", CP-43, Published by the National Research Council of Canada, Ottawa, Ontario, March, 1977.

4. Anderson, S.W., Rich, D.G., and Geary, D.F., "Evaporation of Refrigerant-22 in a Horizontal 3/4-inch O.D. Tube", ASHRAE Transactions Vol. 18, No. 9, 1976.

5. "D.O.E-2 Computer Program for Building Energy Analysis", published by The Building Energy Simulation Group, Lawrence Berkeley Laboratories, University of California, Berkeley, California, January, 1983.

6. "Building Load Analysis and Sytstem Thermodynamics (BLAST) Program", published by the Air Force Environmental Engineering Development Office and the Department of Navy, Washington, D.C., 1977.

7. Elmahdy, A.H., "Analytical and Experimental Multi-Row, Finned-Tube Heat Exchager Performance During Cooling and Dehumidification Process", Ph.D. Thesis, Department of Mechanical Engineering, Carleton University, Ottawa, December, 1975.

8. "Air System Design and Retrofit for Energy/Cost Effectiveness", proceedings of the ASHRAE Professional Development Seminars (PDS), October 27, 28, 1983.

9. Goodman, W., "Performance of Coils for Dehumidifying Air", Heating Piping, Air Conditioning Journal, Vol. 10, No. 11, November, 1938.

10. Webb, R.L., "Air Side Heat Transfer in Finned-Tube Heat Exchangers", Heat Transfer Engineering Journal, Vol. 1, No. 3, January-March, 1980.

11. McQuiston, F.C., "Finned Tube Heat Exchangers - State of the Art for the Air Side", ASHRAE Transactions, Vol. 87, Part-I, 1981.

12. Rich, D.G., Chaddock, J.B., "Design of Direct Expansion Evaporator Coils by Digital Computer", proceedings of the Symposium on 'use of Computers for Environmental Engineering Related to Buildings', Gaithersbug, Maryland, November 30, December 2, 1970, pp. 525-544.

13. McQuiston, F.C., "Heat, Mass and Momentum Transfer Data for Five Plate-Fin-Tube Heat Transfer Surfaces", ASHRAE Transactions, Vol. 84, Part I, 1978.

14. McQuiston, F.C., "Correlations for Heat, Mass and Momentum Transport Coefficients for Plate-Fin-Tube Heat Transfer Surfaces with Staggerd Tubes", AHSRAE Transactions, Vol. 84, Part I, 1978.

15. Pierre, B., The Coefficients of Heat Transfer for Boiling Freon-12 in Horizontal Tubes", Published by Svenska Flaktfabrikent A.B., S.F. Review, Vol. 2, No. 1, 1955.

16. Pierre, B., "Flow Resistance to Boiling Refrigerants, Part I", AHSRAE Journal, September, 1964.

17. Pierre, B., "Flow Resistance to Boiling Refrigerants, Part II", ASHRAE Journal, October, 1964.

18. Rich, D.G., "The Effect of Fin Spacing on the Heat Transfer and Friction Performance of Multi-Row, Smooth Plate Fin-and-Tube Heat Exchangers", ASHRAE Transactions, Vol. 79, Part 2, 1973.

19. Kays, W.M., and London, A.L., "Compact Heat Exchangers", McGraw-Hill Book Company, New York, 1964.

20. Stoecker, W., "Refrigeration and Air Conditioning", McGraw-Hill Book Company, New York, 1972, p. 408.

21. Threlkeld, J.L., "Thermal Environmental Engineering", 2nd. Edition, Prentice-Hall Book Company, Englewood Cliffs, N.J. 1970.

22. Rich, D.G., "The Effect of the Number of Tube Rows on Heat Transfer Performance of Smooth Plate Fin-and-Tube Heat Exchangers", ASHRAE Transactions, Vol. 81, Part I, 1975.

23. Tuve, G.L., "Performance of Fin-Tube Units for Air Heating, Cooling and Dehumidifying", ASHRAE Transactions, Vol. 42, No. 1029, 1936.

24. Briggs, D.E., and Young, E.H., "Convection Heat Transfer and Pressure Drop of Air Flow Across Triangular Pitch Banks of Finned Tubes", Chemical Engineering Progress Symposium Series, Heat Transfer, Vol. 59, No. 41, 1963.

25. Myers, R., "The Effect of Dehumidification on the Air Side Heat Transfer Coefficient for a finned-tube Coil", Masters Thesis, University of Minnesota, 1967.

26. Jameson, S.L., "Tube Spacing in Finned Tube Banks", ASME Transactions, No. 67, November 1945, pp. 633-642.

27. ASHRAE Hand Book, Systems Volume 1984, Chapter 29, published by ASHRAE, Atlanta, Georgia, 1980, p. 29.8.

28. Worse-Schmidt, P., "Some Characteristics of Flow Patterns and Heat Transfer of Freon 12 Evaporating in Horizontal Tubes", The Journal of Refrigeration, Vol. 40, March/April 1960.

29. Green, G.H., Furse, F.G., "Effects of Oil on Heat Transfer from a Horizontal Tube to Boiling R-12 Mixtures", ASHRAE Journal, Vol. 63, October 1963.

30. Chaddock, J.B., "Influence of Oil on Refrigerant Evaporator Performance", ASHRAE Transactions, Vol. 82, Part 1, 1976.

31. ASHRAE Standard 33-78, "Methods for Testing Forces Circulation Air Cooling and Heating Coils", published by ASHRAE, Atlanta, Georgia, 1978.

32. A.R.I. Standard 410-72, "Standard for Forced Circulation Air Cooling and Heating Coils", published by the Air Conditioning and Refrigeration Institute, Arligton, Virginia, 1972.

33. ASHRAE Standard 41.9, "Gravimetric Determination of the Concentration of Oil in a Refrigerant Flow Stream", Published by ASHRAE, Atlanta, Georgia.

34. Draper, N.P., and Smith, H., "Applied Rregression Analysis", John Wiley and Sons, New York, 1963.

35. ASHRAE Handbook and Product Directory, Equipment 1979, Chapter 6, published by ASHRAE Inc., Atlanta, Georgia, 1979, p. 6.13.

36. ASHRAE Handbook - Fundamentals 1981, Chapter 6, published by ASHRAE Inc., Atlanta, Georgia, 1981.

37. Blanchard-ness Inc., Catalog No. 129, Coil No. BNDX 3-10-79, Blanchard-ness Inc. St. Hubert, Quebec, 1979.

38. Young, H.D., "Statistical Treatment of Experimental Data", McGraw-Hill Inc., New York, 1962.

BIBLIOGRAPHY

Air-Side - Studies

B1 Kays, W.M., and London, "Heat Transfer and Flow Friction Characteristics of Some Compact Heat Exchangers, Part I, Test System and Procedure", ASME Transactions, Vol. 72, November 1950.

B2 Gram, A.J., MacKey and Monroe, "Convection Heat Transfer and Pressure Drop of Air Flowing Across In-Line Tube, Banks, II-Correlation of Data for Ten Row Deep Bank", ASME Transactions, Vol. 80, 1958.

B3 Ward, D.J., Young, E.H., "Heat Transfer and Pressure Drop Across Triangular Pitch Banks of Finned Tubes", Chem Eng. Progress Symposium Series, Vol. 53, No. 29, 1959.

B4 Jones and Munroe, "Convection Heat Transfer and Pressure Drop of Air Flowing Across In-Line Tube Banks, Apparatus, Procedure and Special Effects", ASME Transactions, Vol. 80, 1958, pp. 18.

B5 Lapin, A., and Schuring, W., "Heat Transfer Coefficients for Finned Exchangers", Ind. Eng. Chem., Vol. 51, No. 8, August, 1959.

B6 LaHaye, P.G., Skhuja, R.K. and Neugebauer, F.J., "A Generalized Prediction of Heat Transfer Surface Performance and Exchanger Optimization", ASME Paper No. 72-WA/HT-55, 1955.

B7 Ashley, C., "A Method of Analyzing Finned Coil Heat Transfer Performance", Journal of A.S.H.R.A.E., June, 1946.

B8 Kusuda, T., "Coil Performance Solutions without Trial and Error", Air Conditioning, Heating and Ventilating, January, 1960.

B9 Bryan, W.L., "Heat and Mass Transfer in Dehumidifying Surface Coils", ASHRAE Journal, September, 1961.

B10 Bryan, W.L., "Heat and Mass Transfer in Dehumidifying Extended Surface Coils", ASHRAE Journal, April, 1962.

B11 Schmidt, E., "Heat Transfer for Finned Tubes and Computations of Tube Bank Heat Exchangers", Kalttechnik, Vol. 15, No. 4, 1963.

B12 Tamm, H. "Dynamic Response Relations for Multi-Row Cross-Flow Heat Exchangers", ASHRAE Transactions, Vol. 75, Part II, 1969.

B13 McCullagh, Green, G.H., and Sheker, S.C., "An Analysis of Chill Water Cooling Dehumidifying Coils Using Dynamic Relationships", AHSRAE Transactions, Vol. 75, Part II, 1969.

B14 Guillary, J.L., and McQuiston, F.C., "An Experimental Investigation of Air Humidification in a Parallel Plate Exchanger", AHSRAE Transactions, Vol. 79, Part I, 1973.

B15 McQuiston, F., "Fin Efficiency with Combined Heat and Mass Transfer", AHSRAE Transactions, Vol. 81, Part I, 1975.

B16 Trapenese, E., Bettanini, and Di Filippo, P., "Essais Experimentaux Sur L'Influence du Rapport Chaleur Sensible - Chaleur Totale sur le Coefficient de Transmission de Chaleur dans les Batteries de Tubes a Ailettes", International Institute of Refrigeration, Annexe 1964-65 au Bulletine 88R.

B17 Carrier, W.H., and Anderson, S.W., "The Resistance to Heat Flow Through Finned Tubing", Heating, Piping and Air-Conditioning, Vol. 16, 944.

B18 Kasuda, T., "Effectiveness Method for Prediction of the Performance of Finned-Tube Coils", AHSRAE Symposium Publication, June 1969.

B19 Shepherd, D.G., "Performance of One-Row Tube Coils with Thin-Plate Fins, Low Velocity Forced Convection, ASHRAE Transactions, Vol. 62, pp. 505-530, 1956.

B20 McQuiston, F., and Tree, D.R., "Heat Transfer and Flow Friction Data for Two Fin-Tube Surfaces", Heat Tranfer Journal, Vol. 93, pp. 249-250, 1971.

B21 Elmahady, A.H., and Biggs, R.C., "Finned Tube Heat Exchanger", AHSRAE Transactions, Vol. 85, Part 2, pp. 262-273, 1979.

B22 Gebhart, B., "Flow and Heat Transfer Characteristics of Finned-Tube Exchangers", AHSRAE Transactions, Vol. 67, pp. 133-153, 1961.

B23 Forgo, L., "Some Extra-High Capacity Heat Exchangers of Special Design, in Heat Exchangers", Design and Theory Sourcebook", Editors, N.H., Afgan and E.U. Schlunder, pp. 101-120, Hemisphere, Washington, D.C., 1974.

B24 Vlades, I., Theil, H., and Neiss, F., Waermeaus Sauscher mit Flachrohren and Dorchlaufenden Rippen, Heat Transfer 1970, Vol. 1 Paper Hel 5, Elsevier, Amsterdam, 1970.

B25 Zozulya, N.Y., Khavin,A.A., and Kalimn, B.I., "Effect of Fin Deformation on Heat Transfer and Drag in Bundles of Oval Tubes with Transverse Fins, Heat Transfer Sov. Res., Vol. 2, No. 1, pp. 77-79, 1970.

B26 Zozulya, N.Y. Kalinin, B.L., "Effects of Fin Deformation on Heat Transfer and Drag in Bundles of Oval Tubes with Transverse Fins, Heat Transfer Sov. Res., Vol. 7, No. 2, pp. 95-98, 1975.

B27 Fukui, S., and Sakamoto, M., "Some Experimental Results on Heat Transfer Characteristics of Air Cooled Heat Exchangers for Air Conditioning Devices, Ball., JSME, Vol., 11, No. 44, pp. 303-311, 1968.

B28 Saboya, F.F.M., and Sparrow, E.M., "Local and Average Heat Transfer Coefficients for One-Row Plate-Fin and Tube Heat Exchanger Configurations, Heat Transfer Journal, Vol. 96, pp. 265-272, 1974.

B29 Saboya, F.E.M. and Sparrow, E.M., "Transfer Characteristics of Two-Row Plate Fin and Tube Heat Exchanger Configuration, Int. J. Heat Mass Transfer, Vol. 19, pp. 41-49, 1976.

B30 Saboya, F.E.M. and Sparrow, E.M., "Experiments on a Three-Row Fin and Tube Heat Exchanger, Heat Transfer Journal, Vol. 98, pp. 26-34, 1976.

B31 Goldstein, L., Jr. and Sparrow, E.M., "Experiments on the Transfer Characteristics of a Corrugated Fin and Tube Heat Exchanger Configuration, Heat Transfer Journal, Vol. 93, pp. 26-34, 1976.

B32 Goldstein, L.J. and Sparrow, E.M., "Heat Mass Transfer Characteristics for Flow in a Corrugated Wall Channel, Heat Transfer Journal, Vol. 99, 187-195, 1977.

B33 Goldstein, I., Jr. and Sparrow, E.M., "Mass Transfer Experiments on Secondary-Flow Vortices in a Corrugated Wall Channel, Int. J., Heat Mass Transfer, Vol. 19, pp. 1337-1339m 1976.

B34 Madel, S.W., Townshed, M.A. and Parrish, T.F, "Optimal Fin-Side Design of Compact Tube-in-Fin Heat Exchangers with Rippled Fins, J. Heat Transfer, Vol. 101, pp. 514-520, 1979.

B35 Krucckels, S.W. and Kowke, V., "Investigation of the Distribution of Heat Transfer on Fins and Finned - Tubed Models, Chem. Ing. Tech., Vol. 42, pp. 355-362, 1970.

B36 Gunter, A.Y. and Shaw, W.A., "A General Correlation of Friction Factors for Various Types of Surfaces in Crossflow, Trans. ASME, Vol. 67, pp. 643-660, November, 1945.

B37 Katz, D.L. and Young, E.H., Williams, R.B. and Balejiam, G., "How to Design Finned Coils for Cooling", Reinfing Eng., October, 1957.

B38 Katz, D.L. and Young, E.H., Williams, R.B., Balekjiam, G. and Williamson, R.P., "Correlations of Heat Transfer and Pressure Drop for Air Flowing Across Banks of Finned Tubes", University of Michigan, Engineering Research Institute Dept., on Project M592, August, 1952.

B39 Vampola, J., "Heat and Pressure Drop for Gases Flowing through Bundles of Finned Tubes", Strojirensivi, Vol. 16, No. 7, 1966.

B40 Goodman, W., "Performance of Coils for Dehumidifying Air", Heating Piping, Air Conditioning, Vol. 10, No. 11, Nov. 1938.

Refrigerant-Side Studies

B41 Dangler, C.E., Addoms, J.N., "Heat Transfer Mechanism for Vaporization of Water in a Vertical Tube", Chemical Engineering Process, Vol. 52, No. 18, 1956, pp. 95-103.

B42 Lockhart, R.W. and Martinelli, R.C., "Proposed Correlation of Data for Isothermal, Two-Phase, Two Component Flow in Pipes", Chemical Engineering Process, Vol. 45, No. 39, 1949.

B43 Guerrieri, S.A., Talty, R.D., "A Study of Heat Transfer to Organic Liquids in Single-Tube, Natural Circulation, Vertical Tube Boilers", Chemical Engineering Process, Symposium Series, Vol. 52, No. 18, 1956, pp. 69-77.

B44 Pierre, B., "The Coefficient of Heat Transfer for Boiling Freon-12 in Horizontal Tubes", S.F. Review, Vol. 2, No. 1, 1955, published by Svenska Flaktfabriken A.B., Stockholm, Sweden.

B45 Altman, M., Norris, R.H., Staub, F.W., "Local and Average Heat Transfer and Pressure Drop for Refrigerants Evaporating in Horizontal Tubes", A.S.M.E. Heat Transfer Journal, August, 1960, pp. 189-196.

B46 Sachs, P., and Long, R.A.K., "A Correlation for Heat Transfer in Stratified Two-Phase Flow, With Vaporization", International Journal of Heat and Mass Transfer, Vol. 2, No. 3, April, 1961.

B47 Chen, J.C., "A Correlation for Boiling Heat Transfer to Boiling Fluids in Convective Flow", A.I.E. paper 63-Ht-34-1963.

B48 Lavin, J.C. and Young, E.H., "Heat Transfer to Evaporating Refrigerants in Two-Phase Flow", AICHE Journal, Vol. II, NO. 6, 1965.

B49 Chaddock, J.B., Noerager, J.A., "Evaporation of Refrigerants-12 in a Horizontal Tube with Constant Wall Heat Flux", ASHRAE Transactions, Vol. 72, Part I, 1966, pp. 90-100.

B50 Geary, D.F., "Flow Resistance with Boiling Refrigerants - Part II", ASHRAE Journal, Vol. 81, Part I, 1975.

B51 Shah, R.K., "Advances in Compact Heat Exchange Technology and Design Theory", Proceedings of the Seventh International Heat Transfer Conference, Munchen, West Germany, 1982, pp. 137.

B52 Chaddock, J.B. and Brunemann, H., "Forced Convection Boiling of Refrigerants in Horizontal Tubes", - Phase 3, Report HL - 113, Research Project RP-45, ASHRAE Publications, 1967.

B53 Anderson, S.W., discussion onf Ref. [8] A.S.M.E. Heat Transfer Journal, August, 1960, pp. 196-198.

B54 Shah, M.M., "A New Correlation for Heat Transfer During Boiling Flow Through Pipes", ASHRAE Transactions, Vol. 82, Part I, 1976.

B55 Chaddock, J.B., Varma, H.K., "An Experimental Investigation of Dry-Out with R-22 Evaporating in a Horizontal Tube", ASHRAE Transactions, Vol. 85, Part II, 1979.

B56 Varma, H.K., "Experimental Investigation of Dry-Out in Forced Convection Evaporation", Ph.D. Thesis, Department of Mechanical Engineering, Duke University, 1970.

B57 Sthapak, B.K., Varma, H.K., Gupta, C.P., "Heat Transfer Coefficients in Dry-Out Region of Horizontal Tube, Water R-12 Evaporator", ASHRAE Transactions, Vol. 82, Part II, 1976.

B58 Sthapak, B.K., Varma, H.K., Gupta, C.P., "Mass Vaport Fraction at the On-Set of Dry-Out in a Horizontal Tube Evaporator", paper B.1.39, International Congress of Refrigeration, Mascow, 1975.

APPENDIX - I

Coil Geometric Data - Present Study

1. Fixed Parameters: D_o = 13.4 mm; D_I = 12.6 mm; $S_T = S_L$ = 38.1 mm; Y_f = 0.16 mm; fin type - flat plate fin; fin material - aluminium; C_H = 55.9 cm; C_w = 121.9 cm

2. Variable parameters:

COIL NO.	N_R	P_s (fins/cm)	D_h (cm)	A_{mf}/A_F	N_{TR}	L_d (cm)	A_o/A_p	A_o/A_I	S_f/Y_f
01	3	3.9	0.32	0.58	15	11.4	26.5	27.0	17.2
02	3	4.7	0.27	0.57	15	11.4	31.8	32.2	14.4
03	3	5.5	0.22	0.56	15	11.4	37.2	37.4	12.3
04	4	5.5	0.22	0.56	15	15.2	37.2	37.4	12.3
05	6	3.1	0.40	0.60	15	22.9	21.2	21.8	21.6
06	6	3.9	0.32	0.58	15	22.9	26.5	27.0	17.2
07	6	4.7	0.27	0.57	15	22.9	31.8	32.2	14.4
08	8	3.1	0.40	0.60	15	30.5	21.2	37.4	12.3
09	8	3.9	0.32	0.58	15	30.5	26.5	27.0	17.2
10	8	5.5	0.22	0.56	15	30.5	37.2	37.4	12.3

APPENDIX - I (cont'd)

Coil Geometric Data - Existing Studies [7.13]

fin material - aluminum
tube material - copper
tube management - stagered
flat plate fins

McQuiston [13]

COIL NO.	N_R	P_s (mm)	D_o (mm)	D_I (mm)	S_L (mm)	S_T (mm)	Y_f (mm)	C_H (mm)	C_W (cm)	L_d (cm)	D_h (cm)	$A_{m,f}/A_F$	N_{TR}	A_o/A_p	S_f/Y_f
11	4	3.1	10	--	22	25.4	0.15	30.5	30.5	8.8	0.40	0.58	5	11.2	20.8
12	4	4.7	10	--	22	25.4	0.15	30.5	30.5	8.8	0.26	0.57	5	16.7	13.9
13	4	5.5	10	--	22	25.4	0.15	30.5	30.5	8.8	0.22	0.56	5	19.6	11.9

ELMAHDY [7]

14	8	4.7	15.9	14.6	33	38.1	0.17	61.0	61.0	34.3	0.34	0.54	16	22.3	13.0

APPENDIX - 2

MAJOR EQUIPMENT SPECIFICATIONS

1.	AIR HANDLING UNIT:		
	Rated volume rate	600 ft^3/min	[2833 1/s]
	Rated air static pressure	5.5 in. w.g.	[1.369 kPa]
	Type of fan	Centrigugal	
	Air volume control	Front-face damper	
2.	STEAM BOILER:		
	Rated capacity	60 kW 600V; 3-phase	
	Rated steam pressure	34.7 Lb/in^2	[239.08 kPa]
	Rated steam flow rate	172 Lb_m/hr, 212°F	[21.67 g/s 100°C]
3.	HEATING COIL:		
	Rated capacity	120,000 Btu/Hr	[35.kW]
	Number of rows	6	
	Number of fins	12 fins/in.	[4.7 fins/cm]
	Face area	7.5 ft^2	[0.697 m^2]
	Tube Material	Copper	
	Fin Material	Alluminum	
4.	REFRIGERATION SYSTEM:		
	Number cylinder in compressor	6	
	Compressor type	Reciprocating - open type	
	Refrigerant	R-22	
	Rated capacity	30 tons	[105.6 kW]
	Capacity control	Cylinder unloading	
	Condensor shell-tube, rated pressure	414.7 Lb/in^2	[2857.3 kPa]
	Condensor tube-side, rated pressure	164.7 Lb/in^2	[1134.8 kPa]

APPENDIX - 3

TEST COIL REF NO. 01* $N_R = 3$ $p_s = 3.9$ fin/cm

TEST NO	V_a (m/s)	Δt_a (°C)	ΔH_a (kJ/kg)	Q (kW)	h_a (W/m²°C)	j_a x10²	Δp_a (Pa)	f_a x10²	m_r (kg/s)	Δx	K_f x10⁻²	h_rx10⁻² (W/m²°C)	Nu_r	Δp_r (kPa)	f_r x10²	$Re_{r,l}$ x10⁻²	Re_a
WET SURFACE TESTS																	
01	2.0	11.8	16.0	26.7	77.8	1.21	59.8	5.93	0.14	0.85	39.93	22.5	280	1.3	2.36	42.3	690
02	2.3	8.5	18.2	34.3	83.3	1.15	69.7	5.41	0.17	0.90	40.96	28.1	350	1.9	2.30	51.7	778
03	3.5	4.8	10.8	30.9	91.6	0.82	129.5	4.29	0.19	0.83	40.19	28.2	351	2.1	2.35	56.2	1200
DRY SURFACE TESTS																	
04	2.0	10.9	11.1	18.6	48.9	0.91	44.8	4.42	0.11	0.75	29.11	15.7	196	0.9	2.40	34.0	690
05	2.3	8.7	8.9	16.7	53.9	0.89	57.3	4.22	0.09	0.78	29.92	13.4	168	0.6	3.12	27.4	778
06	3.5	7.9	8.0	23.3	71.1	0.76	107.1	3.56	0.14	0.75	31.13	18.9	236	1.5	2.36	42.7	1200
PARTIALLY WET SURFACE TEST (for validation of the selection method)																	
07	2.3	8.3	12.58	22.9			67.2		0.16					1.9			778

*See Appendix-1

APPENDIX - 3 (cont'd)
TEST COIL REF NO. 02 $N_R = 3$ $p_s = 4.7$ fin/cm

TEST NO	V_a (m/s)	Δt_a (°C)	ΔH_a (kJ/kg)	Q (KW)	h_a (W/m²·°C)	j_a x10²	Δp_a (Pa)	f_a x10²	m_r (kg/s)	Δx	K_f x10⁻²	h_rx10⁻² (W/m²·°C)	Nu_r	Δp_r (kPa)	f_r x10²	$Re_{r,l}$ x10⁻²	Re_a
WET SURFACE TESTS																	
08	1.8	13.0	20.1	28.4	93.7	1.59	57.3	5.76	0.17	0.79	39.6	23.7	304	2.0	2.36	51.8	530
09	2.3	12.5	18.4	34.8	98.8	1.34	82.2	5.27	0.18	0.89	41.3	24.2	311	2.0	2.36	52.4	664
10	2.9	10.2	11.7	27.6	92.6	0.99	117.0	4.62	0.17	0.85	40.3	26.2	336	1.8	2.34	49.9	842
DRY SURFACE TESTS ($q_s/q = 1$)																	
11	1.8	11.6	11.8	17.6	42.9	0.87	43.1	4.34	0.09	0.85	21.5	15.2	195	0.7	3 12	26.8	530
12	2.3	12.2	12.4	23.2	51.2	0.83	67.2	4.23	0.14	0.80	30.7	22.0	283	1.4	2.36	42.3	664
13	2.9	9.7	9.8	23.4	64.2	0.82	99.6	3.86	0.15	0.80	31.7	19.0	244	1.4	2.36	43.2	842
PARTIALLY WET SURFACE TEST (for validation of the selection method)																	
14	8.1	12.6	23.4				74.7		0.15					1.7			664

APPENDIX - 3 (cont'd)
TEST COIL REF NO. 03 $N_R = 3$ $p_s = 5.5$ fin/cm

TEST NO	V_a (m/s)	Δt_a (°C)	ΔH_a (kJ/kg)	Q (kW)	h_a (W/m²°C)	j_a x10²	Δp_a (Pa)	f_a x10²	m_r (kg/s)	Δx	K_f x10⁻²	h_rx10⁻² (W/m²°C)	Nu_r	Δp_r (kPa)	f_r x10²	$Re_{r,l}$ x10⁻²	Re_a
WET SURFACE TESTS																	
15	2.0	12.2	20.9	34.1	82.8	1.24	87.2	5.54	0.02	0.81	38.7	24.8	354	2.7	2.35	60.4	487
16	2.5	9.1	19.6	39.8	98.4	1.18	119.5	4.83	0.21	0.90	41.3	28.3	364	2.7	2.36	61.4	621
17	3.5	6.4	11.9	34.1	85.6	0.73	194.2	4.0	0.20	0.79	41.0	28.1	362	2.7	2.35	59.8	873
DRY SURFACE TESTS																	
18	2.0	12.8	13.1	21.3	45.8	0.82	67.2	4.29	0.11	0.75	30.2	15.4	198	1.0	3.12	32.3	497
19	2.5	11.3	11.6	23.5	54.4	0.78	104.6	4.27	0.15	0.80	31.0	21.6	278	1.4	2.36	43.2	621
20	3.5	9.2	9.3	26.7	68.7	0.70	179.3	3.88	0.16	0.77	30.0	20.1	259	1.8	2.36	48.6	873
PARTIALLY WET SURFACE TEST (for validation of the selection method)																	
21	2.5	10.0	12.6	25.3			110.1		0.18					2.7			621

APPENDIX - 3 (cont'd)
TEST COIL REF NO. 04 N_R = 4 p_s = 5.5 fin/cm

TEST NO	V_a (m/s)	Δt_a (°C)	ΔH_a (kJ/kg)	Q (kW)	h_a (W/m²°C)	j_a x10⁻²	Δp_a (Pa)	f_a x10²	m_r (kg/s)	Δx	K_f x10²	h_rx10² (W/m²°C)	Nu_r	Δp_r (kPa)	f_r x10²	$Re_{r,l}$ x10⁻²	Re_a
WET SURFACE TESTS																	
22	2.5	7.3	17.8	36.3	89.5	1.07	149.4	4.53	0.19	0.94	29.6	25.6	329	3.0	2.35	56.1	623
23	2.8	7.2	16.8	37.5	91.6	1.0	179.3	4.52	0.23	0.95	29.5	28.9	371	4.6	2.35	68.3	682
24	3.2	6.5	15.0	38.7	104.7	0.99	234.1	4.43	0.24	0.95	29.7	28.9	372	4.9	2.34	70.6	789
DRY SURFACE TESTS																	
25	2.5	11.3	11.5	23.5	56.7	0.81	137.0	4.15	0.14	0.70	21.3	15.4	194	2.3	2.58	43.1	623
26	2.8	10.7	10.9	24.3	57.5	0.75	159.4	4.05	0.15	0.70	21.8	17.3	222	2.5	2.58	44.7	682
27	3.2	10.9	11.1	28.7	63.8	0.72	209.2	3.96	0.15	0.74	22.5	17.9	231	2.4	2.58	44.8	789
PARTIALLY WET SURFACE TEST (for validation of the Selection method)																	
28	2.8	8.1	15.2	37.2			170.1		0.20					4.1			682

APPENDIX - 3 (cont'd)
TEST COIL REF NO. 05 $N_R = 6$ $p_s = 3.1$ fin/cm

TEST NO	V_a (m/s)	Δt_a (°C)	ΔH_a (kJ/kg)	Q (kW)	h_a (W/m²·°C)	j_a x10²	Δp_a (Pa)	f_a x10²	m_r (kg/s)	Δx	K_f x10⁻²	h_rx10⁻² (W/m²·°C)	Nu_r	Δp_r (kPa)	f_r x10²	$Re_{r,l}$ x10⁻²	Re_a
WET SURFACE TESTS																	
29	2.2	11.6	19.0	33.1	107	1.60	97.1	5.71	0.15	0.95	19.3	18.3	235	5.4	2.34	46.2	914
30	2.6	8.7	18.5	38.6	126	1.59	124.5	5.12	0.24	0.90	19.5	20.1	259	12.4	2.29	70.7	1094
31	3.4	7.4	15.2	41.3	107	1.03	194.2	4.81	0.26	0.89	18.8	23.4	301	14.1	2.30	76.1	1429
DRY SURFACE TESTS																	
32	2.2	11.0	11.2	19.6	49.8	0.89	74.7	4.41	0.10	0.82	14.9	11.1	143	2.1	2.46	30.3	914
33	2.6	10.5	10.7	22.3	57.6	0.86	104.6	4.29	0.16	0.72	15.0	14.2	183	3.9	2.30	48.6	1094
34	3.4	9.7	9.9	27.0	70.9	0.81	149.4	3.52	0.17	0.75	15.4	15.9	204	4.1	2.30	50.1	1429
PARTIALLY WET SURFACE TEST (for validation of the selection method)																	
35	2.6	9.3	17.4	35.9			120.5		0.2					6.1			

APPENDIX - 3 (cont'd)
TEST COIL REF NO. 06 N_R = 6 p_s = 3.9 fin/cm

TEST NO	V_a (m/s)	Δt_a (°C)	ΔH_a (kJ/kg)	Q (kW)	h_a (W/m²°C)	j_a x10²	Δp_a (Pa)	f_a x10²	m_r (kg/s)	Δx	K_f x10⁻²	h_rx10⁻² (W/m²°C)	Nu_r	Δp_r (kPa)	f_r x10²	$Re_{r,l}$ x10⁻²	Re_a
WET SURFACE TESTS																	
36	2.3	9.2	22.3	40.9	113.8	1.74	144.4	5.49	0.21	0.95	19.5	19.7	254	5.5	2.31	62.3	776
37	2.7	6.8	20.2	42.9	111.8	1.31	166.8	4.81	0.26	0.90	18.6	18.5	335	8.3	2.25	76.4	918
38	3.4	5.2	14.5	43.0	97.1	0.89	249.0	4.30	0.27	0.90	19.0	18.1	319	9.4	2.29	80.7	1174
DRY SURFACE TESTS																	
39	2.3	14.8	15.0	27.7	54.8	0.91	124.5	4.27	0.15	0.75	14.4	14.3	183	3.5	2.30	44.0	776
40	2.7	12.7	12.9	28.2	62.1	0.87	146.9	4.15	0.17	0.78	15.3	15.4	198	4.0	2.30	50.0	918
41	3.4	11.2	11.4	32.7	67.6	0.74	221.6	3.82	0.18	0.82	14.8	15.9	205	4.6	2.30	62.3	1174
PARTIALLY WET SURFACE TEST (for validation of the selection method)																	
42	2.7	10.8	18.1	38.5			149.5		0.20					8.4			918

APPENDIX - 3 (cont'd)
TEST COIL REF NO. 07 N_R = 6 p_s = 4.7 fin/cm

TEST NO	V_a (m/s)	Δt_a (°C)	ΔH_a (kJ/kg)	Q (kW)	h_a (W/m²·°C)	j_a x10²	Δp_a (Pa)	f_a x10²	m_r (kg/s)	Δx	K_f x10⁻²	h_rx10⁻² (W/m²·°C)	Nu_r	Δp_r (kPa)	f_r x10²	$Re_{r,l}$ x10⁻²	Re_a
WET SURFACE TESTS																	
43	2.2	9.9	23.8	41.5	96.5	1.40	149.4	5.42	0.22	0.9	19.9	19.9	256	6.1	2.31	66.1	620
44	2.8	7.9	19.3	43.7	87.6	0.98	214.1	4.62	0.26	0.88	20.0	23.9	307	8.0	2.11	76.7	804
45	3.2	9.1	17.0	43.8	88.6	0.87	261.5	4.32	0.27	0.82	19.2	22.5	289	9.7	2.29	80.5	916
DRY SURFACE TESTS																	
46	2.2	16.8	17.0	29.8	52.5	0.91	119.5	4.31	0.16	0.82	14.4	15.1	194	3.2	2.30	45.7	620
47	2.8	13.1	13.3	30.1	62.8	0.84	189.2	4.06	0.19	0.78	14.2	16.9	218	5.1	2.29	55.5	804
48	3.2	12.0	12.2	31.4	63.0	0.74	239.0	3.94	0.20	0.71	14.5	16.3	209	5.7	2.29	58.3	916
PARTIALLY WET SURFACE TEST (for validation of the selection method)																	
49	2.8	8.1	18.3	41.1			200.5		0.24					7.0			804

APPENDIX - 3 (cont'd)
TEST COIL REF NO. 08 $N_R = 8$ $p_s = 3.1$ fin/cm

TEST NO	V_a (m/s)	Δt_a (°C)	ΔH_a (kJ/kg)	Q (kW)	h_a (W/m²°C)	j_a x10²	Δp_a (Pa)	f_a x10²	m_r (kg/s)	Δx	K_f x10⁻²	h_rx10⁻² (W/m²°C)	Nu_r	Δp_r (kPa)	f_r x10²	$Re_{r,l}$ x10⁻²	Re_a
WET SURFACE TESTS																	
50	1.7	14.5	33.1	44.3	91.9	1.79	89.6	6.66	0.23	0.90	14.2	18.6	327	9.6	2.61	68.3	702
51	2.2	12.4	27.3	49.1	118.1	1.71	137.0	5.61	0.30	0.80	14.6	21.0	370	12.5	1.72	92.1	945
52	2.9	12.9	21.3	49.1	106.3	1.19	199.2	4.85	0.31	0.84	13.9	23.1	401	14.5	1.99	93.8	1222
DRY SURFACE TESTS																	
53	1.7	21.8	22.1	29.7	43.8	1.02	59.8	4.37	0.15	0.86	11.0	11.7	206	3.8	2.66	46.1	702
54	2.2	18.8	18.7	34.5	54.9	0.95	107.1	4.37	0.22	0.72	10.3	18.6	328	7.9	2.02	65.2	945
55	2.9	16.0	16.3	38.0	65.0	0.87	154.4	3.91	0.24	0.79	11.3	16.4	289	9.2	2.0	72.3	1222
PARTIALLY WET SURFACE TEST (for validation of the selection method)																	
56	2.2	12.8	25.2	40.3			128.1							11.2			945

APPENDIX - 3 (cont'd)
TEST COIL REF NO. 09 $N_R = 8$ $p_s = 3.9$ fin/cm

TEST NO	V_a (m/s)	Δt_a (°C)	ΔH_a (kJ/kg)	Q (kW)	h_a (W/m²°C)	j_a x10²	Δp_a (Pa)	f_a x10²	m_r (kg/s)	Δx	K_f x10⁻²	h_rx10⁻² (W/m²°C)	Nu_r	Δp_r (kPa)	f_r x10²	$Re_{r,l}$ x10⁻²	Re_a
WET SURFACE TESTS																	
57	2.2	12.4	29.0	50.6	103.9	1.52	171.8	5.62	0.26	0.90	14.5	20.2	260	9.7	2.08	77.0	735
58	2.8	10.8	24.4	55.0	125.2	1.42	265.5	5.21	0.27	0.91	13.7	20.4	263	10.7	2.15	80.8	948
59	3.1	10.7	23.6	58.8	11[illegible]	1.19	278.9	4.49	0.36	0.90	14.2	23.8	305	20.3	2.15	108.4	1050
DRY SURFACE TESTS																	
60	2.2	21.8	22.1	38.9	53.2	0.93	139.4	4.56	0.20	0.91	10.7	15.1	195	5.7	2.02	59.6	735
61	2.8	17.4	17.7	40.0	64.2	0.87	211.7	4.17	0.25	0.78	11.0	16.7	214	10.1	2.0	76.0	948
62	3.1	16.1	16.3	41.1	64.6	0.79	236.6	3.89	0.28	0.75	11.3	18.6	239	12.5	2.0	83.2	1050
PARTIALLY WET SURFACE TEST (for validation of the selection method)																	
63	2.8	12.8	23.1	52.0			250.1		0.25					11.0		74 8	948

APPENDIX - 3 (cont'd)
TEST COIL REF NO. 10 N_R = 8 p_s = 5.5 fin/cm

TEST NO	V_a (m/s)	Δt_a (°C)	ΔH_a (kJ/kg)	Q (kW)	h_a (W/m²°C)	j_a x10²	Δp_a (Pa)	f_a x10²	m_r (kg/s)	Δx	K_f x10⁻²	h_rx10⁻² (W/m²°C)	Nu_r	Δp_r (kPa)	f_r x10²	$Re_{r,l}$ x10⁻²	Re_a
WET SURFACE TESTS																	
64	1.5	14.2	41.9	52.3	81.3	1.59	159.4	6.8	0.33	0.89	14.0	20.7	267	12.9	1.51	99.0	381
65	2.1	14.1	35.6	9.5	63.8	0.93	263.9	6.0	0.36	0.85	14.4	25.7	331	13.8	1.34	106.5	511
66	2.7	14.0	28.3	61.3	70.9	0.84	343.6	4.67	0.39	0.80	13.9	27.7	355	17.6	1.51	116.5	662
DRY SURFACE TESTS																	
67	1.5	26.6	27.0	33.8	40.7	0.95	117.0	4.68	0.26	0.70	11.0	18.6	239	11.4	2.0	78.3	381
68	2.1	22.7	23.0	38.8	48.9	0.85	179.3	4.06	0.28	0.73	11.3	13.3	234	12.9	2.0	82.2	511
69	2.2	17.7	18.0	39.1	54.2	0.73	268.9	3.86	0.28	0.70	11.0	14.2	249	13.1	2.0	83.8	662
PARTIALLY WET SURFACE TEST (for validation of the selection method)																	
70	2.1	15.8	31.1	52.0			254.2		0.31	0.80				13.0		91.7	511

APPENDIX-4

SAMPLE TEST DATA

TEST REF. NO. 01 (SEE APPENDIX-1)

ASHRAE STANDARD 33-78

TEST RUN			AIR SIDE TEST DATA										
①	②	④	COIL READINGS								NOZZLE READINGS		
	READING		⑤	⑥	⑦	⑧	⑨	⑩	⑪	⑫	⑬	⑭	⑮
No.	No.	Time (Min.)	P_b (In. Hg)	t_3 (°F)	t_3 (°F)	t_4 (°F)	t_5 (°F)	t_5 (°F)	ΔP_n (In. H_2O)	P_{s1} (In. H_2O)	ΔP_{sn} (In. H_2O)	P_{sn} (In. Hg)	t_{sn} (°F)
1	1	23.0	30.80	80.16	71.70	58.94	57.52	77.60	0.219	2.411	4.483	-0.171	61.08
	2	20.0	30.80	80.18	71.68	58.94	57.49	77.60	0.219	2.412	4.483	-0.171	61.09
	3	18.0	30.80	80.18	71.68	58.94	57.48	77.60	0.219	2.415	4.483	-0.171	61.12
	4	21.0	30.80	80.17	71.68	58.94	57.50	77.60	0.219	2.412	4.483	-0.171	61.11
Average	⑨		30.80	80.17	69.68	58.94	57.50	77.60	0.219	2.413	4.483	-0.171	61.10
Average	⑨												
Average	⑨												

VOLATILE REFRIGERANT COIL TEST DATA - REFRIGERANT SIDE

Test Point No.	Reading No.	REFRIGERANT SIDE								LIQUID FLOW METER	
①	②	⑯ t_{r2} (°F)	⑰ P_{r1} (psig)	⑱ t_{r0} (°F)	⑲ P_{r0} (psig)	⑳ ΔP_r (psi)	⑳a ΔP_{rc} (psi)	㉑ h_{r1} (Btu/lb)	㉒ h_{r2} (Btu/lb)	㉓ t_{rf2} (°F)	㉔ w_r (lb/hr)
1	1	49.72	68.35	68.37	91.92					91.94	1082.12
	2	49.72	68.36	68.37	91.92					91.94	1082.12
	3	49.72	68.37	68.37	91.92					91.94	1082.12
	4	49.72	68.39	68.37	91.92					91.94	1082.12
Average	③	49.72	68.37	68.37	91.92			25.68	110.37	91.94	1082.12
Average	③										
Average	③										

SAMPLE TEST DATA SUMMARY

APPENDIX-4 (CONT'D)

VOLATILE REFRIGERANT COIL TEST DATA — REFRIGERANT SIDE

CONDENSER WATER METHOD

Test No.	Reading No.	㉒ t_{w1} (°F)	㉓ t_{w2} (°F)	㉔ W (lb)	㉕ Σ (min)	㉖ t'_{c1} (°F)	㉗ p_{c1} (psig)	㉘ t_{c1} (°F)	㉙ p_{c2} (psig)	㉚ t_s (°F)	㉛ t_c (°F)	㉜ A_m (sq ft)	㉝ U_c (Btu/(hr)(sq ft)(°F))
1	1	72.5	104.5	52.1			200.0			86.96			
	2	70.5	102.2	51.9			200.0			86.96			
	3	71.0	103.4	52.0			200.0			86.96			
	4	68.5	100.2	50.9			200.0			86.96			
Average	⑨	70.9	102.6	51.8			200.0			86.96		15.70	0.04
Average	⑩												
Average	⑪												

SAMPLE TEST DATA SUMMARY

PAGE 3 of 3

APPENDIX - 5

SAMPLE CALCULATIONS

Sample Calculations (see Appendix-4)

Test reference No.: 01 (see Appendix-3)

Number of tube rows: 3

Coil fin spacing : 10 fins/inch

The following calculations are based on the procedures outlined in the ASHRAE and A.R.I. Standards [31 and 32]:

1. Air mass flow rate (m_a) is given by:

$$m_a = 200.4\ C_N\ A_N\ N_N\ [(\Delta P_N)\ (P_N+P_s)/V_N\ (1+W_N)]^{0.5}\ (lb/min) \qquad (9.1)$$

where,

C_N - nozzle flow coefficient

A_N - cross section area of nozzle (ft^2)

N_N - number of nozzles used in test

ΔP_N - air pressure drop across the nozzles (In. water)

P_N - air static pressure at the nozzle throat (In. of mercury)

V_N - specific volume of air at standard air condition (ft^3/lb of dry air)

P_B - barometer pressure (in. of mercury)

W_N - humidity ratio of air at the standard air conditions (lb of moisture / lb of dry air)

2. The specific volume of air at standard conditions (v_N) is given by:

$$v_N = 0.025\ (t_N + 460)\ (1+1.6078\ W_N)\ (ft^3/lb) \qquad (9.2)$$

where t_N is the air temperature at the nozzle throat.

From the test data:

$C_N = 0.99$

$A_N = 0.349\ (ft^2)$

$N_N = 1$

$P_N = -0.171$ (in. of H_g)

$vP_N = 4.483$ (in. of water gauge)

nence,

$$v_N = 0.025\ (61.1 + 460)\ (1 + 6078) \times 0.011)$$

$$= \underline{13.3\ (ft^3/lb)}$$

$$m_a = 200.4 \times 3.19 = 221.28\ (lb/min.)$$

3. Air velocity at standard conditions (V_a):

$$V_a = m_a\ v_N/A_F \qquad (ft/min.)$$

where

m_a - defined in eqn. 9.1

v_N - defined in eqn. 9.2

A_F - coil face area

V_a = 221.26 x 13.3/7.5 = <u>393.3</u> (ft/min.)
= 2 m/s

4. <u>Coil Capacity Calculations</u>:

<u>Test Data</u>: (from Appendix-4)

Entering air D.B. Temp ($t_{a,2}$)	: 80.17 (°F)
Entering air W.B. temp. ($t'_{a,1}$)	: 71.68 (°F)
Entering air enthalpy ($H_{a,1}$)	: 30.66 (Btu/lb)
Leaving air D.B temp. ($t_{a,2}$)	: 58.94 (°F)
Leaving air W.B. temp. ($t'_{a,2}$)	: 57.50 (°F)
Leaving air enthalpy ($H_{a,2}$)	: 25.64 (Btu/lb)
Entering refrigerant enthalpy ($H_{r,1}$)	: 25.64 (Btu/lb)
Leaving refrigerant enthalpy ($H_{r,2}$)	: 110.37 (Btu/lb)
Refrigerant mass flow rate (m_r)	: 1082.12 (lb/hr.) (0.14 kg/s)

4.1 <u>Air-Side Total Capacity (Q_a) is given by (from Eqn. 4.27):</u>

$Q_a = [60\ m_a[(H_{a,1} - H_{a,2})]$ (Btu/hr.)

= [221.28 (30.66 - 23.79) x 60]

= <u>906610.0</u>

4.2 Refrigerant-Side Capacity (Q_r) is given by:

$$Q_r = m_r (H_{r,2} - H_{r,1}) \qquad \text{(Btu/hr)}$$

$$= 1082.12 (110.37 - 25.64)$$

$$= \underline{91773.0}$$

4.3 Coil Average Total Capacity (Q_T) is give by (from Eqn. 4.28)

$$Q_T = \frac{Q_a + Q_r}{2} \qquad \text{(Btu/hr)}$$

$$= \frac{90610 + 91773}{2} = \underline{91191.0} = 26.7 \text{ kw}$$

4.4 Heat Balance Total Difference (HBT) is given by (from Eqn. 4.29)

$$HBT = 100 \left(\frac{Q_a - Q_r}{Q}\right) \quad (\%)$$

$$= 100 \left(\frac{90610 - 91773}{91191}\right) = \underline{- 1.28\%}$$

5. Heat Transfer Surface Area Calculations:

The heat transfer surface area calculations are performed from the equations listed in the Table 4.1. The calculated heat transfer surface areas for the coil are as follows:

primary surface area (A_p) = 23.81 (ft^2)

total surface area	(A_o)	= 630.10	(ft^2)
tube inside surface area	(A_I)	= 23.31	(ft^2)
coil face area	(A_F)	= 7.50	(ft^2)
Ratio of total surface area to tube inside surface area	$\frac{A_o}{A_I} = (B)$	= 27.28	
Ratio of minimum flow area to coil face area	$(A_{m,f}/A_F = \sigma)$	= 0.584	
coil hydraulic diameter (D_h)		= 0.01 (ft)	(Eqn. 2.3)
refrigerant circuit equivalent length lengtn (for the coil):		= 15.4 ft	

6. Heat Transfer and Pressure Drop factor Calculations:
Test Data for Test A01 (Appendix - 4):

Average tube surface temperature row - 1 $(t_{s,1})$	60.4	(°f)
Average tube surface temperature row - 3 $(t_{s,3})$	55.5	(°F)
Temperature of the liquid refrigerant entering the coil circuit $(t_{r,1})$	45.8	(°F)
Pressure of the liquid refrigerant entering the coil circuit $(P_{r,1})$	82.9	(Lbf/in^2)

vapour quality of the refrigerant entering coil ciruit (from the condenser leaving conditions)	0.15	
Refrigerant vapour temperature leaving the coil circuit ($t_{r,2}$)	49.7	(°F)
Refrigerant vapour pressure leaving the coil circuit ($P_{r,2}$)	83.1	(lbf/in^2)
Super heat of the refrigerant vapour leaving the coil circuit ($t_{r,SH}$)	9.7	(°F)
Average refrigerant pressure drop (ΔP_r)	0.19	(lbf/in^2)
Average air pressure drop across the coil (ΔP_a)	0.22	in. of water gauge

The measured average tube surface temperature for the first and the last row of the coil ($t_{s,1}$ and $t_{s,3}$) are lower than the corresponding saturation temperatures for the air ($t_{a,1,sat}$ and $t_{a,3,sat}$ respectively). Hence, the coil surface is completely wet. The overall heat transfer coefficient ($h_{a,w}$) and the finned tube material thermal resistance (R_m), computed from Eqns. 4.31, 4.35 and 4.16 respectively, are as follows:

$h_{o,w}$ = 6.45 (Btu/hr. ft^2.°F)

$h_{a,w}$ = 13.69 "

= 77.8 (W/m^2.°C)

R_m = 0.0108 (hr.ft^2. °F/Btu)

The refrigerant side average thermal resistance (R_r) is given by (from Eqn. 4.15).

$$R_r = \left(\frac{1}{h_{o,w}}\right) - \left(\frac{1}{h_{a,w}} + R_m\right)$$

= 0.12 (hr.ft^2.°F/Btu)

and the corresponding average heat transfer coefficient is given by (Eqn. 4.18)

$$h_r = A_o/(A_i R_r)$$

= 27.28/0.07 = 389.2 Btu/hr ft^2. °F

7. Calculation of the average heat transfer and pressure drop factors:

The average heat transfer and pressure drop coefficients for the air-side and the refrigerant sides, are as follows:

$J_{a,w}$ = 0.0121 (from Eqn. 4.36)

$f_{a,w}$ = 0.0593 (from Eqn. 2.4)

Nu_r = 280.4 (from Eqn. 2.26)

f_r = 0.0236 (from Eqn. 2.33)

The refrigerant liquid flow Reynolds number ($Re_{r,l}$) is as follows:

$Re_{r,l}$ = 4230 (from Eqn. 2.31)

The corresponding average number (k_f) is as follows:

k_f = 3993 (from Eqn. 2.32)

The air flow Reynolds number (Re_a) is as follows:

Re_a = 690 (from Eqn. 2.2)

APPENDIX - 6

APPLICATIONS OF THE DX-COIL SELECTION METHOD

Selection of DX-coils, for comfort air conditioning applications involves the selection of the coil (configuration) which would satisfy the required design conditions [heat transfer rate (Q), and the air side leaving conditions (dry and wet bulb temperatures)] determined from the building thermal loads calculations and the air conditioning system requirements. The choice for the coil configurations are generally pre determined from the market requirements, manufacturing constraints and economic considerations [35]. In addition to meeting the heat transfer rate requirements, the selected coil should also have the least possible air-side and refrigerant-side pressure drop, at the corresponding design conditions, in order to minimize energy consumption.

The applications of the DX-coil selection method (see Chapter 7) arepresented through the following illustrative example.

EXAMPLE

Application of the Selection Method for Coil Selection

STEP 1: Required Selection Conditions for the Coil

Heat transfer capacity (Q)	=	34 ± 0.5	KW
Entering air dry-bulb temperature ($t_{a,1}$)	=	27 ± 1	°C
Entering air wet-bulb temperature ($t'_{a,1}$)	=	23 ± 1	°C

(From building thermal load calculations)

Leaving air dry-bulb temperature ($t_{a,2}$) = 16 ± 1 °C

Leaving air wet-bulb temperature ($t'_{a,2}$) = 15 ± 1 °C

Air mass flow rate across the coil (m_a) = 2 kg/s

(From the system specifications)

Leaving refrigerant vapor pressure ($P_{r,2}$) = 571 ± 2 kPa

Leaving refrigerant vapor temperature ($t_{r,2}$) = 5 ± 1 °C

(From compressor inlet requirements)

STEP 2. IDENTIFY COIL CONFIGURATION CHOICES:

For illustrative purpose, coils 01, 02 and 03 (from Appendix-1) are chosen as alternatives, for this example. For actual selections, however, the choices are generally of much wider range (typically 4 to 6 alternatives).

STEP 3: DETERMINE THE PERFORMANCE DATA (Q, $t_{a,2}$, ΔP_a and ΔP_r) FOR THE SELECTED COILS:

The refrigerant mass flow rate (m_r) may be determined from the procedure described in Chapter-7.

Then, the performance data for the selected coils may be determined from the computer assisted selection method. The results for the coils

selected are shown in Table a6.1. From this data (table a6.1), coil-02 may be selected since the coil meets the required conditions and has the least air and refrigerant side pressure drop.

In typical selection applications where wide choice of coil configurations alternatives exist, the computer assisted selection method can provide substantial savings in the selection time and the corresponding cost.

STEP 4:

The selection method developed may also be used to predict the part load performance of a given coil for variable air volume systems where the air volume flow rate (at a given dry and wet bulb temperatures) is modulated in accordance with the building thermal load requirements.

The coil performance (Q, ΔP_a, Δt_r, and $t_{a,2}$) at part loads may be computed by the selection method for given increments of the air mass flow rate (or the corresponding velocity). The corresponding refrigerant mass flow rate (m_r) may be computed from the required heat transfer rate (at part loads) similarly to that at the selection condition. A comparison of the part-load data computed by the selection method and from the coil manufacturer's data [37] (from the A.R.I. tests) for coil No. 2 are shown in Fig. a6.1. The computed performance data (Q, ΔP_a, and ΔP_r) for the coil agreed within $\pm$ 10% with the corresponding data from the coil manufacturer [37].

Hence, the selection method may be used for prediction of the part load performance of DX-coils in the range of validity of the selection method (see Chapter 7 - Section 2).

TABLE a6.1 - SIMULATED PERFORMANCE DATA (Example Problems)

* Coil Ref. No.	No. of Rows	Fins/cm	Coil Total Capacity (Q_T) (kW)	Leaving air Conditions		Pressure drop		Refrig. Flow/Rate Circuit (M_r) (l/s)
				($t_{a,2}$) (°C)	(W_2)	Air Side (ΔP_a) (Pa)	Refrig. Side (ΔP_a) (kPa)	
01	3	3.9	29.76	16.69	0.012	0.076	2.80	11.55
02	3	4.7	34.76	16.68	0.012	0.097	2.91	11.71
03	3	5.5	34.85	14.12	0.010	0.122	3.65	13.34

* See Appendix-1

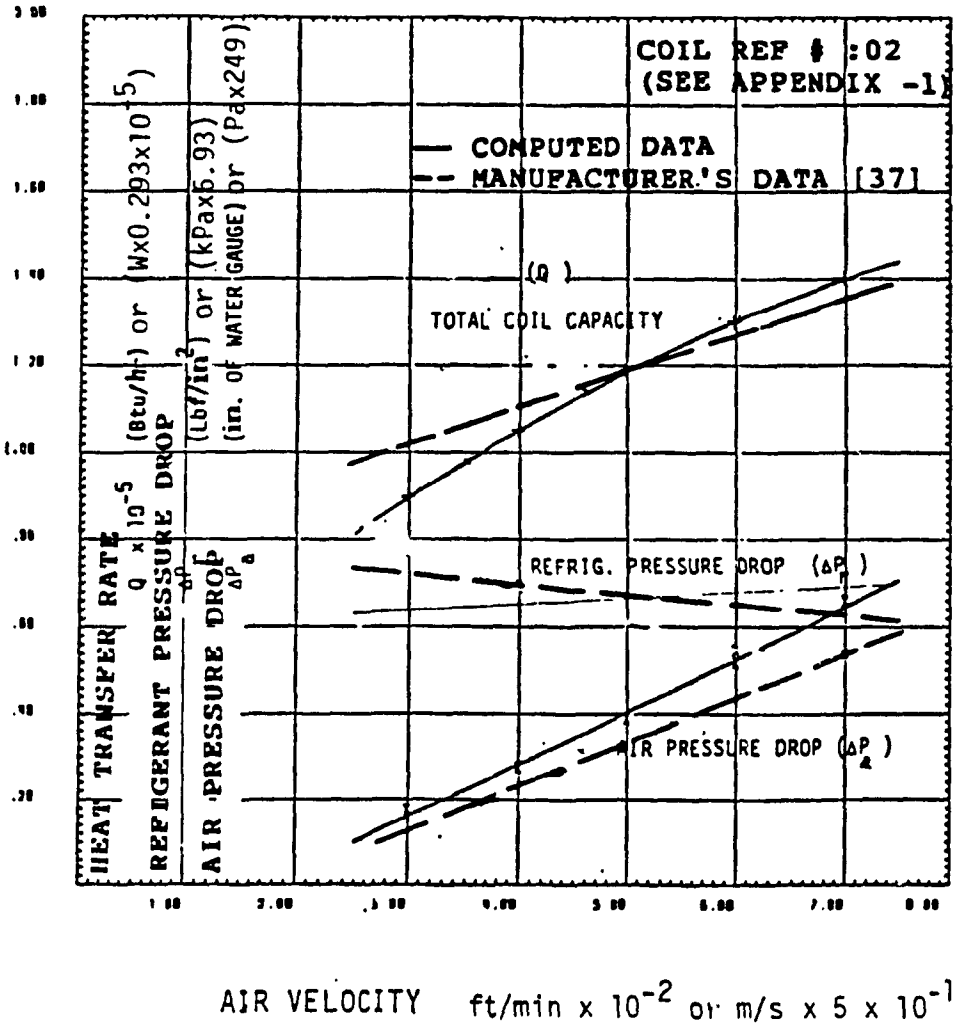

FIG.a6.1 COIL PART-LOAD PERFORMANCE DATA

APPENDIX - 7

UNCERTAINTY ANALYSIS

Statistical methods for evaluation of the uncertainties associated with the experimental measurements are described in Ref. [38]. The uncertainty of a variable (x) in terms of the standard deviation ( ) may be expressed as follows:

$$\sigma = \frac{1}{(N-1)} \sum_{i=1}^{N} [(X_i - x_m)^2]^{\frac{1}{2}} \qquad (a7.1)$$

where

σ - standard deviation

N - Number of measurements

X_m - Mean value of the variable

X_i - Given value of the variable

In the following analysis, it is assumed that the uncertainties of the experimental measurements are known in terms of absolute limits. Normal distribution of the error is assumed where, 95% confidence level corresponds to 2 .

For a variable X, which is a function of other variables a, b, c, etc., the combined uncertainty (x) may be expressed as follows:

$$\sigma_x^2 = (\frac{\delta x}{\delta a})^2 \sigma_a^2 + (\frac{\delta x}{\delta b})^2 \delta_b^2 + ... \qquad (a7.2)$$

The uncertainties of the measured and derived variables used in the experimental study are presented in the following sections. A summary of the uncertainties are shown in Section-3 of this Appendix.

1. AIR-SIDE MEASUREMENTS

a) Air dry-bulb temperature:

The thermocouples used for the air dry-bulb measurement are calibrated to an accuracy of $\pm$ 0.2 °F.

Hence $\sigma = \frac{0.2}{2} = 0.1$ °F

To express the standard deviation as a percentage of the mean temperature (which is 80°F),

$$\sigma_t = \frac{0.1}{80} \times 100 = 0.13\%$$

b) Air relative humidity measurement:

The relative humidity sensor is calibrated to an accuracy of $\pm$ 0.2%. To express the standard deviation as a percentage of the mean value (80%) [based on the calibration data (document No. 76 - 867)]

$$\sigma_{RH} = \frac{0.1}{80} \times 100 = 0.1\%$$

c) Air flow measurement:

The air mass flow rate (m_a) from the pilot-tube traverse method may be expressed as follows:

$$m_a = \rho_a A_F V_a \qquad (a7.3)$$

where,

$$V_a = K \sqrt{[(\Delta p/p) / T]} \qquad (a7.4)$$

A_F - coil face area

V_a - average velocity

ΔP - air pressure drop across the coil

p - absolute pressure

t - average air temperature (absolute)

from Eqns. a7.3 and a7.4

$$m_a \propto A_F [(\Delta p/p)/T]^{0.5} \qquad (a7.5)$$

The uncertainties associated with the variables are as follows (in the range $1 > V_a > 3$ m/s)

$\sigma_{\Delta p}$	= 1.5%	(estimated from the uncertainty in the pressure measurements)
σ_p	= 1.0%	(see Section-1, Item 4)
σ_T	= 0.13%	
σ_{A_F}	= 2.0%	(estimated)
σ_{m_a}	= 3.0%	

d) Air flow Reynolds number (Re_a):

The air flow Reynolds number may be expressed as follows:

$$Re_a \propto m_a/\mu_a \qquad (a7.6)$$

The associated uncertainties are as follows:

σm_a = 3.0%

$\sigma \mu_a$ = 0.5% (estimated)

σRe_a = 3%

e) **Heat transfer rate (Q):**

1. **Dry surface tests:**

The heat transfer rate (Q_D) may be expressed as follows:

$$Q_D = m_a C_p (\Delta t_a) \qquad (a7.7)$$

The associated errors are as follows:

σm_a = 3%

σc_p = 0.5% (estimated)

Δt_a = 1% (estimated)

σQ_D = 3.2%

2. **Wet surface tests:**

$$Q_w = m_a (\Delta H_a) \qquad (a7.8)$$

σm_a = 3%

$\sigma(\Delta H_a)$ = 3% (estimated)

σQ_w = 4.2%

f) Heat transfer factor:

1. Dry surface tests:

$$h_{a,D} = Q_D/A_o\ (\Delta t_a) \qquad \text{(a7.9)}$$

$\sigma_{Q_D} = 3.2\%$

$\sigma_{A_D} = 3\%$

$\Delta t_a = 1\%$

$\sigma_{n_{a,D}} = 4.5\%$

2. Wet surface tests:

$$h_{a,w} = \frac{Q_w\ C_p}{A_o\ (\Delta H_a)} \qquad \text{(a7.10)}$$

$\sigma_{Q_w} = 4.2\%$

$\sigma_{C_p} = 0.5\%$ (estimated) $\sigma_{ha,w} = 6\%$

$\sigma_{\dot{m}_o} = 3.0\%$

$\sigma_{\Delta H_a} = 3.0\%$

g) Air-side heat transfer factor (j_a):

1. Dry surface tests:

$$j_{a,D} \propto (A_o\ h_{a,D}/m_a)\ (\mu_a\ Cp_a/K_a) \qquad \text{(a7.10)}$$

$\sigma_{A_o} = 3\%$

$\sigma_{n_{a,D}} = 4.5\%$

m_a = 3.0%

μ_a = 0.5% (estimated) $\sigma_{j_{a,D}} = 6.2\%$

C_{p_a} = 0.5%

K_a = 0.5% (estimated)

2. **Wet surface tests:**

From the computed percentage error for $h_{a,w}$

$\sigma_{J_{a,w}} = 7.4\%$

h) **Air-side pressure drop factor: (f_a)**

1. **Dry surface tests**

$$f_{a,D} \propto \frac{h_{a,D}}{C_p \Delta P_a V_a} \qquad (a7.11)$$

Air pressure drop is measured by the strain gauge of the pressure transducers, calibrated to an accuracy of $\pm$ 0.02 inches of water gauge, in the range $0.1 < \Delta p_a < 2$ inches of water gauge.

$$\sigma_{\Delta p_a} = \frac{0.01}{1} \times 100 = 1\%$$

$\sigma_{h_{a,D}} = 4.5\%$

$\sigma_{c_p} = 0.5\%$

$\sigma_{V_a} = 3.5\%$

$\sigma_{f_{a,D}} = 5.9\%$

2. **Wet surface tests**

From the computed error for $h_{a,w}$ (6%)

$$\sigma_{f_{a,w}} = 7\%$$

2. REFRIGERANT-SIDE MEASUREMENTS:

a) Refrigerant temperature (t_r):

The refrigerant temperature is measured by a plantinum resistance thermometer, calibrated to an accuracy of $\pm$ 0.1°F. The standard deviation expressed as a percentage of the mean value (40 °F) is,

$$\sigma_{t_r} = \frac{0.05}{40} = 0.01\%$$

b) Refrigerant pressure (p_r):

The refrigerant pressure transducer is calibrated to an accuracy of $\pm$ 0.2 Lbf/in^2 in the range $60 < p_r < 120$ Lbf/in^2. The standard deviation expressed as percent of the mean value (80 Lbf/in^2),

$$\sigma_{p_r} = 0.11\%$$

c) Refrigerant liquid mass flow rate (m_r):

The refrigerant liquid mass flow rate is measured by a variable area flow meter. The flow meter is calibrated by the manufacturer

for an accuracy of + 50 lbm/hr (of R-22) in the range $1000 < m_{r,l} < 10{,}000$ lbm/hr. The corresponding standard deviation, expressed as a percentage of the mean value (5000 lbm/hr) is:

$$\sigma_{m_{r,l}} = \frac{25}{5000} \times 100 = 0.5\%$$

d) **Refrigerant liquid flow Reynolds number ($Re_{r,l}$):**

$$Re_{r,l} \propto m_{r,l}/\mu_{r,l} \qquad (a7.12)$$

$$\sigma_{m_{r,l}} = 0.5\%$$

$$\sigma_{\mu_{r,l}} = 0.5\% \qquad \text{(estimated)}$$

$$\sigma_{Re_{r,l}} = 0.7\%$$

e) **Refrigerant-side average heat transfer coefficient (h_r):**

The refrigerant-side thermal resistance (R_r) is computed from the overall thermal resistance (R_o) and the corresponding air-side and finned-tube material thermal resistance (R_a and R_m) as follows:

for the air-side dry surface tests

$$R_o = \frac{A_o\,(\Delta H_{a,r})}{C_p\,Q_D} \qquad (a7.13$$

$$\sigma_{A_o} = 3\%$$

$$\sigma_{(\Delta H_{a,r})} = 3\% \qquad \text{(estimated)}$$

$$\sigma_{C_p} = 0.5$$

$$\sigma_{Q_D} = 3.2\%$$

$$\sigma_{R_o} = 5.3\%$$

The corresponding uncertainty for the wet surface test (R_o) is as follows:

$$\sigma_{R_o} = 6.5\% \quad \text{(assuming } H_{a,w} = 4\%)$$

The percentage error in the air side thermal resistance (R_a) is as follows:

(from Eqns. a7.9 and a7.10)

$$\sigma_{R_{a,D}} = 4.5\%$$

$$\sigma_{R_{a,w}} = 6\%$$

The percentage error in R_m is as follows (from Eqn. 4.16)

$$R_m = (A_o/A_p)\ (t_t/k_f)$$

$$\sigma_{A_o} = 3\%$$

$$\sigma_{A_p} = 3\% \qquad \text{(estimated)}$$

$$\sigma_{t_t} = 1\% \qquad \text{(estimated)}$$

$$\sigma_{k_f} = 0.5\% \qquad \text{(estimated)}$$

$$\sigma_{R_m} = 4.5\%$$

From Eqn. 4.15

$$R_r = R_o - (R_a + R_m) \qquad \text{(a7.14)}$$

$$\sigma_{R_{r,min}} = 8.2\% \ ; \ \sigma_{R_{r,max}} = 9.8\%$$

$$h_r = A_o/(A_I\ R_r) \qquad \text{(a7.15)}$$

σ_{A_o} = 3%

σ_{A_I} = 2% (estimated)

$\sigma_{h_{r,min}}$ = 8.9% and $\sigma_{h_{r,max}}$ = 10.4%

from Eqn. 4.15

$$R_r = R_o - (R_a + R_m) \qquad \text{(a7.14)}$$

$\sigma_{R_{r,min}}$ = 8.2% ; $\sigma_{R_{r,max}}$ = 9.8%

$$h_r = A_o/(A_I R_r) \qquad \text{(a7.15)}$$

σ_{A_o} = 3%

σ_{A_I} = 2% (estimated)

$\underline{\sigma_{h_{r,min}} = 8.9\%}$ and $\underline{\sigma_{h_{r,max}} = 10.4\%}$

f) Refrigerant-side Nusselt number (Nu_r)

(from Eqn. 4.26)

$Nu_r = h_r D_I/K_{r,l}$

σ_{D_I} = 0.5% (estimated)

$\sigma_{K_{r,l}}$ = 0.5% (estimated)

$\underline{\sigma_{Nu_{r,min}} = 8.9\%}$; $\underline{\sigma_{Nu_{r,max}} = 10.4\%}$

g) Refrigerant pressure drop factor (f_r):

From Eqn. 2.33

$$f = [\Delta p_r / (DP)] + DX$$

$\sigma_{(\Delta p_r)}$ = 0.5% (estimated from the uncertainties in the measurement of P_r)

from Eqn. 2.34

$DX = (v_x)\ D_I/x_m L$

$\sigma_{\Delta x}$ = 5% (estimated)

σ_{x_m} = 4% (estimated)

σ_{D_I} = 0.5% (estimated)

σ_L = 2% (estimated)

$\sigma_{(DX)}$ = 6.7%

from Eqn. 2.36

$(DP) = G_{r,1}^2\ X_m\ v_m\ L/D_I$

$\sigma_{G_{r,1}}$ = 1.0% (estimated from errors in m_r and the tube cross sectional area)

σ_{v_m} = 3% (estimated)

$\sigma_{(DP)}$ = 5.4%

Hence, σ_{f_r} = 8.7%

3. SUMMARY OF THE UNCERTAINTIES:

Item	σ %	
Re_a	3%	
Q_D	3.2%	
Q_W	4.2%	
$h_{a,D}$	4.5%	
$h_{a,w}$	6%	
$j_{a,D}$	6.2%	
$j_{a,w}$	7.4%	
$f_{a,D}$	5.9%	
$f_{a,w}$	7%	
$Re_{r,1}$	0.7%	
f_r	8.7%	
v_{p_a}	1%	
v_{p_r}	1.1%	
	min	max
h_r	8.9%	10.4%
Nu_r	8.9%	10.4%